ALMA MATER STUDIORUM - UNIVERSITÀ DI BOLOGNA

SCUOLA DI INGEGNERIA E ARCHITETTURA

DIPARTIMENTO DI INGEGNERIA CIVILE, CHIMICA, AMBIENTALE E DEI MATERIALI - DICAM

CORSO DI LAUREA IN INGEGNERIA CHIMICA E DI PROCESSO – CURRICULUM "SUSTAINABLE TECHNOLOGIES AND BIOTECHNOLOGIES FOR ENERGY AND MATERIALS"

TESI DI LAUREA
in
Fluid Mechanics and Transport Phenomena

APPLICATION OF AN AMMONIA-BASED PROCESS WITH CONTROLLED SOLID FORMATION FOR POST-COMBUSTION CO_2 CAPTURE

CANDIDATO
Davide Bernardo Preso

RELATORE
Chiar.ma Prof.ssa Maria Grazia De Angelis

CORRELATORI
Chiar.mo Prof. Marco Mazzotti
Federico Milella
José Francisco Pérez Calvo
Dott. Daniel Sutter

Anno Accademico 2017/2018

Sessione III

Abstract

CO_2 capture and storage is needed to reduce the carbon footprint related to industrial activities. Among the different available technologies, CO_2 removal from power/cement plant's flue gases is of particular interest due to its versatility and retrofit opportunities for existing plants. In this framework, the Chilled Ammonia Process (CAP) is a promising technology for post-combustion CO_2 capture. Besides its competitive energetic performance compared to conventional amines, the use of aqueous NH_3 as a solvent offers advantages concerning global availability, environmental footprint and cost compared to most amine processes.

A new ammonia-based process for CO_2 capture from flue gas has been developed, which found its origin in the Controlled Solid Formation - Chilled Ammonia Process (CSF-CAP), developed by Sutter et al. [1]. A controlled solid precipitation carried in a dedicated unit of the plant lead to a reduction of the energy penalty of the process without hindering its operability, since the mass flow rate sent to regeneration can be substantially reduced by means of CO_2 concentration in the solid phase rather than the liquid phase. Differently from the original CSF-CAP, where ammonium bicarbonate has been exploited in the crystallization section, in this new process ammonium carbonate monohydrate is formed, which promises numerous advantages in terms of the overall energy efficiency of the process.

Initially, the process synthesis has been performed, followed by a rigorous optimization and performance evaluation. The work have been carried out coupling Aspen Plus V8.6 and Matlab. The speciation model developed by Thomsen et al. [2] has been used for the calculations in the CO_2 -NH_3 -H_2O system.

Under the assumptions considered in this work and discussed in Sec. 6, the new CSF-CAP has been found to require $0.84\,\mathrm{MJ/kg_{CO_2}}$ of electrical energy, which corresponds to a reduction of 5% of the overall energy duty of the plant, compared to the original CSF-CAP, which needs $0.89\,\mathrm{MJ/kg_{CO_2}}$ [1].

Acronyms

CCS	Carbon Capture and Storage
PCC	Post Combustion Capture
MEA	Monoethanolamine
DEA	Diethanolamine
MDEA	Methyldiethyl-ethanolamine
SI	Supersaturation Index
CAP	Chilled Ammonia Process
DCC	Direct Contact Cooler
L-CAP	Liquid-CAP
CSF-CAP	Controlled Solid Formation-CAP
BC-CSF-CAP	Ammonium Bicarbonate-CSF-CAP
CB-CSF-CAP	Ammonium Carbonate Monohydrate-CSF-CAP

Contents

1 Introduction

1.1 Global emissions and future scenarios

The report of the Inter Governmental Panel on Climate Change [3] states that anthropogenic activities are the main responsible for the greenhouse gases (GHGs) emitted into the atmosphere. These gases are carbon dioxide (CO_2), methane (CH_4), chlorofluorocarbons (CFCs) and nitrous oxide (N_2O). Among them, carbon dioxide (CO_2) is the largest fraction of emitted GHGs. Consequently, CO_2 has been assumed to be the greatest responsible for the GHGs effect, accounting for approximately 55% of the global warming [4].

The combustion of fossil fuels, which is employed for approximately 85% of the world's energy supply, is the main source of CO_2 emissions [5], contributing to 70% of the overall CO_2 emissions due to power production [4].

In this contex, during the 21st conference of the Parties of the United Nations Framework Convention on Climate Change in 2015, the Paris agreement was stipulated to agree on common objectives concerning the climate change. In particular, the Parties agreed on *"holding the increase in the global average temperature to well below 2°C above pre-industrial levels and pursuing efforts to limit the temperature increase to 1.5°C […]"* [6].

As a consequence of the increasing demand of consumer goods in the last years and the relative increase of industrial plants capacities, the actual scenario sees a continuously increasing trend of the GHGs emissions. Figure 1 shows the trend of CO_2 emissions in the last years.

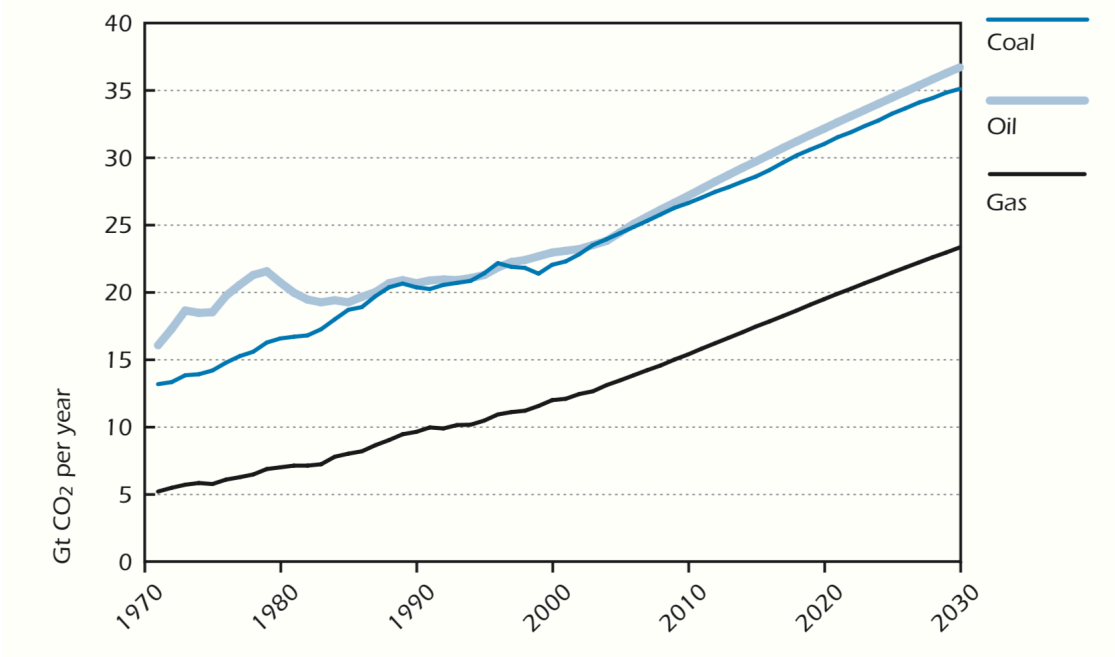

Figure 1: Energy-related CO2 emissions by fuel (1973-2030). Based on IEA data from IEA, 2004a © OECD/IEA 2004, www.iea.org/statistics, Licence: www.iea.org/tc [7]

With the aim of reducing the CO_2 emissions and achieving the objectives of the Paris agreement, two emission pathway scenarios have been identified, concerning the drop of the CO_2 emissions near to zero in a short time or that negative emissions are realized in the second half of the century [3] [8].
The trend of net CO_2 emissions is shown in Figure 2, concerning the 2°C scenario.

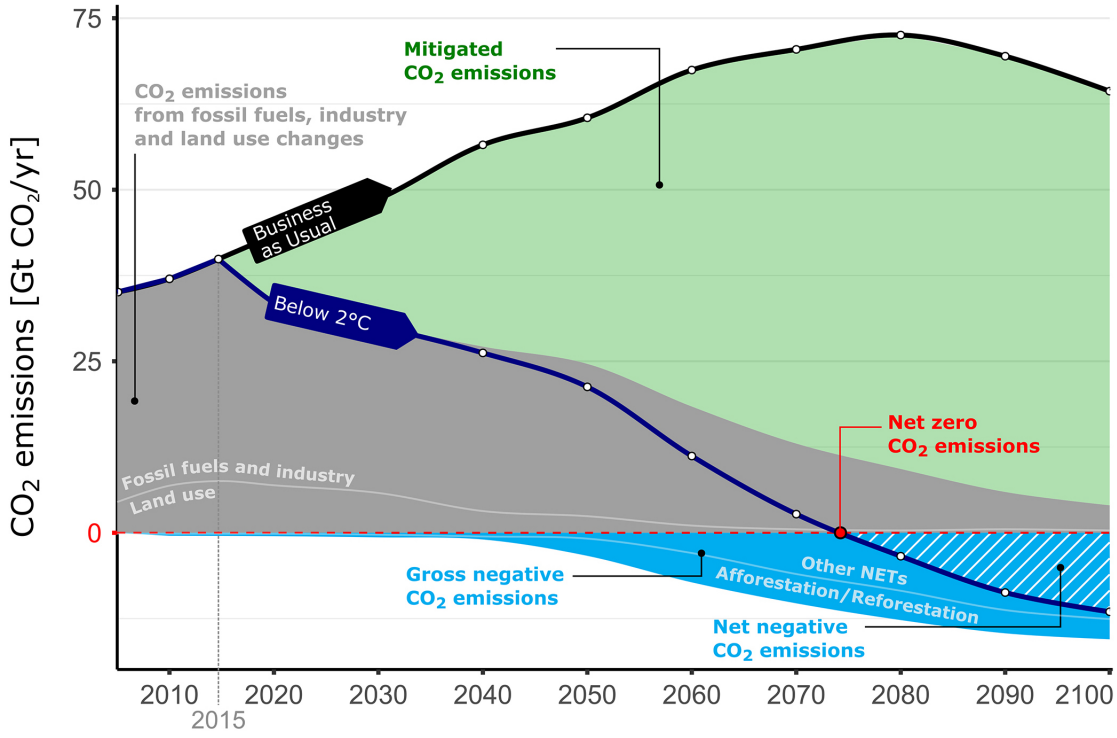

Figure 2: "The role of negative emissions in climate change mitigation" adapted from Fuss et al. [8] is licensed under CC BY 3.0

For this purpose, different approaches have been considered. Among them, the Carbon Capture and Storage (CCS) has earned much credit, becoming a fundamental tool for the achievement of both the scenarios [1].

1.2 Carbon capture and storage and post-combustion CO_2 capture

CCS is mainly divided into 4 categories: post-combustion capture (PCC), pre-combustion capture, oxyfuel conbustion and electrochemical separation. [9].

This thesis focuses on the PCC, which separates the CO_2 from the flue gas after the combustion, by keeping unaltered the existing power plant. Although PCC is one of the most challenging approaches due to presence of dilute CO_2 in the treated gas and the low pressure of the flue gas, it can be considered the easiest technology to be integrated in existing power plants [10] [11].

1.2.1 PCC by chemical absorption

Several techniques are available for PCC, which exploit physical absorption, absorption with chemical solvents (reagents), cryogenic separation and biological fixation [4]. Nowadays, the most employed PCC technique is the chemical absorption.

An ideal solvent for this purpose should meet the following features [4] [12]:

- high CO_2 absorption capacity;
- rapid and reversible reaction with CO_2 , with minimal heat requirement;
- good oxidative and thermal stability;
- low vapor pressure;
- low toxicity;
- low flammability;
- availability at low cost;
- less corrosivity.

Usually, alkanolamine-based and ammonia-based solutions are used in this framework.

1.2.2 Alkanolamine-based processes

Aqueous alkanolamines solutions are the most diffused solvents in CO_2 capture processes [12]. Among them, monoethanolamine (MEA), diethanolamine (DEA) and methyldiethylethanolamine (MDEA) can be mentioned.

The wide use of amine-based solutions for CO_2 absorption makes this process one of the most well-understood. In fact, amine-based processes have been know for more than 80 years [13] [4].

Besides the positive aspects, they have some disadvantages [4] [12] [11]:

- low CO_2 loading capacity ($mol_{CO_2,absorbed}/mol_{absorbent}$);
- active at low CO_2 partial pressure, because CO_2 chemically reacts with amines (tipically 13-14% from coal-fired power plants) [12];
- oxidative degradation due to the presence of SO_2, NOx, HCl, HF and O_2 in the flue gas;
- high equipment corrosion;
- high heat duty due to solvent regeneration;

The general reaction scheme of absorption of CO_2 by amines was proposed by Kohl and Nielsen [14]:

$$H_2O \rightleftharpoons H^+ + OH^- \quad \text{(ionization of water)} \tag{1}$$

$$CO_2 + H_2O \rightleftharpoons HCO_3^- + H^+ \quad \text{(hydrolysis,ionization of } CO_2\text{)} \tag{2}$$

$$RNH_2 + H^+ \rightleftharpoons RNH_3^+ \quad \text{(protonation of alkanolamine)} \tag{3}$$

$$RNH_2 + CO_2 \rightleftharpoons RNHCOO^- + H^+ \quad \text{(carbamate formation)} \tag{4}$$

The scheme applies to primary (i.e. MEA), secondary and tertiary amines, although the latter cannot react directly with CO_2 to form carbamates (reaction 4). Scheme 5 [12] resumes the absorption reaction of CO_2 by primary and secondary amine to form carbamate, where reaction 4 is predominant:

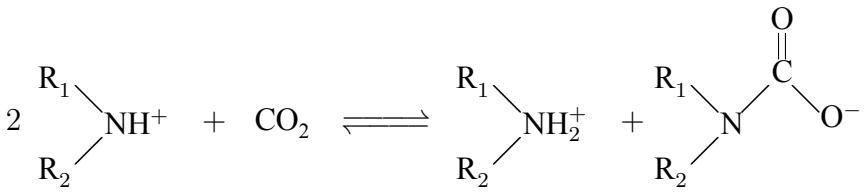

(5)

Carbamate is a stable compound, which does not easily undergo hydrolysis to bicarbonate. Tertiary amines absorb CO_2 by forming bicarbonate, as shown in scheme 6:

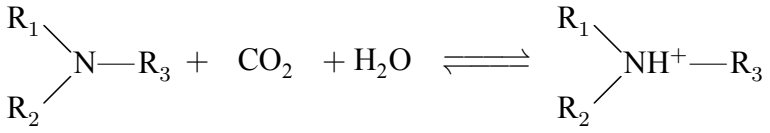

(6)

The differences between the two reaction schemes are:

- in general, scheme 5 is faster than scheme 6;
- in scheme 5, the loading capacity of the solution is 0.5 mol of CO_2 per mol of amine, whereas in scheme 6 only one mole of amines is consumed per mole of CO_2 absorbed.

1.2.3 Ammonia-based processes

From a chemical point of view, NH_3 and amines (which are in turn produced from NH_3) are very similar [jason e.]. Aqueous ammonia can therefore be directly employed as a solvent in CO_2 capture processes.

With regard to safety, NH_3 is a hazardous substance, which is very harmful if inhaled. Moreover, NH_3 is explosive, in fact NH_3 can be burned .

In comparison with amine-based solvents, aqueous ammonia has better features [4] [15] [1]:

- high CO_2 loading capacity;
- high rate of CO_2 absorption;
- non corrosive solution;
- stable in presence of O_2 and other flue gas impurities;
- generally lower liquid to gas flow ratio in the absorption process;
- multi-pollutant capture capability (in particular SO_2 and NOx), so that further pre-treatment of the flue-gas is not required;
- less energy demand for solvent regeneration;
- low cost product, cheaper than MEA and other amines;
- higher worldwide availability;
- regeneration at elevated pressures.

Details on the thermodynamics of the NH_3 -CO_2 -H_2O system are given in section 2. Furthermore, the employment of aqueous ammonia for the absorption of CO_2 could lead to the formation of different salts, i.e. ammonium bicarbonate, ammonium carbonate mono-hydrate, ammonium sesqui-carbonate and ammonium carbammate [16].

1.3 Comparison between ammonia and amine processes

Several comparative works that analyze both NH_3 -based and MEA-based CO_2 capture processes have been published.

As a result of the analyses, the costs associated with amine-based CO_2 capture have led the research toward the development of processes which exploit different solvents. Minimum energy requirement and lower equipment size have been the challenges to overcome the amine-based process limitations [4]. In this framework, aqueous ammonia is playing an important role.

In general, studies show that CO_2 capture with aqueous NH_3 solution is better in terms of performance (CO_2 removal efficiency and absorption capacity) [4]. Bandyopadhyay [4] presented a comparative study on the energy penalty of NH_3 -based and MEA-based CO_2 -capture processes. As reported, MEA-based processes require 4215 $kJ/kg_{CO_{2,captured}}$, employing 30% wt. MEA solutions, whereas the NH_3 -based process energy duty is only about 27% of the latter, with 1147 $kJ/kg_{CO_{2,captured}}$.
Furthermore, Luis [10] reported that energy requirements of processes operated with 30%

wt. MEA solution ranges from 3200 to 5500 $kJ/kg_{CO_{2,captured}}$, which is in any case higher than the ones of NH_3 -based processes.

The regenerative desorption for the regeneration of the solvent is endothermic and it is the main energy consumption associated to the process, which is much higher in MEA-based processes than in NH_3 -based processes. The energy requirements of the desorption strongly depends on the composition of the solvent loaded with CO_2 .

In conclusion, combining such processes with power plants implies a net power output reduction of around 30% [17], as well as a reduction of the overall efficiency of the plant. This is due to the energy required to operate the CO_2 capture in the plant.

1.4 Applications to cement plants

1.4.1 Introduction to cement plants

Coal-fired power plants are certainly the largest producers of CO_2 , but technologies for CO_2 emissions reduction are not focused only on these plants.

Lately, the application of CCS to power plant has lost attention, because of the still increasing employment of renewable energies. Furthermore, the integration of CO_2 capture processes have been studied with other manufacturing processes. In this regard, cement plants have gained the attention of the researchers.

The cement sector is among the biggest manufacturing industrial sectors. Cement is involved in the production of concrete, the most consumed product in the world. Consequently, cement industry accounts for 7% of the global industrial energy consumption [18]. It is also responsible for 5% of the global CO_2 emissions [19] and it is the second largest sector for total direct industrial CO_2 emissions, with 2.2 Gt_{CO_2} /year in 2014 [18].

The Technology Roadmap of the International Energy Agency [18] sets a strategy for CO_2 emissions reduction in the 2 °C scenario framework, although the concrete production is expected to increase by 12-23% by 2050. The strategy is based on four main actions:

- improving energy efficiency;
- using less carbon intensive fuels;
- reducing the clinker to cement ratio;
- implementing technologies such as CCS.

1.4.2 Overview of cement manufacturing

Cement is produced in a three-stage process: initial preparation of raw material, production of clinker and grinding of clinker with other components to get cement. A simple scheme is showed in Figure 3.

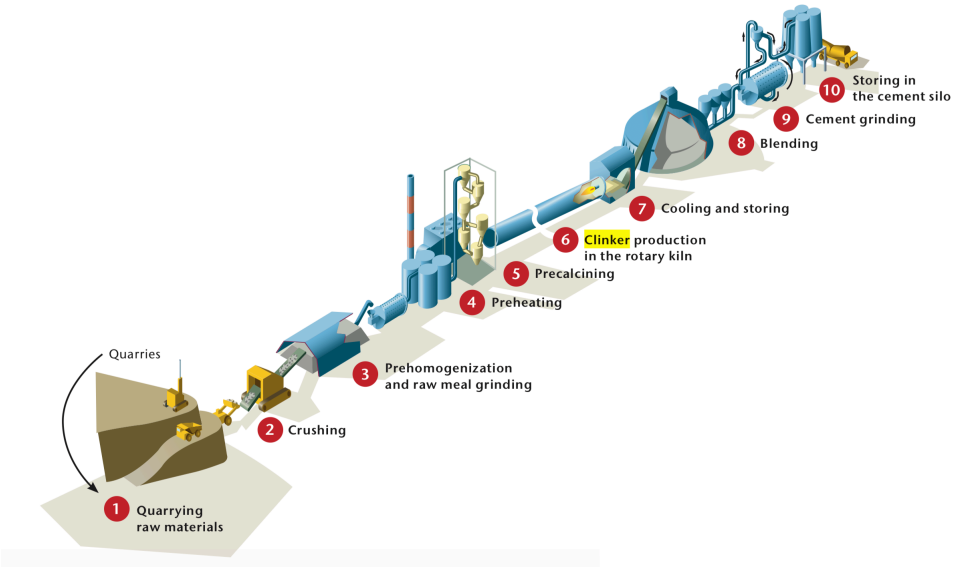

Figure 3: Cement manufacture at a glance. © OECD/IEA 2009, Cement Technology Roadmap 2009 - Carbon emissions reductions up to 2050, IEA Publishing. Licence: www.iea.org/tc [19]. 1) Quarrying raw materials, 2) crushing, 3) preparing raw meal, 4) preheating and co-processing, 5) pre-calcining, 6) producing clinker in the rotary kiln, 7) cooling and storing, 8) blending, 9) grinding, 10) storing in silos for loading and packaging

Clinker can be produced in "wet" or "dry" processes, depending on the moisture concentration in the raw materials. The wet process needs a higher amount of energy due to the moisture vaporization.

Typically, 30-40% of total CO_2 emissions comes from the combustion of fuels, while the other 60-70% comes from the calcination, defined by IUPAC as "heating to high temperatures in air or oxygen". The chemical reaction that decomposes limestone into lime, with release of CO_2 is:

$$CaCO_3 \rightleftharpoons CaO + CO_2 \quad \text{(calcination)}$$

Calcination mostly occurs in the "precalciner" (step 5, Figure 3) and it is completed in the "clinker" or kiln (step 6, Figure 3).

2 Thermodynamic model and process simulation

2.1 The CO_2 -NH_3 -H_2O system

The NH_3 -CO_2 -H_2O system can be modeled using the so called "Thomsen model", which is a thermodynamic model originally developed by Thomsen and Rasmussen [2] and successively upgraded by Darde et al. [20].

Several equilibrium processes are considered in the CO_2 -NH_3 -H_2O system:

- vapor-liquid equilibria:

$$CO_2\ (g) \rightleftharpoons CO_2\ (aq) \tag{7}$$
$$NH_3\ (g) \rightleftharpoons NH_3\ (aq) \tag{8}$$
$$H_2O\ (g) \rightleftharpoons H_2O\ (l) \tag{9}$$

- speciation equilibria (in the liquid phase):

$$H_2O\ (l) \rightleftharpoons OH^- + H^+ \tag{10}$$
$$NH_3\ (aq) + H^+ \rightleftharpoons NH_4{}^+ \tag{11}$$
$$CO_2\ (aq) + H_2O\ (l) \rightleftharpoons HCO_3{}^- + H^+ \tag{12}$$
$$HCO_3{}^- \rightleftharpoons CO_3{}^{2-} + H^+ \tag{13}$$
$$NH_3\ (aq) + HCO_3{}^- \rightleftharpoons NH_2COO^- + H_2O\ (l) \tag{14}$$

- liquid-solid equilibria:

$$NH_4{}^+ + HCO_3{}^- \rightleftharpoons NH_4HCO_3(s) \tag{15}$$
$$NH_4{}^+ + NH_2COO^- \rightleftharpoons NH_2COONH_4(s) \tag{16}$$
$$2NH_4{}^+ + CO_3{}^{2-} + H_2O \rightleftharpoons (NH_4)_2CO_3 \cdot H_2O(s) \tag{17}$$
$$4NH_4{}^+ + CO_3{}^{2-} + 2HCO_3{}^- \rightleftharpoons (NH_4)_2CO_3 \cdot NH_4HCO_3(s) \tag{18}$$
$$H_2O\ (l) \rightleftharpoons H_2O\ (s) \tag{19}$$

As shown, the model considers the formation of 5 different solids:

NH_4HCO_3	ammonium bicarbonate (BC)
$(NH_4)_2CO_3 \cdot NH_4HCO_3$	ammonium sesqui-carbonate (SC)
$(NH_4)_2CO_3 \cdot H_2O$	ammonium carbonate monohydrate (CB)
NH_2COONH_4	ammonium carbamate (CM)
H_2O(s)	ice

In the Thomsen model, the extended UNIQUAC model is used in calculating the activity coefficients of the aqueous species, while the gas phase fugacity coefficients are calculated using the SRK equation of state.

A schematic summary of phase equilibria and reactions is reported in Figure 4

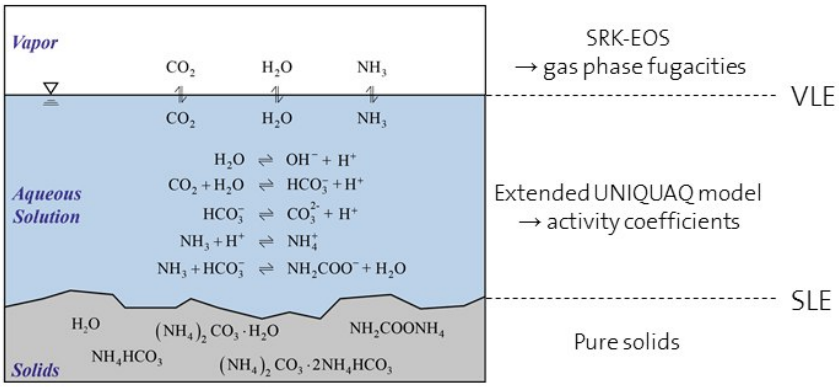

Figure 4: The CO_2 –NH_3 –H_2O system as described in the Thomsen model [20]. Reprinted from Chemical Engineering Science, 133 (2015), Daniel Sutter, Matteo Gazzani, Marco Mazzotti , Formation of solids in ammonia-based CO_2 capture processes — Identification of criticalities through thermodynamic analysis of the CO_2 –NH_3 –H_2O system, Pages No. 170-180, Copyright 2015, with permission from Elsevier [2]

2.2 Equilibria calculations

Each equilibrium equation described in 2.1 can be written in the form of equation 20:

$$-\frac{\Delta G_j^0(T)}{RT} = \sum_i v_{i,j} \ln a_i \tag{20}$$

where ΔG_j^0 is the standard state Gibbs energy of formation increment for process j at a specific temperature T, a_i is the activity and $v_{i,j}$ is the stoichiometric coefficient of component i in process j.

Equilibrium composition is calculated by solving the system of equations (7)-(14). Afterwards, solids formation has to be verified by checking equations (15)-(19). If one or more solid phases form, the system of equations needs to be integrated with equilibrium equation (among (15)-(19)) of the solids formed and solved again.

2.2.1 Speciation equilibria

In the Thomsen model, the extended UNIQUAC model is used to calculate the activity coefficients of the aqueous species. The original UNIQUAC model, originally developed by Abrams and Prausnitz [21] and Maurer and Prausnitz [22], was extended by Thomsen

and Rasmussen [23] by the addition of a Debye-Hückel term:

$$G^E_{\text{extendedUNIQUAC}} = G^E_{\text{combinatorial}} + G^E_{\text{residual}} + G^E_{\text{Debye-Hückel}} \tag{21}$$

in which G^E_i is the excess Gibbs energy for the generic term i in the equation. So equation 21 is the sum of an entropic term (combinatorial), an enthalpic term (residual) and the Debye-Hückel electrostatic term. The latter term takes into account ionic species in solution. In this way, the extended UNIQUAC model is able to account for the electrostatic interactions in the system.

At equilibrium conditions, for each reaction, the sum of the chemical potential of the reactants is equal to the sum of the chemical potentials of the products. The chemical potentials must be written by following some conventions. In the "Thomsen model", water has been considered the solvent in the system, while NH_3 is considered as a solute. Therefore, the symmetrical convention has been adopted for water, whereas the rational unsymmetrical potential has been chosen for all the other species. So, the chemical potential of water in liquid phase is calculated as:

$$\mu_{\text{H}_2\text{O(l)}} = \mu^0_{\text{H}_2\text{O(l)}} + RT \ln a_{\text{H}_2\text{O(l)}} = \mu^0_{\text{H}_2\text{O(l)}} + RT \ln \left(\gamma_{\text{H}_2\text{O(l)}} x_{\text{H}_2\text{O(l)}}\right) \tag{22}$$

where $\mu^0_{\text{H}_2\text{O(l)}}$ is the standard state chemical potential of water at temperature T, R is the gas constant, $a_{\text{H}_2\text{O(l)}}$ is the activity, $\gamma_{\text{H}_2\text{O(l)}}$ is the activity coefficient and $x_{\text{H}_2\text{O(l)}}$ is the mole fraction of water in the liquid phase. While, for the other species in the liquid phase, the chemical potential can be written as:

$$\mu_{\text{i(aq)}} = \mu^*_{\text{i(aq)}} + RT \ln a^*_{\text{i(aq)}} = \mu^*_{\text{i(aq)}} + RT \ln \left(\gamma^*_{\text{i(aq)}} x^*_{\text{i(aq)}}\right) \tag{23}$$

where the lettering is the same as equation 22, but the "*" indicates the unsymmetrical convention.

The chemical potential is calculated as the standard state chemical potential, plus the concentration dependence term, where the latter is calculated by means of the thermodynamic model.

So one can solve the system of speciation equilibria equations (10-14).

2.2.2 Vapor-liquid equilibria

At equilibrium, the fugacity of the liquid phase equals the fugacity of the vapor phase. Therefore, equation 24 is obtained:

$$P y_i \phi_i = H^*_{i,w}(T, P^s_w) \exp \frac{v^\infty_{i,w} \times (P - P^s_w)}{RT} \gamma^*_i x_i \tag{24}$$

The solution of the system returns the mole fraction of the vapor phase. If the sum is

different from 1, a new pressure is guessed and the system is solved again.

The bubble point of the aqueous electrolyte solution is calculated by a $\gamma - \phi$ approach, paired with equilibrium speciation reactions [2] [24] [25].

The phase equilibrium is found by guessing the pressure and the vapor composition. For each component i, the vapor-phase fugacity can be written as follow:

$$\bar{f}_i^V = y_i \Phi_i P \tag{25}$$

where y_i is the mole fraction of component i, Φ_i is the fugacity coefficient of component i and P the total pressure. The Thomsen model exploits the SRK equation of state to calculate the gas phase fugacity coefficients.

At this point, the existence of the vapor phase is checked by running bubble pressure calculations. In case of vapor-liquid phase coexistence, Henry's law is exploited for the calculation of the liquid phase fugacity, in which a Poynting factor has been used for pressure correction of Henry's law constant:

$$\bar{f}_i^L = H_{i,w}^*(T, P_w^s) \exp \frac{v_{i,w}^\infty \times (P - P_w^s)}{RT} \gamma_i^* x_i \tag{26}$$

where P is the pressure of the system, $H_{i,w}^*(T, P_w^s)$ is the Henry's constant of compound i in pure water on the mole fraction scale, P_w^s is the saturation pressure of water at the specified temperature, $v^{\text{inf}_{i,w}}$ is the partial volume of compound i at infinite dilution.

Equation for ammonia in water comes from Rumpf and Maurer [26]:

$$\ln H_{\text{NH}_3,w}^* \times M_w = 3.932 - \frac{1879.02K}{T} - \frac{355134.1K^2}{T^2} \tag{27}$$

where H is the Henry's law constant in MPa, M_w is the molar weight of water in kg/mol^{-1} and T the temperature in K. Equation for carbon dioxide in water comes also from Rumpf and Maurer [26]:

$$\ln H_{\text{CO}_2,w}^* \times M_w = 192.876 - \frac{9624.4K}{T} - 1.441 \times 10^{-2}\text{K}^{-1} \times T - 28.749 \times \ln T \tag{28}$$

where the same units as equation 27 are used.

2.2.3 Solid-liquid equilibria

As described before, the $j - th$ equilibrium process between an aqueous phase and a solid i is described by the following equation:

$$\ln K_j(T) = -\frac{\Delta G_j^0(T)}{RT} = \sum_i v_{i,j} \ln a_i \tag{29}$$

from which the equilibrium constant of the $j-th$ equilibrium process can be defined. The equilibrium constant can be rearranged in the following form:

$$K_j = \prod_i a_i^{\upsilon_{i,j}} \tag{30}$$

where $a_i = m_i \gamma_i$ is the activity coefficient for the ions and $a_{\mathrm{H_2O}} = x_{\mathrm{H_2O}} f_{\mathrm{H_2O}}$ is the activity coefficient for the water. The activity of the salt is in its standard state, therefore is equal to 1.

In this field, the equilibrium constant of a dissolution reaction of a salt in a solution is also called "ionic product", calculated at the conditions of the solution considered:

$$K_I(T, P, \bar{x}) = \prod_i a_i^{\upsilon_{i,j}} \tag{31}$$

The equilibrium constant calculated at saturation is called "solubility product" of the generic salt i, function of the temperature alone: $K_j(T)$. The temperature dependence of the solubility product can be computed using the van't Hoff equation.

To verify solids formation in the system, the "supersaturation index" (SI) can be exploited. It is defined as the ionic product of a generic dissolution reaction of a salt divided by its solubility product [27]:

$$SI = \frac{K_I(T, P, \bar{x})}{K_j(T)} \tag{32}$$

If:

- $SI = 1$, the solution is at saturation;
- $SI > 1$, the solution is supersaturated and precipitate is formed;
- $SI < 1$, the solution is unsaturated.

2.3 Thomsen model development

UNIQUAC volumes, UNIQUAC surface area and temperature dependent binary interaction energy parameters are required by the extended UNIQUAQ model, which need to be fitted on experimental data [25] [2] [20]. SRK equation is applied with standard mixing rules. No interaction parameters are taken into account. Further details can be found in the work of Thomsen et al. [23].

In general, the Thomsen model parameters for the CO_2 -NH_3 -H_2O system have been fitted based on more than 3700 data [20]. The model is able to describe the system in a range of ammonia concentrations up to 80 molal, temperatures between 0 and 150 °C, and pressures up to 10 MPa.

2.4 Ternary phase diagrams

Ternary phase diagrams are a very powerful tool to describe the CO_2 -NH_3 -H_2O system. An example of ternary phase diagram at 10 °C and 1.013 bar is shown in Figure 5.

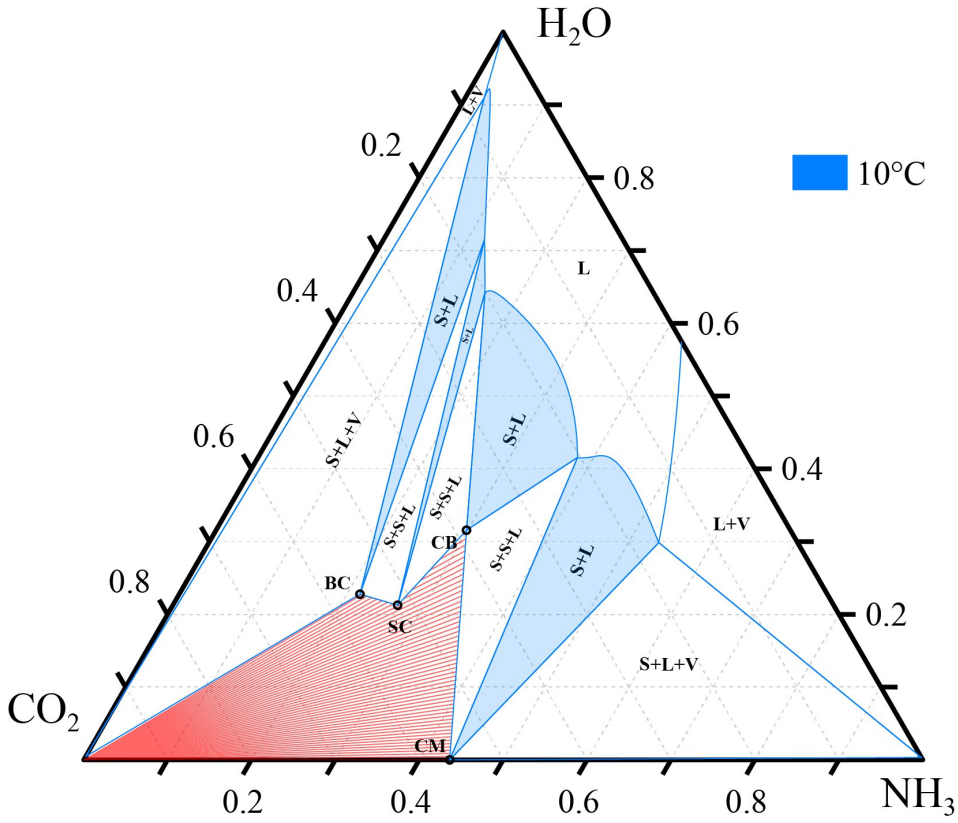

Figure 5: Isothermal ternary phase diagram at 10 °C and 1.013 bar, compositions in weight fractions

Due to different equilibria in the CO_2 -NH_3 -H_2O system, more than three species are present in a solution. What the ternary phase diagrams show is the overall mass fraction of CO_2 , NH_3 and H_2O , with respect of the real speciation. These mass fractions will be referred as apparent composition CO_2 , NH_3 and H_2O , respectively.

Each solid is indicated with a circle, which is invariant. Solid phase is indicated with S, liquid phase with L and vapor phase with V.

Each colored S-L region belong to one solid, in which the solid coexists with the liquid phase. The regions are bound by two straight lines and a curve, which is the “solubility isotherm”. The solubility isotherms separate the liquid phase region from the region in which solids formation occurs. If a generic system composition is chosen within one of the S-L regions and a tieline is drawn, which connects the system composition with the corresponding solid, the line crosses the solubility isotherm. The intersection point gives the composition of the mother liquor in equilibrium with the solid phase.

The solid-to-liquid ratio can be obtained by applying the lever arm rule.

S-L regions are separated by S-S-L regions, in which two solids coexist with the liquid phase. The composition of the mother liquor is the corner of the triangular region, intersection point of two solubility isotherms.

These are the relevant information useful for the purpose of this thesis. Further details about ternary phase diagrams have been reported by Sutter et al. [15].

The variation of the solubility as a function of the temperature is shown in Figure 6. The S-L regions are highlighted based on a temperature-dependent colorcode. As shown,

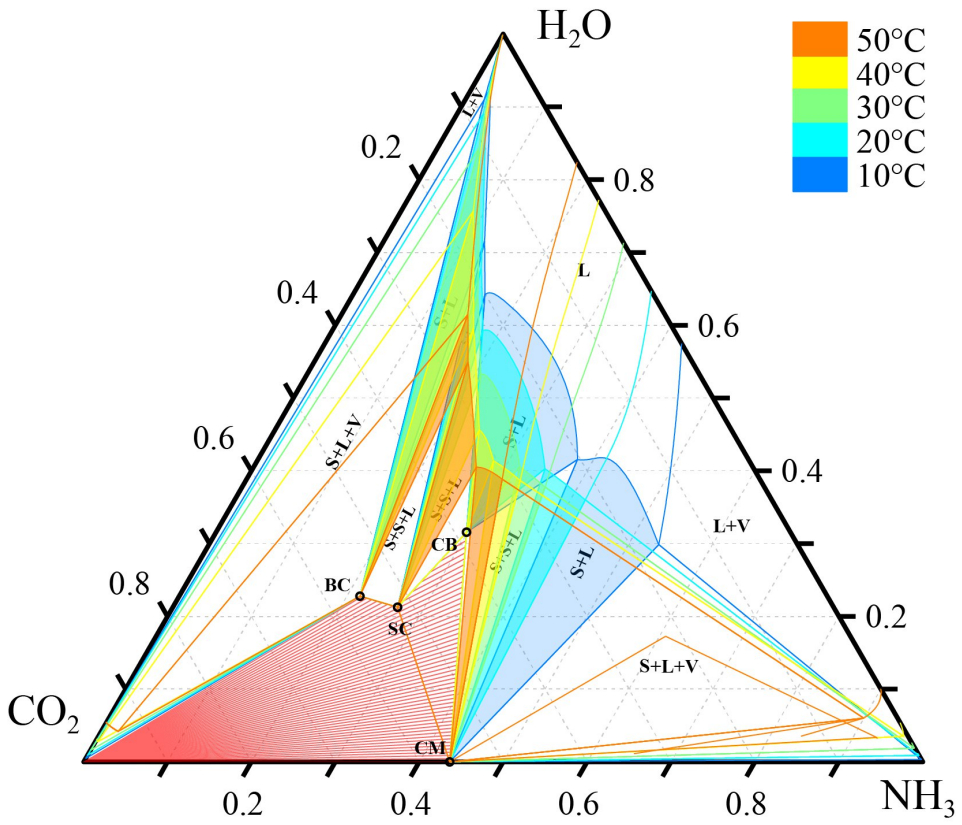

Figure 6: Isothermal ternary phase diagram at 1.013 bar and 10, 20, 30, 40 and 50 °C, compositions in weight fractions. Labels and phase boundaries are only shown for 10 °C for better visibility

the S-L regions become smaller as the temperature increases, except for the region related to the ammonium sesqui-carbonate, which expands.

Important information can be gathered about ammonium carbonate monohydrate. As shown in Figure 6, ammonium carbonate monohydrate does not appear at 50 °C. In fact, at 43 °C the S-L region related to ammonium carbonate monohydrate collapses into a line, whose endpoint falls at the intersection of the solubility curves of ammonium sesqui-carbonate and ammonium carbamate, which meet at 43 °C [15].

2.5 Aspen Plus® implementation

The standard model to describe the CO_2 -NH_3 -H_2O system in Aspen Plus is the electrolite-Non-Random Two-Liquid model (e-NRTL), which is implemented as default.

Recently, also the Extended UNIQUAC model has been implemented in Aspen Plus [24]. Darde et al. [24] has shown that the Extended UNIQUAC model describes better the CO_2 -NH_3 -H_2O system rather than the e-NRTL model.

The implementation of the model on Aspen Plus has been used for the aim of this thesis to simulate the CSF-CAP plant.

3 Process description

3.1 MEA-based processes

The absorption/stripping process configuration for CO_2 removal with MEA is shown in Figure 7.

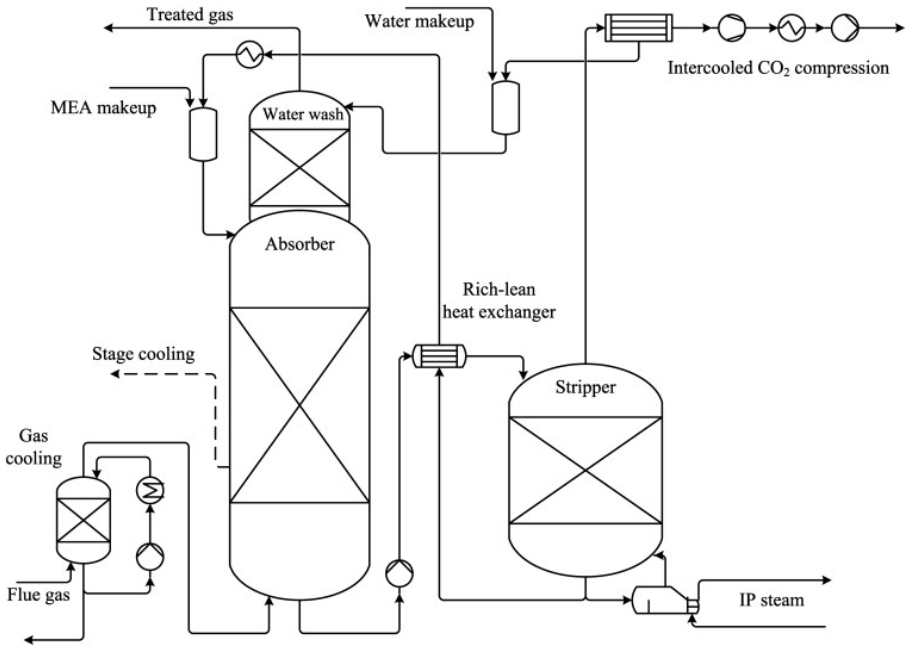

Figure 7: Flowsheet for CO_2 removal with MEA. Reprinted from Energy, 36 (2011), R. Strube, G. Pellegrini, G. Manfrida, The environmental impact of post-combustion CO_2 capture with MEA, with aqueous ammonia, and with an aqueous ammonia-ethanol mixture for a coal-fired power plant, Pages No. 3763-3770, Copyright 2011, with permission from Elsevier [17]

It mainly consists of two columns, an absorber and a desorber (stripper). The flue gas is cooled down and fed to the packed bed absorption tower, in which contact with the aqueous solution of MEA occurs, referred as CO_2 -lean stream. The absorption process triggers several reactions in the liquid phase, described in Section 2. At the exit of the absorber, the flue gas is washed to decrease MEA losses, and emitted to atmosphere. The liquid stream exiting the absorber, concentrated in CO_2 , which will be referred as CO_2 -rich stream, is heated up and sent to the desorber where CO_2 is stripped by steam produced at the bottom of the column.

At the top, the stream of H_2O and CO_2 is collected and sent to a condensation step to recover water and obtain a CO_2 stream with high purity, to be further sent to compression. The regenerated solvent, obtained in the desorber, is cooled down by means of the heat exchanged with the stream loaded in CO_2 coming from the absorber and is recirculated to

Table 1: Operating conditions and specifications of the MEA-based processes [28]

Unit operations specifications		
	Absorber	Desorber
T [°C]	40-60	100-120
P [atm]	1	1.5-2
Streams specifications		
	CO_2 -rich	CO_2 -lean
CO_2 -lean loading ($mol_{CO_2,absorbed}/mol_{MEA}$)	0.4-0.5	
MEA [% wt.]		30

the absorber.

Specifications of the MEA-based processes are reported in table 1.

3.2 Chilled Ammonia Process

Two different variants for CO_2 capture operation with ammonia-based solutions currently exist, based on the absorption temperature adopted [16]. The first process is the Chilled Ammonia Process (CAP) in which the absorption of the CO_2 occurs at low temperature (2-10°C), whereas the second process includes the absorption section which works at higher temperature (25-40°C).

3.2.1 Liquid - Chilled Ammonia Process

The standard CAP, which will be referred as liquid-CAP (L-CAP), avoids solids formation throughout the whole plant, in contrast to the new generation process that exploits solid formation, described in section 3.2.2. The L-CAP is quite similar to the absorption/stripping process based on amines. It was patented in 2008 from Gal [29] and, in the same year, Alstom® started the development of L-CAP for commercialization purposes. The scheme of the process is shown in Figure 8.

The process is mainly divided in 5 sections, as shown in Figure 8:

- Flue gas cooling section: since the absorption occurs at low temperature, from which the lettering "chilled", the hot flue gas which usually is at 100-110°C needs to be cooled down. This is accomplished by direct contact coolers (DCC). This also allows moisture, particulate and acidic or volatile species to condense into water, thus reducing their concentration in the gas phase [30];

- CO_2 capture section: in this section an absorption-desorption process allows the separation of the CO_2 and the regeneration of the solvent. After cooling, the flue gas enters the absorption unit. The flue gas is fed to the bottom of the absorber, where

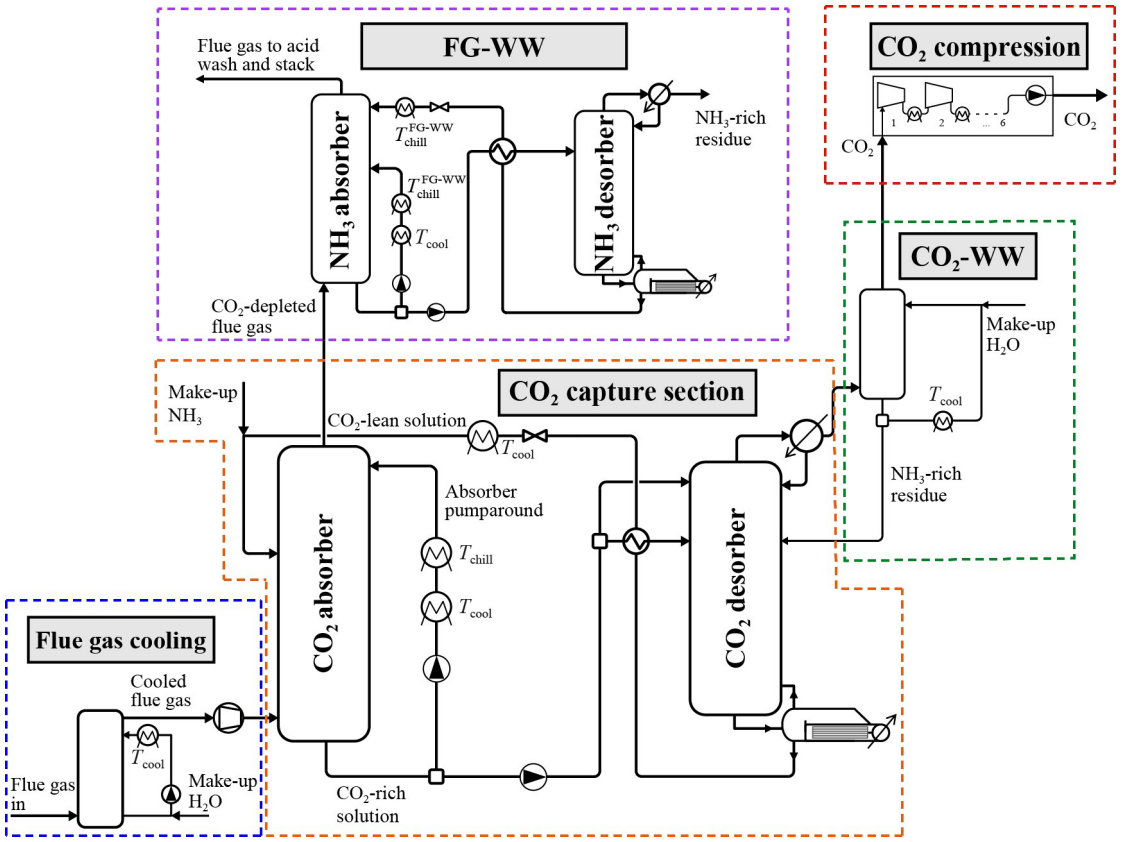

Figure 8: Flow scheme for the L-CAP process. Republished with permission of Faraday Discussions, from A low-energy chilled ammonia process exploiting controlled solid formation for post-combustion CO_2 capture, Daniel Sutter, Matteo Gazzani and Marco Mazzotti, 192, 2016; permission conveyed through Copyright Clearance Center, Inc. [1]

is put into contact with the absorptive solvent, which will be referred as CO_2 -lean stream, in a counter-current arrangement.

The liquid stream leaving from the bottom of the absorber is loaded in CO_2 and will be referred as CO_2 -rich stream. It passes through a heat exchanger, where it is cooled down. A part of it is recycled to the absorber, as also mentioned in the patent [29] and it will be referred as pumparound. The pumparound is fundamental to increase the CO_2 concentration of the CO_2 -rich stream and decrease the temperature in the absorber. The remaining part is pressurized, to reduce the vaporization of ammonia and water, and heated up by means of a heat exchanger with the regenerated solvent exiting the desorber, for heat recovery purposes, prior to be sent to the desorber. The desorption units operate at higher pressure than the absorption ones. The regenerated solvent collected at the bottom of the desorber is the CO_2 -lean stream, which is recirculated to the top of the absorber.

- CO_2 wash section: CO_2 is collected from the top of the desorber as a vapor mixture containing ammonia and water. The latter are further recovered with a cold wash in a dedicated column. Highly pure CO_2 is obtained.

- CO_2 compression section: the highly pure CO_2 stream is sent to compression and storage. CO_2 already exits the desorber at high pressure, with further reduction of the energy penalty in this section.

- Flue gas water wash section: after absorption, the processed flue gas exits the absorber. The ammonia content of the stream is usually very high and prior to the emission of the flue gas to the environment, the concentration of ammonia needs to be reduced. This occurs by means of washings with cold water and an acidic solution. Although the numerous good features, the most relevant disadvantage of the process is the high evaporation rate of NH_3 , which will be referred as "ammonia slip phenomena". This leads to additional washing units in the plant required for its abatement. Further studies demonstrate that auxiliary loads for chilling and ammonia emissions control (later explained) could affect the process to the point that it would not be competitive anymore, although its advantages [31] [32].

Some zones of the L-CAP are prone to solids formation, because the operating conditions are close to the saturation. In particular, the absorber, the pumparound stream, the condenser of the desorber in the CO_2 capture section, the liquid stream exiting the desorber in the flue gas water wash section and the column in the CO_2 water wash.

3.2.2 Controlled Solid Formation - Chilled Ammonia Process

Recent developments of the CAP process have led to a different configuration of the plants, shown in Figure 9. The CSF-CAP (Controlled Solid Formation-Chilled Ammonia Process) is an implementation of the process by Sutter et al. [1] in which a crystallization section for precipitation, separation and dissolution is integrated in the CO_2 capture section, with the aim to concentrate CO_2 in the stream exiting the absorber, decreasing the flow rates sent to the desorber and so the heat duty required at the reboiler.

This thesis focuses on the CSF-CAP process.

3.2.3 CAP and cement plants

Although CAP could readily be applied to the power industry, its application to cement plants is still under development compared to the CO_2 in power plant flue gases. The main problem stems from the difference of CO_2 concentration of the flue gas. Typical values of flue gas composition from power plants are about 10-14% vol. [12] [4], while CO_2 concentration in the flue gas from cement plants could exceed 16% vol.

The application of the CAP to cement plants is one of the most promising example of technology for CO_2 capture and storage. As stated before, ammonia solutions can hold higher CO_2 loading, a fundamental feature for cement plant application. Furthermore, the stability of ammonia solutions to impurities makes this process suitable for flue gas from

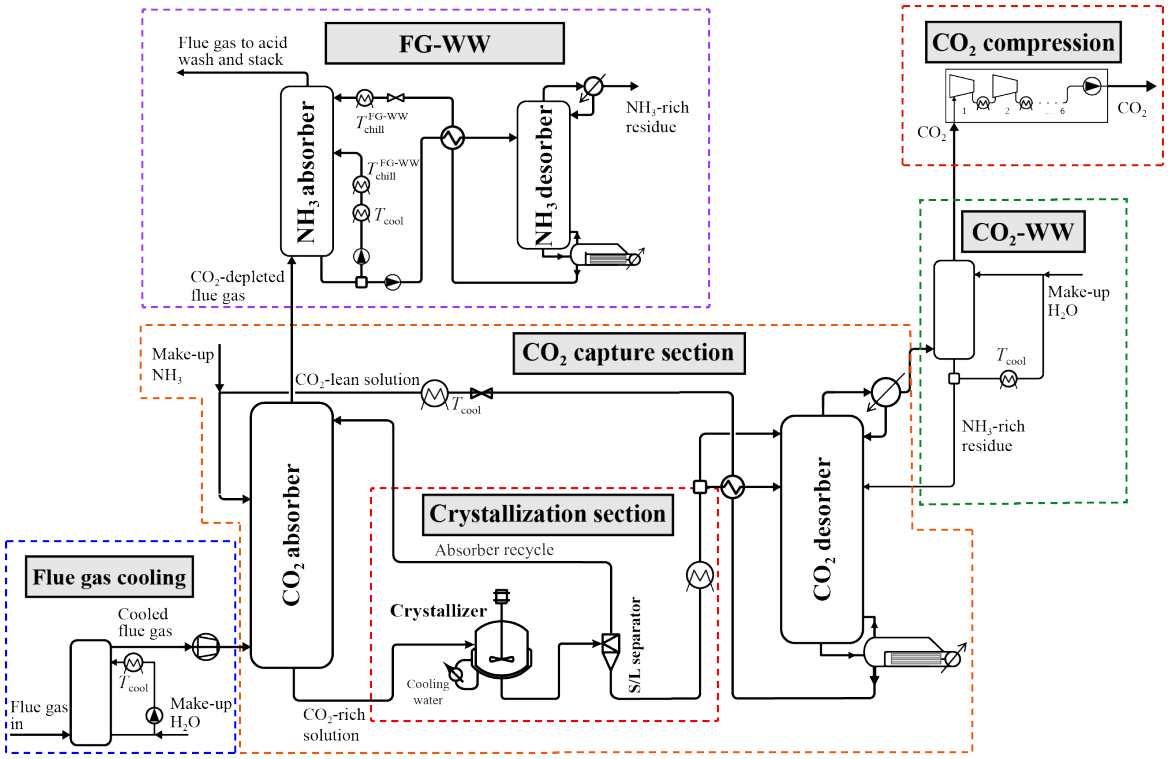

Figure 9: Flow scheme for the CSF-CAP process. Republished with permission of Faraday Discussions, from A low-energy chilled ammonia process exploiting controlled solid formation for post-combustion CO_2 capture, Daniel Sutter, Matteo Gazzani and Marco Mazzotti, 192, 2016; permission conveyed through Copyright Clearance Center, Inc. [1]

various industrial sources, such as cement plant. [1].

3.3 Aims of the Thesis

Based on the probable widespread utilization of CCS processes in the next future, even small developments of the process could lead to substantial improvements of CO_2 capture at global level.

As explained before, ammonium bicarbonate (NH_4HCO_3) formation in the crystallization section is actually the state of the art of the Controlled Solids Formation-Chilled Ammonia Process. This thesis aims to find a new set-point of the CSF-CAP, in which ammonium carbonate monohydrate ($(NH_4)_2CO_3 \cdot H_2O$) crystallization is exploited, with the aim to obtain a less energy-intensive process.

4 Theoretical potential of ammonium carbonate monohydrate

Ammonium bicarbonate (NH_4HCO_3) formation within the crystallization section is actually the state of the art of the CSF-CAP. This thesis aims to find a new set-point of the CSF-CAP, in which ammonium carbonate monohydrate ($(NH_4)_2CO_3 \cdot H_2O$) crystallization is exploited, with the aim to obtain a less energy-intensive process. The idea is supported by some theoretical potential.

4.1 CO_2 capture yield

The first theoretical potential can be explained by looking at the variation of the solubility curves of the relevant salts as a function of the temperature. Figure 10 shows the ternary phase diagram for the CO_2 -NH_3 -H_2O system at 10 and 30 °C, and 1 bar. The solubility of ammonium carbonate monohydrate at 30 and 10 °C is indicated in the diagram as A and A', respectively. Similarly, the points B and B' indicate the solubility of ammonium bicarbonate

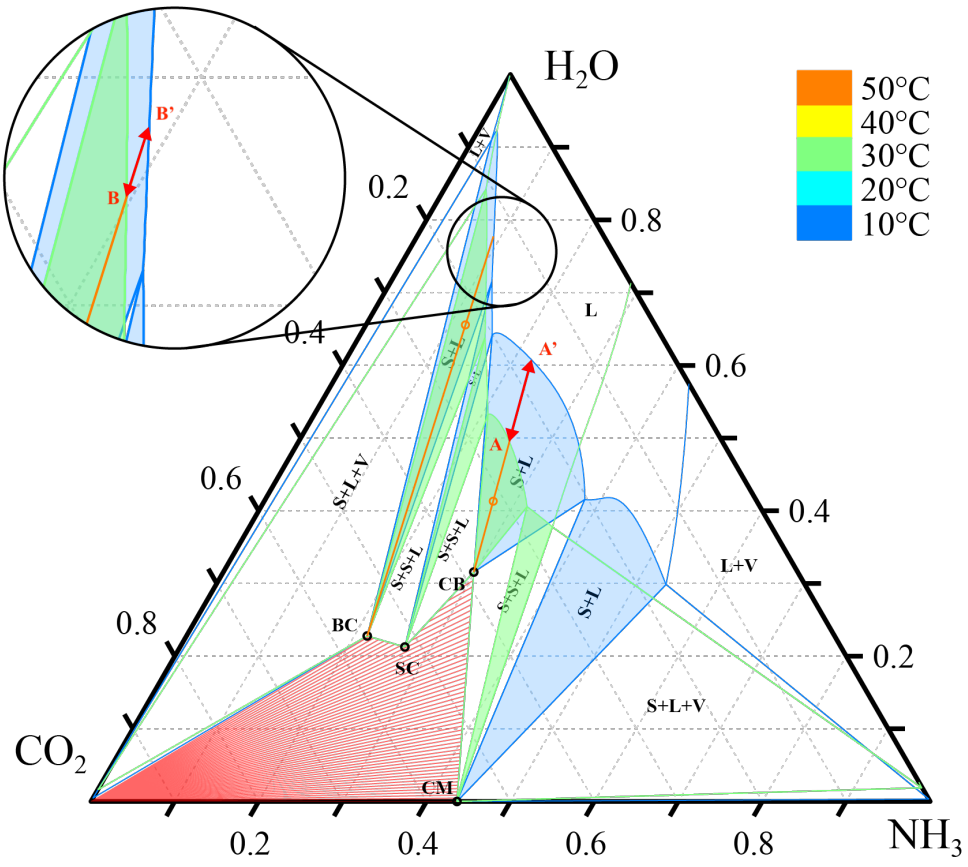

Figure 10: Isothermal ternary phase diagram for the CO_2 -NH_3 -H_2O system, at 10 and 30 °C and 1.013 bar

at 30 and 10 °C, respectively.

If crystallization occurs, two phases in equilibrium form in the mixture, a solid phase and a liquid phase. The latter is also called "mother liquor". The composition of the mother liquor in equilibrium with the solid phase is the intersection between the solubility curve at 10 °C and the tie line passing through the point of the initial mixture at 30 °C at saturation and its relative pure solid (point A' and B' in Figure 10).

As can be seen, applying the lever arm rule, for a given temperature difference, the yield of solid formation is always higher exploiting ammonium carbonate monohydrate crystallization compared to the case of ammonium bicarbonate.

Another way to visualize the above mentioned theoretical potential is in Figure 11, which shows the CO_2 molality in an aqueous-ammonia solution as a function of the temperature, for different NH_3 concentrations in the mixture. The Thomsen model has been exploited for the calculation of the solubilities of the ammonium carbonate monohydrate and the ammonium bicarbonate. In particular, solubility data of both solids have been collected at different temperatures and ammonia concentrations in the ternary CO_2 -NH_3 -H_2O system. The data

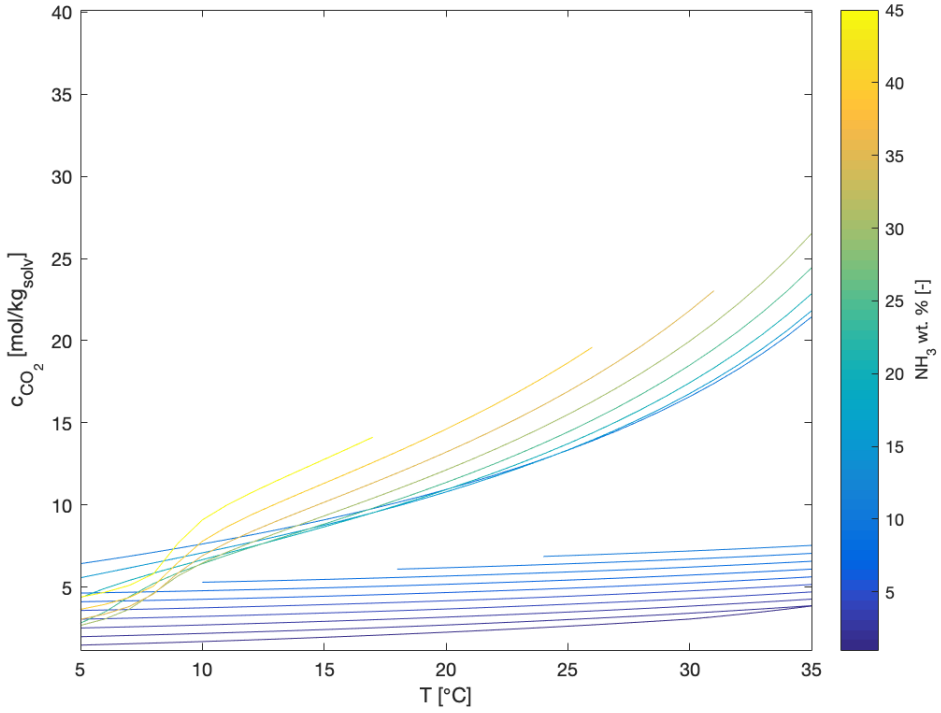

Figure 11: CO_2 concentration in aqueous-ammonia solution as a function of the temperature of the system, for different NH_3 concentration in mixture

in the bottom part of the plot refers to a lower ammonia concentration, which corresponds to the case in which ammonium bicarbonate is crystallized. Whereas, the data in the upper part refer to higher ammonia concentration, which could lead to ammonium carbonate monohydrate formation. As shown, for a given temperature difference, the change in concentration

of CO_2 in solution is more accentuated when a higher ammonia content is employed. This means that, when crystallization is exploited, for a given temperature difference, a higher CO_2 difference is obtained in the mother liquor, thus a higher amount of CO_2 is transferred to the solid phase, if a higher ammonia concentration is exploited in the solvent.

The crystallization yield, in terms of equivalent CO_2 , can be defined as:

$$Y = \frac{m_{CO_2}\left(T_{\text{mix}}\right) - m_{CO_2}\left(T_{\text{crystallization}}\right)}{m_{CO_2}\left(T_{\text{mix}}\right)} \times 100 \tag{33}$$

where $m_{CO_2}\left(T_{\text{i}}\right)$ is the molality of the apparent CO_2 in the liquid phase at a certain temperature, T_{mix} is the temperature of the mixture leaving the absorber that you want to crystallize, $T_{\text{crystallization}}$ is the temperature at which crystallization occurs. In the previous example, T_{mix} is 30 °C and $T_{\text{crystallization}}$ is 10 °C.

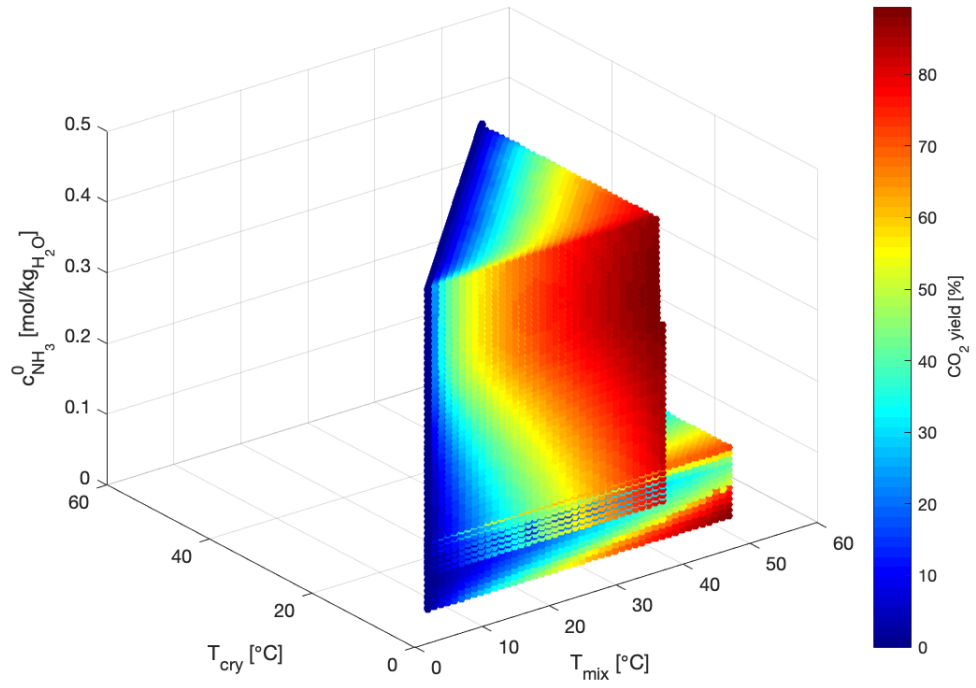

Figure 12: Coloured points showing the yield percent of CO_2 obtained in a crystallization process for a given mixture temperature, crystallization temperature and ammonia concentration in solution.

Based on this definition, the CO_2 capture yield has been calculated as a function of the mixture temperature T_{mix}, crystallization temperature T_{cry}, and concentration of ammonia $\omega^0_{NH_3}$ in the aqueous-ammonia solution employed. The mixture temperature and the crystallization temperature define the temperature difference used in the crystallization section.

Figure 12 shows the CO_2 capture yield percent obtained for a given temperature difference in a crystallization process and for a given ammonia concentration in aqueous-ammonia

solution. As shown, in the region at higher ammonia concentration, the same CO_2 capture yield can be obtained exploiting lower temperature differences, compared with the case at lower ammonia concentration.

4.2 CO_2 absorption rate

The second theoretical potential can be explained by looking at the plot in Figure 13. It shows the CO_2 partial pressure in aqueous solutions at different fixed amounts of NH_3 and various amounts of CO_2 , at constant temperature.

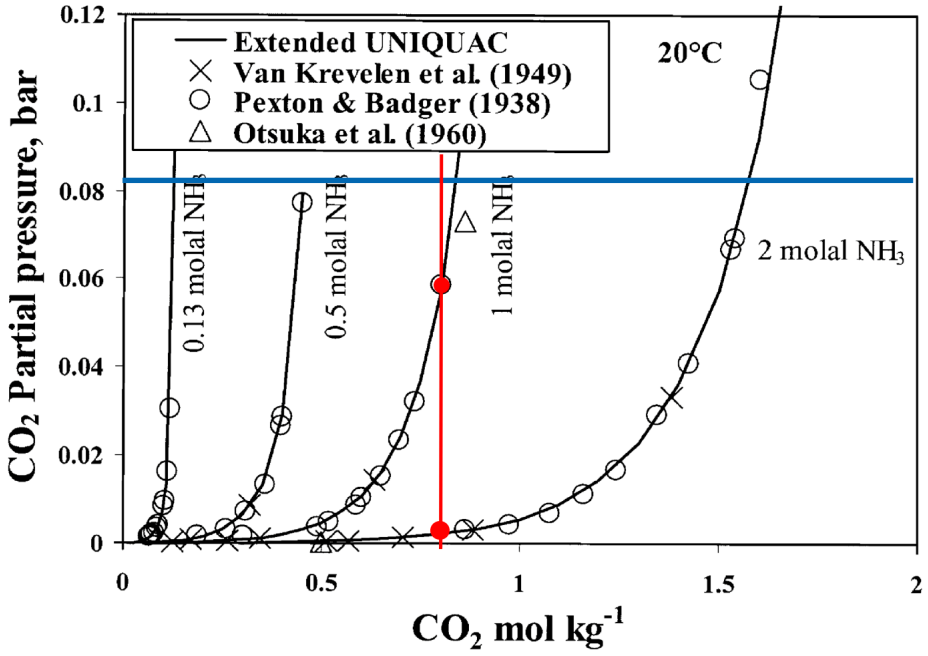

Figure 13: The partial pressure of carbon dioxide in aqueous solutions of fixed amounts of ammonia and various amounts of carbon dioxide. Comparison of experimental and calculated values at 20 °C. Reprinted from Chemical Engineering Science, Vol. 54 (1999), Kaj Thomsen, Peter Rasmussen, Modeling of vapor—liquid—solid equilibrium in gas—aqueous electrolyte systems, Pages No. 1787—1802, Copyright 1999, with permission from Elsevier [2]

Data showed does not refer to the real values, but they merely serve explanation purposes. The flue gas flowing at each section of the absorption column is at constant CO_2 partial pressure. In Figure 13 it is indicated by a horizontal blue line. Concerning the aqueous phase in the column, for a given CO_2 concentration in solution, the CO_2 partial pressure decreases as the NH_3 content in solution increases. This means that the CO_2 solubility in aqueous ammonia solutions increases as the ammonia concentration increases. The red line in Figure 13 indicates an aqueous solution at constant CO_2 concentration. The difference in CO_2 partial pressure between the flue gas and the gas in equilibrium with the aqueous

phase, at each section of the column, is the driving force for mass transfer in the absorption column. For a given absorbant solvent with a certain NH_3 concentration sent to the column, the driving force will be different. In particular, considering an aqueous ammonia solution at constant CO_2 concentration, for a given ammonia content there will be a certain driving force ($\Delta p_{CO_2,1}$ in Figure 13). If the ammonia concentration of the solution increases, the CO_2 partial pressure will be lower, so the driving force for CO_2 transfer from the flue gas to the absorbant will be greater ($\Delta p_{CO_2,2}$ in Figure 13).

In conclusion, this is an advantage when ammonium carbonate monohydrate is exploited in CSF-CAP, because higher concentrations of ammonia are used compared to the ammonium bicarbonate-exploiting CFS-CAP. This translates to faster absorption rates and therefore smaller equipment are required to perform the absorption operation.

5 Process analysis, optimization, and performance evaluation

The optimization of the CO_2 -capture process described in this thesis encountered a series of challenges [sutter2]:

- The complexity of the thermodynamic model describing the systems;
- A relatively complex flowscheme consisting of several different units controlled by a large number of decision variables;
- Different types of energy duties (*e.g.* heating, cooling, chilling, and electric);
- A multi-objective optimization is required for the evaluation of the process performance, often leading to conflicting objectives (*e.g.* capital costs and operative costs).

The literature lack of works focused on a rigorous optimization of the CAP. Some research proposed a single-variable sensitivity analysis, but their efficacy is strongly affected by the inter-dependency of the operating variables in the system [1].

In the work of Sutter et al. [1], the optimization is based on a multiple-variable sensitivity analysis, which can overcome the problems due to inter-dependencies. This kind of analysis is referred as heuristic optimization, since it screens the design space with a brute force approach.

The optimization algorithm proposed in this work is schematically shown in Figure 14.

Matlab launches simulations in Aspen Plus and acts as the data manager. Each of the four coloured section is analyzed alone. Input variables for the analyses are the parameters indicated with the same colour as the section in which they are used. Dashed lines indicate the data flux among blocks. The algorithm is divided into 5 main parts:

1. At the beginning, a set of feasible operating conditions for the new set-point of the plant has been found.
2. An optimization which concerns three different sections of the plant (flue-gas cooling section, absorption section and regeneration section) is performed sequentially, till convergence is reached. The set of feasible operating conditions found in the previous section is used in this step as an initial guess. In contrast to previous work present in literature, a rigorous optimization has been then performed. The algorithm uses the *patternsearch* function implemented in the optimization toolbox of Matlab [33] and it is interfaced with Aspen Plus. Furthermore, a preliminary multi-variable sensitivity analysis is performed on the regeneration section, in order to reduced the

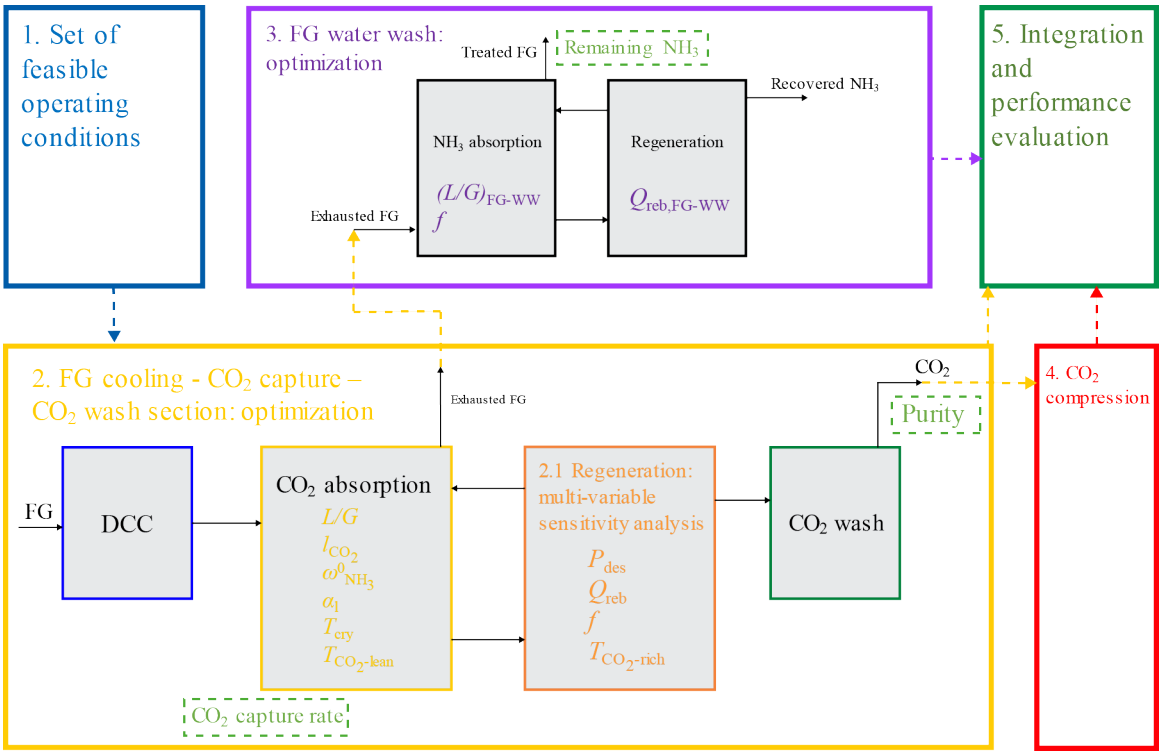

Figure 14: Scheme of the algorithm used for the optimization of the CSF-CAP plant

number of operating variables employed in the overall optimization, thus reducing the computational power and the time required for the simulations, as well as the size of the design space.

3. The results obtained for the exhaust flue gas stream leaving the absorber are the inputs of a rigorous optimization of the flue-gas water wash section, performed in Aspen Plus.

4. The information collected for the purified CO_2 -stream leaving the CO_2 -wash section are used for the compression section duty calculation.

5. The results from block 2, 3 and 4 in Figure 14 are collected for the performance evaluation of the overall plant.

5.1 Range of feasible operating conditions

The CSF-CAP flowscheme used for the simulations is the one presented in Section 3.2.2.

Due to the complexity of the plant, each section has been previously analyzed alone. The aim was to find a set of feasible operating conditions which allows the proper operation of the plant, with ammonium carbonate monohydrate formation in the crystallization section, and to understand how the plant behaves under different operating conditions. The study has allowed to identify the performance of the different unit operations and the criticalities when the process variables have been modified.

The work has not only shown that different operating conditions are required for the new set-point of the plant, but also a resizing of some unit operation is needed. Nevertheless, a goal has been to keep the flowscheme of the plant as similar as possible to the one of the CSF-CAP, for comparison purposes.

5.1.1 Absorption section

The CO_2 absorber, coupled with the crystallizer and the solid-liquid separator has been analyzed. This has been chosen as the starting point of the analysis since it represents the most critical part of the plant. Figure 15 shows the flowscheme used in the analysis. Further

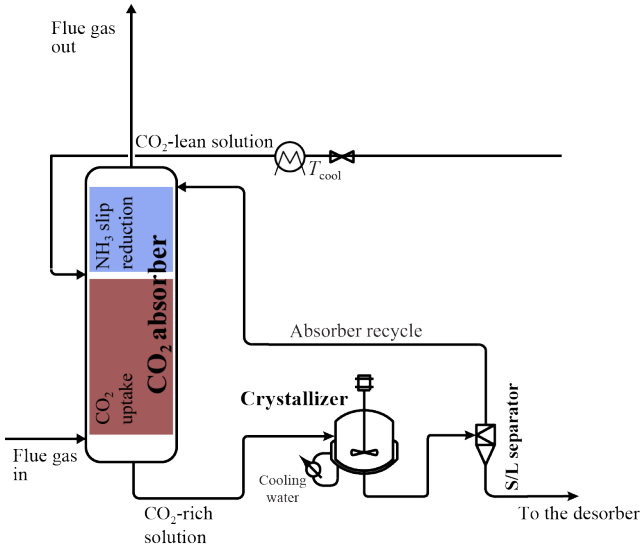

Figure 15: Detailed flowscheme of the CO_2 absorber, the crystallizer and the solid-liquid separator from the CSF-CAP

details are:

- The absorber is mainly composed by two sections, separated where the CO_2 -lean stream enters the column. The top part of the column is the so called "NH_3 slip reduction section", in which the treated flue gas, which has been enriched in ammonia, flows counter-currently with respect to the pumparound stream entering the column at the top. This allows for a reduction of the ammonia content in the flue gas. Ammonia slip is usually given in part-per-million (ppm_v) with respect to the treated flue gas stream. The bottom of the column is the "CO_2 uptake section". The CO_2 -lean stream, which mixes with the liquid coming from the top, absorbs the CO_2 from the flue gas, fed to the bottom part of the column.

- The crystallizer is treated as an equilibrium stage. The solid product collected is a solid phase in equilibrium with its mother liquor.

- The solid-liquid separator is an hydrocyclone, which allows for solid-liquid separation of the solids, accordingly to the splitting factor chosen.

For the analysis, several process variables have been taken into account:

- Liquid-to-gas flow rate ratio (L/G): is the ratio between the mass flow rate of the CO_2 -lean stream and the mass flow rate of the flue gas to be treated.

- CO_2 loading (l_{CO_2}): defined as the apparent molar flow rate of CO_2 in the lean stream, divided by the apparent molar flow rate of NH_3 in the same stream:

$$l_{CO_2} = \frac{\dot{n}_{CO_2}^{CO_2\text{ -lean}}}{\dot{n}_{NH_3}^{CO_2\text{ -lean}}} \tag{34}$$

- Mass fraction of ammonia in the CO_2 -lean stream on a carbon free basis ($\omega_{NH_3}^0$) defined as the ratio between the mass flow rate of NH_3 in the lean stream and the sum of the mass flow rate of NH_3 and H_2O in the same stream:

$$\omega_{NH_3}^0 = \frac{\dot{m}_{NH_3}^{CO_2\text{ -lean}}}{\dot{m}_{NH_3}^{CO_2\text{ -lean}} + \dot{m}_{H_2O}^{CO_2\text{ -lean}}} \tag{35}$$

- Hydrocyclone splitting factor (α_l): defined as the mass flow rate of the mother liquor in the slurry phase sent to the desorber, divided by the mass flow rate of mother liquor in the stream entering the hydrocyclone:

$$\alpha_l = \frac{\dot{m}_{\text{mother liquor}}^{\text{slurry out}}}{\dot{m}_{\text{mother liquor}}^{\text{in}}} \tag{36}$$

- Crystallization temperature (T_{cry}), defined as the temperature exploited in the crystallization section.

- Temperature of the CO_2 -lean stream ($T_{CO_2\text{ -lean}}$).

The l_{CO_2} and the $\omega_{NH_3}^0$ determine the composition of the CO_2 -lean stream.

To be in line with the ammonium bicarbonate-crystallizing CSF-CAP, CO_2 capture rate greater or equal than 90% wt. has been set as a process constraint. The CO_2 capture rate is defined as:

$$\psi_{CO_2} = \frac{\dot{m}_{CO_2}^{\text{in}} - \dot{m}_{CO_2}^{\text{out}}}{\dot{m}_{CO_2}^{\text{in}}} \times 100 \tag{37}$$

After the simulation converges, a key output parameter has been checked, which can give a feedback on the proper functionality of the unit operations. In particular, the ammonia slip has been checked, which is a criticality in this system and it cannot be easily controlled.

Figure 16 shows the equilibrium partial pressures of ammonia $p_{NH_3}^{\text{eq}}$ at 1 bar and 10 °C which is approximately the temperature of the absorber top stage. The gray area represents

the region proposed in the literature where the compositions in the CO_2 -absorber should lie. The left and right borders are the minimum and maximum CO_2 -loading (0.25-0.67), respectively, suggested in the patent of Gal [29]. The upper and lower borders are suggested by Yu et al. [34] and Darde et al. [16], respectively. They correspond to the minimum and maximum ammonia mass fraction on a carbon free basis proposed. Formation of ammonium

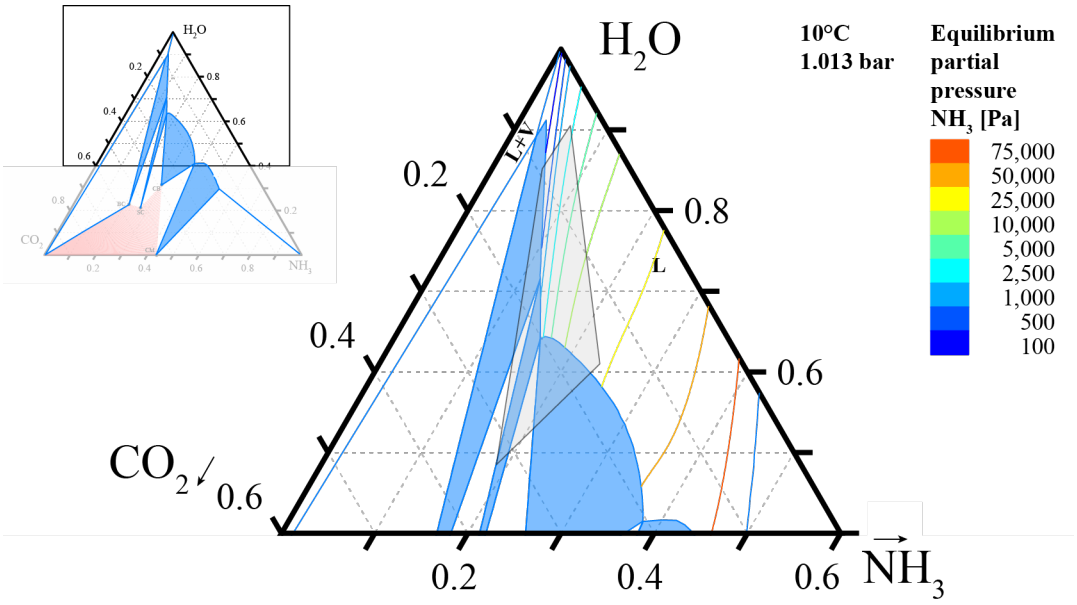

Figure 16: Equilibrium partial pressure of NH_3 at 1.013 bar and 10 °C in the ternary phase diagram at the same conditions. The gray area represents the expected compositions range in the CO_2 -absorber from literature data [29] [34] [16]

carbonate monohydrate is achieved if the operating range of the absorber is in the lower part of the gray area, hence at higher ammonia concentration. Due to higher ammonia partial pressure, so higher ammonia slip is obtained in the ammonium carbonate monohydrate-crystallizing CSF-CAP when compared to the ammonium bicarbonate-crystallizing CSF-CAP. Moreover, the higher the values of ammonia slip, the higher the energy required for its abatement in the flue gas water wash section. Therefore, the ammonia slip needs to be kept as low as possible to decrease the energy duty of the plant.

The interplay between the different operating variables chosen is important to understand how the NH_3 slip can be controlled. In particular, NH_3 and CO_2 concentrations and temperatures in the absorber have to be analyzed as shown in the work of Sutter et al. [1]

The temperature, as well as the CO_2 -loading, strongly affects the ammonia partial pressure. The pumparound is the parameter that mostly influence the ammonia slip phenomenon. The low temperature and the acidic conditions (high CO_2 concentration) of the stream lead to a decrease of the ammonia equilibrium partial pressure [15]. Additionally, if other parameters lead to a decrease of the temperature and the pH, this would positively influence the ammonia slip phenomenon. Clearly, temperature and pH can be lowered down to a certain

extent, to still enable the proper functioning of the CO_2 absorption process.

Furthermore, the ammonia slip itself could also affect the temperature profile, in particular if the ammonia slip is too high, since the evaporation of ammonia is an endothermic process. So, a strong interplay is present between ammonia slip and the temperatures in the absorber.

A typical good temperature profile of the absorber is shown in Figure 17. Since the absorption process is exothermic, the temperatures are expected to increase from the top to the bottom. The temperature profile is not completely linear, but two jumps are present, relative to the feed of the CO_2 -lean stream and the flue gas.

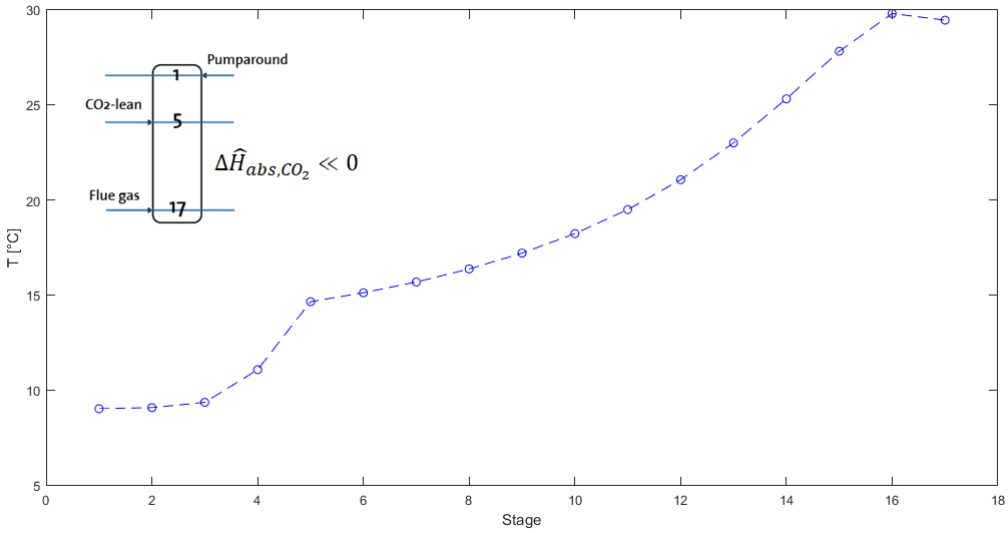

Figure 17: Typical temperature profile of the CO_2 absorber operated in a proper mode

The ternary phase diagram in Figure 18 shows the liquid composition on each stage along the CO_2 absorber, as well as the composition of the liquid feed sent to the absorber and the compositions of the streams obtained after the crystallization and the separation. Each point is coloured according to a temperature colorcode. The pumparound is fed at the top of the absorber. The pumparound composition lies very close to the solubility curve at the crystallization temperature. Thus, the pumparound is heated up of 1 °C to avoid solids formation. From the pumparound, a number of points extends, pointing towards the NH_3 vertex. This segment is representative of the NH_3 slip reduction section. The low temperature of the pumparound and its high loading in CO_2 allow the uptake of NH_3 in the liquid phase.
The composition of the CO_2 -lean stream is chosen for each simulation. At the stage where the CO_2 -lean stream is fed, the composition of the liquid phase lies on the tie line between the last stage of the NH_3 slip reduction section and the CO_2 -lean stream, from which the points representing the CO_2 uptake section depart, pointing towards the CO_2 vertex. The CO_2 -rich stream is sent to the solid handling section at the end of which the hydrocyclone

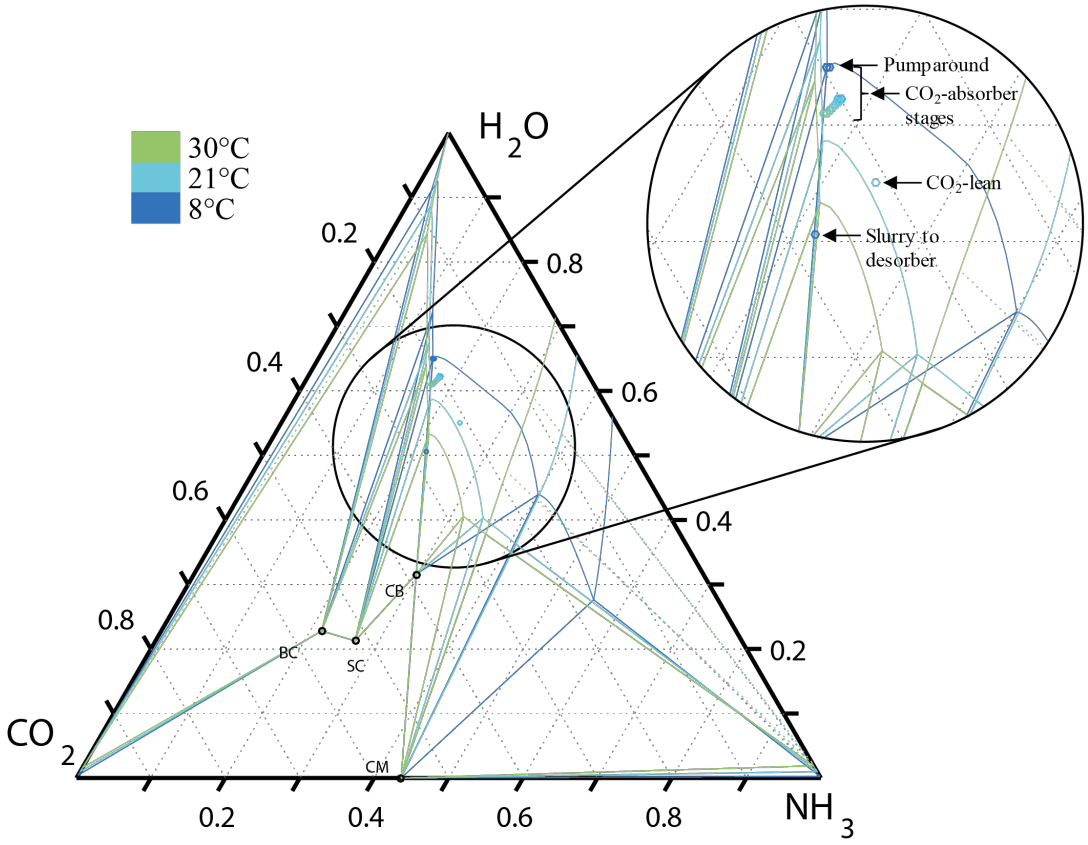

Figure 18: Ternary phase diagram at 8, 21 and 30 °C and 1.013 bar showing the liquid composition of the CO_2 -absorber stages and its related feed stream. Both isotherms and concentration points follow the same colorcode shown.

separates a slurry phase from the mother liquor. The composition of the slurry phase lies on the tie line between the CB point and the CO_2 -rich stream composition. The position of the point depends on the hydrocyclone splitting factor chosen. The lower the α_l, the closer to the CB point the slurry phase is. Whereas, the composition of the pumparound, which corresponds to the separated mother liquor, is constant. The composition of the pumparound on the ternary phase diagram is at the intersection of the tie line indicated before with the solubility curve at the crystallization temperature. The lever arm rule can be exploited to calculate the amount of solid formed in the crystallizer.

With the aim to increase the yield of solid formation and explore a wider region of the ternary phase diagram, different simulations have been performed, which are shown Figure 19. Based on the preliminary knowledge on the absorber, different decisions have been made to run the simulations. The loading of the CO_2 -lean stream has been chosen as the maximum possible, since it impacts positively the NH_3 slip phenomena. Therefore, the CO_2 -lean stream lies close to the solubility curve at its temperature. For this purpose, different operating conditions have been used. In particular, higher ammonia concentration in the CO_2 -lean stream. The different cases shown in Figure 19 have been obtained, where

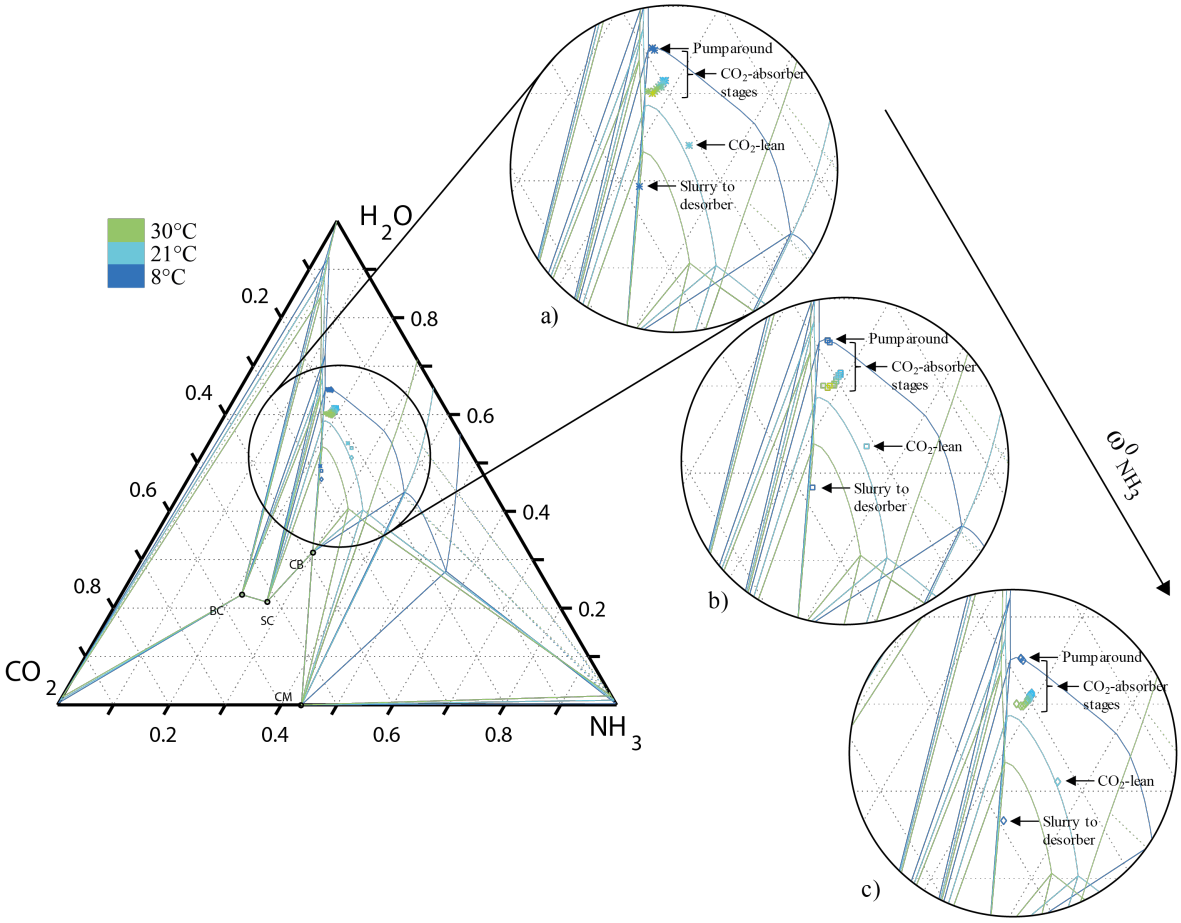

Figure 19: Ternary phase diagram at 8, 21 and 30 °C and 1.013 bar showing the liquid composition of the CO_2 -absorber stages and its related feed stream. Both isotherms and concentration points follow the same colorcode shown. The magnifications refers to three different processes with three CO_2 -lean stream used. Ammonia concentration in the CO_2 -lean stream increases from a) to c).

the concentration profile of the CO_2 uptake section has been moved down in the plot due to higher ammonia concentrations. As expected, higher ammonia slip has been achieved with increasing ammonia concentration.

If the ammonia concentration is still increased, as in the case shown in Figure 20, the concentration profile of the CO_2 -capture section starts to bend towards the direction of a decrease of ammonia content in the liquid, which indicates ammonia evaporation from the solution. In fact, the bottom part of concentration profile is directed in the reversed direction of the NH_3 vertex, which means that NH_3 is being lost.

Finally, a different simulation at higher ammonia composition of the CO_2 -lean stream has been performed, shown in Figure 21. In this case, the ammonia slip is so high that the concentration profile is not only bent, but it has a complete different direction with respect to the CO_2 vertex. Therefore, in the CO_2 uptake section not only CO_2 capture occurs, but

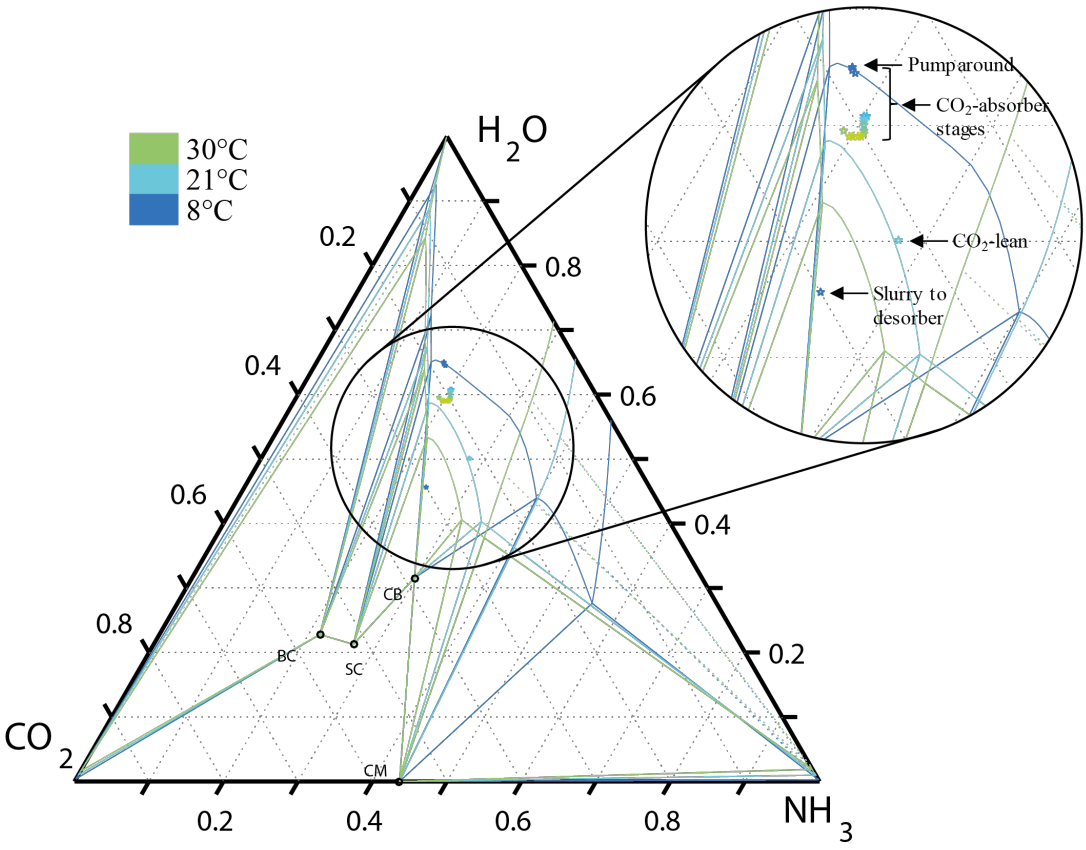

Figure 20: Ternary phase diagram at 8, 21 and 30 °C and 1.013 bar showing the liquid composition of the CO_2 -absorber stages and its related feed stream. The CO_2 -absorber concentration profile is bent due to ammonia slip phenomena. Both isotherms and concentration points follow the same colorcode shown.

other phenomena like ammonia and water evaporation or condensation are occurring.

In conclusion, a higher NH_3 concentration and ammonium carbonate monohydrate formation can be exploited in a CO_2 capture process with similar CO_2 capture rates. Table 2 resumes the NH_3 slip ranges obtained for the different CAP. The maximum ammonia slip for the CB-CSF-CAP has been set to 45000 ppm_v, because a feasible control of the absorber is not possible when this critical value is reached.

A set of feasible operating conditions for the CO_2 absorber, crystallizer and hydrocyclone has been identified.

The four simulations shown before in Figure 18 and in Figure 19 fulfil all specifications and constraints in terms of ammonia slip and CO_2 capture rate, and guarantee stable convergence. This lays the foundations to the feasibility of operating the CSF-CAP at higher ammonia concentrations. Although this preliminary analysis has shown that a proper control of the absorber is not possible under certain conditions, the optimization presented in Section 5.2.2 explores a wider range of operating conditions, whose combination leads to

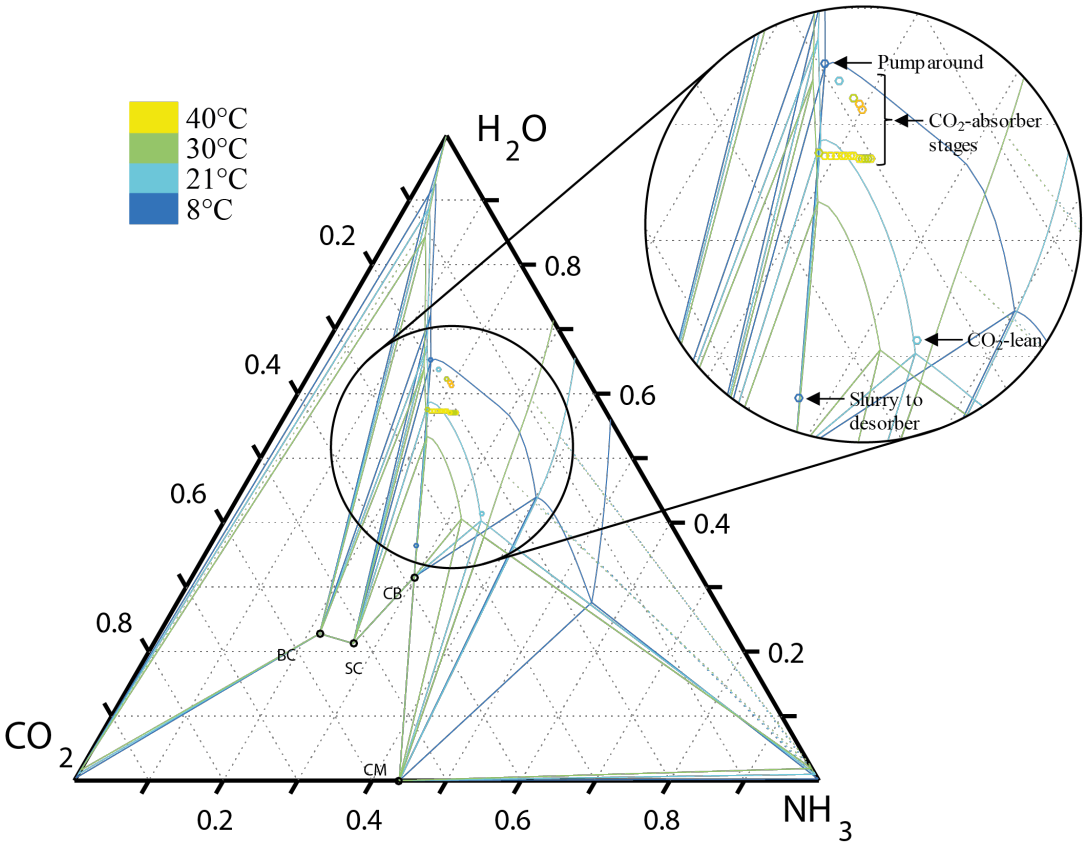

Figure 21: Ternary phase diagram at 8, 21 and 30 °C and 1.013 bar showing the liquid composition of the CO_2 -absorber stages and its related feed stream. The concentration profile is not pointing towards the CO_2 vertex. Other phenomena in the CO_2 -absorber are not negligible compared with the CO_2 absorption. Both isotherms and concentration points follow the same colorcode shown.

find other feasible operating points.

The operating conditions for the simulation shown in Figure 18 and the three simulations shown in Figure 19 are resumed in Table 3.

5.1.2 Dissolution and regeneration section

The solvent regeneration section, which includes the dissolution section, the heat integration, and the CO_2 desorber has been analyzed. The flowscheme of this section is shown in Figure 22. Further details are:

- The dissolution section in Figure 22 is indicated as an heat exchanger for simplicity, but in reality the dissolution of the solids is made in a dedicated unit. In the work of Sutter et al. [1], sufficient residence time, good mixing, and efficient heat transfer are listed as requirements for this unit. The requirements match the ones of the crystallizer. Furthermore, it also states that it is energetically more efficient to oper-

Table 2: NH_3 slip ranges in the exhausted flue-gas leaving the absorber for different CAP [1]

	min [ppm_v]	max [ppm_v]
L-CAP	6300	11900
BC-CSF-CAP	1200	3500
CB-CSF-CAP	18300	45000*

*maximum value set for screening results

Table 3: Feasible operating conditions and specifications for the absorption section

	Case 1	Case 2	Case 3	Case 4
L/G	3.1	3.0	2.9	2.9
$\omega^0_{NH_3}$	0.30	0.32	0.33	0.35
l_{CO_2}	0.339	0.325	0.313	0.315
T_{cry} [°C]	8	8	8	8
α_l	0.18	0.2	0.18	0.15
T_{CO_2-lean} [°C]	21.2	21.2	21.2	21.2

ate the dissolution section at higher pressure, because either problems due to vapor phase formation are reduced, and the required work for pumping is reduced at lower temperature.

- The CO_2 -rich stream coming from the dissolution section is split. The first part is sent to heat recovery with the regenerated CO_2 -lean stream, before entering the desorber at around two thirds of the stages (counting from the top). The second part is directly fed to the top of the desorber. In comparison with the ammonium bicarbonate-crystallizing CSF-CAP, the condenser at the top of the desorber has been eliminated. Condensation at the top can be still achieved with a suitable extent with the split of the cold CO_2 -rich stream.Therefore, issues related to solids formation are completely avoided. Furthermore, as shown later in this work, the split of the CO_2 -rich stream positively impact the energy duty when compared with the flowscheme that includes the condenser.

- The reboiler temperature has always been kept lower than 150 °C, due to severe corrosion problems occurring above that temperature.

The composition of the liquid phase and the slurry phase after the hydrocyclone are shown only for “Case 1” from the previous analysis in Figure 23. The liquid phase composition and the slurry phase composition exiting the hydrocyclone lie on the tie line passing the hydrocyclone feed composition and the stationary point of the ammonium carbonate monohydrate. The solubility curve at 50 °C is plotted to show that the slurry phase coming from the hydrocyclone becomes liquid at that temperature. 50 °C has been chosen as the temperature for the dissolution section. Basically, the complete dissolution temperature is

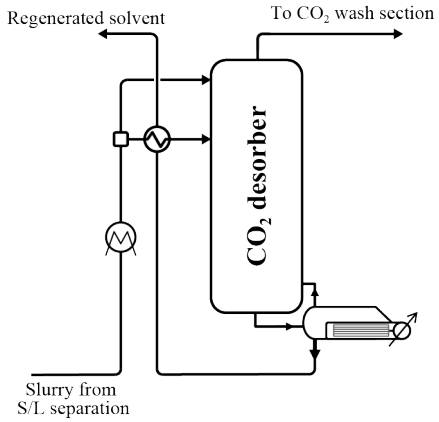

Figure 22: Detailed flowscheme of the dissolution section and solvent regeneration desorber with heat integration

slightly lower (about 45 °C), but a conservative temperature has been chosen to avoid solids presence. This stream is the so-called CO_2 -rich stream, which is sent to the desorber.

Figure 24 shows the liquid composition along the desorber in the ternary phase diagram. In this case, the simulation has been done with a pressure in the desorber of 25 bar. The CO_2 -rich stream sent to the desorber is the one obtained in "Case 1" from the previous analysis. The pressure of the desorber has been set to 25 bar, while in the ammonium bicarbonate-crystallizing CSF-CAP the pressure was 10 bar. This allows to reduce the ammonia partial pressure in the gas phase, so its content in the gas sent to the CO_2 -wash section. Further details are given in Section 5.2.1.

The reboiler duty of the desorber is chosen based on the CO_2 composition of the regenerated CO_2 -lean stream required. A make-up of NH_3 and H_2O is required by the regenerated CO_2 -lean stream, in order to account for losses of aqueous-ammonia in the exhausted flue gas and in the purified CO_2 stream. CO_2 can not be added with a make-up stream, therefore :

- If the reboiler duty is lower than needed, the CO_2 content in the lean stream will be higher than required;
- If the reboiler duty is higher than needed, the CO_2 content in the lean stream will be lower than required.

5.1.3 CO_2 wash section

Although a very high purity of CO_2 (about 99% wt.) in the gas stream recovered at the top of the desorber is obtained, the ammonia content is still relatively high, so a further purification step is required. The goal is achieved in a water wash section, where the gas stream is put in contact with a cold water stream. The liquid stream leaving the bottom of the wash column is split. The majority is recycled to the wash column, to decrease the amount of fresh water

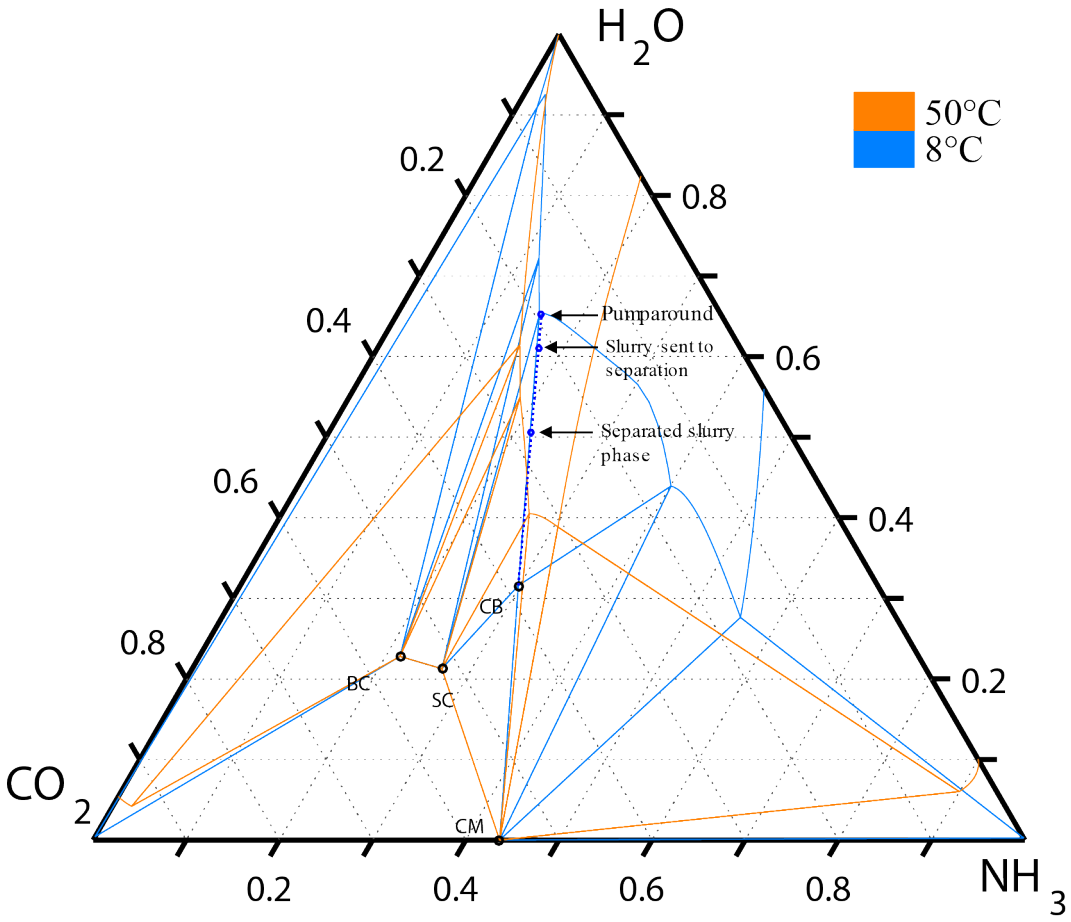

Figure 23: Ternary phase diagram at 8, and 50 °C and 1.013 bar showing the composition of the hydrocyclone feed, as well as the composition of the liquid phase and the composition of the slurry phase obtained after separation.

used. The remaining part is recycled to the desorber in the CO_2 -capture section. The flow rate of the latter is very low, so its effect on the performance of the desorber is negligible.

The ammonia content in the gas stream leaving the desorber is higher with compared to the L-CAP and BC-crystallizing CSF-CAP, because of the higher ammonia concentration exploited. Therefore, the operating conditions of the CO_2 -wash section, as well as the size of the unit operation, have been modified. In particular, the number of stages of the column and the $(L/G)_{CO_2\text{ -wash}}$ have been increased to achieved an higher capture of ammonia, thus obtain an ammonia concentration in the CO_2 -stream sent to compression that observe the constrain (<50 ppm_v).

Table 4 resumes the main differences between the CO_2 -wash section of the BC-CSF-CAP and CB-CSF-CAP.

Table 4: CO_2 -wash section features for different CSF-CAP

	BC-CSF-CAP	CB-CSF-CAP
$(L/G)_{\text{wash section}}$	0.3	0.5
Absorber stages	4	8

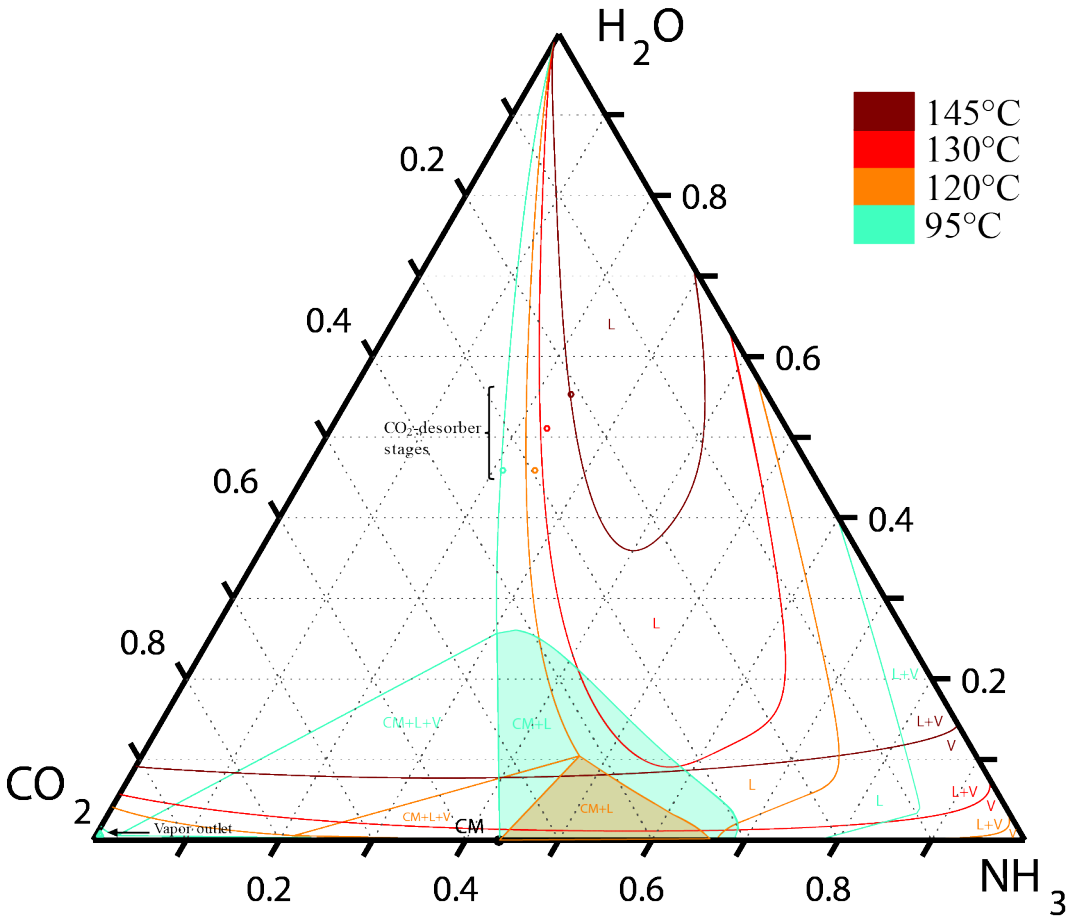

Figure 24: Ternary phase diagram at 95, 120, 130, and 145 °C and 25 bar showing the liquid composition of the solvent regeneration desorber stages. Liquid composition is indicated with a circle. The vapor composition of the vapor leaving the top of the desorber is shown with a triangle. Both isotherms and concentration points follow the same colorcode shown.

5.1.4 Flue gas water wash section

There are no conceptual differences in the flue-gas water wash section between the different CAP described so far.

Higher energy consumption is expected in this section when ammonium carbonate mono-hydrate is exploited in the CSF-CAP, due to the higher ammonia slip phenomena in the CO_2 -capture section.

An automated optimization of this section has been performed in Aspen Plus, which is described in details in Section 5.3.

5.2 Process optimization

As explained before, the optimization of the process focuses on the minimization of the energy consumption of the capture plant.

The optimization has been restricted to the whole plant, apart from the flue-gas water

wash section, which is later evaluated.

In a preliminary study, a multi-variable sensitivity analysis has been performed on the solvent regeneration section. Afterwards, exploiting the results previously obtained, the optimization on the whole plant has been performed.

Other operating conditions and assumptions for the simulations are reported in Table 5. The ranges of the operating variables varied during the optimization are further resumed in Table 7.

Table 5: Operating conditions and assumptions for the CO_2 capture section

CO_2 capture section	
Temperature of cooled streams (T_{cool}) [°C]	18
CO_2 capture rate [% wt.]	> 85
$\eta_M^{CO_2}$ absorber top/bottom	0.015/0.15
Flue gas cooling section	
Blower inlet/outlet pressure [bar]	1.013/1.05

5.2.1 Multi-variable sensitivity analysis on the solvent regeneration section

The aim of this analysis was to find an optimal point at which the regeneration section can be operated. Four operating variables have been employed in the sensitivity analysis:

- The splitting factor of the CO_2 -rich stream, defined as the mass flow rate of CO_2 -rich stream sent to the top of the desorber, without heat recovery, divided by the mass flow rate of CO_2 -rich stream coming from the dissolution section:

$$f = \frac{\dot{m}_{\text{to the top}}}{\dot{m}_{CO_2\text{-rich}}} \tag{38}$$

- the temperature difference of the energy recovery heat exchanger, defined as the difference between the temperature of the cold CO_2 -rich entering the exchanger and the hot regenerated solvent exiting the exchanger:

$$\Delta T = T_{\text{cold } CO_2\text{-rich}} - T_{\text{hot } CO_2\text{-lean}} \tag{39}$$

- The pressure of the section P_{des};

- The specific reboiler duty of the desorber, defined as the ratio between the reboiler duty and the CO_2 stream sent to compression (after the CO_2 -wash section):

$$\hat{Q} = \frac{\dot{Q}}{\dot{m}_{CO_2 \text{ to compression}}} \tag{40}$$

With this aim, also the CO_2 -wash section has been simulated. Two different composition for the CO_2 -rich stream coming from the S/L separator are exploited. Particularly, the ones obtained in Case 1 and Case 4.

The heat exchanger simulated in Aspen is the "Mheatx" type, which can perform a zone analysis, to calculate the temperature profiles of both streams along the heat exchanger, via a pinch point temperature analysis. Therefore, since vapor formation may occur, crossover issues are avoided. The minimum pinch point has been chosen as 3 °C.

The sensitivity analysis finds and collects data for the specific reboiler duty obtained as a function of the pressure P_{des} and the splitting factor f, when the pinch point is minimized. The minimum pinch point is obtained by varying the ΔT. Figure 25 shows the results of the multi-variable sensitivity analysis. In the ammonium bicarbonate-crystallizing CSF-CAP

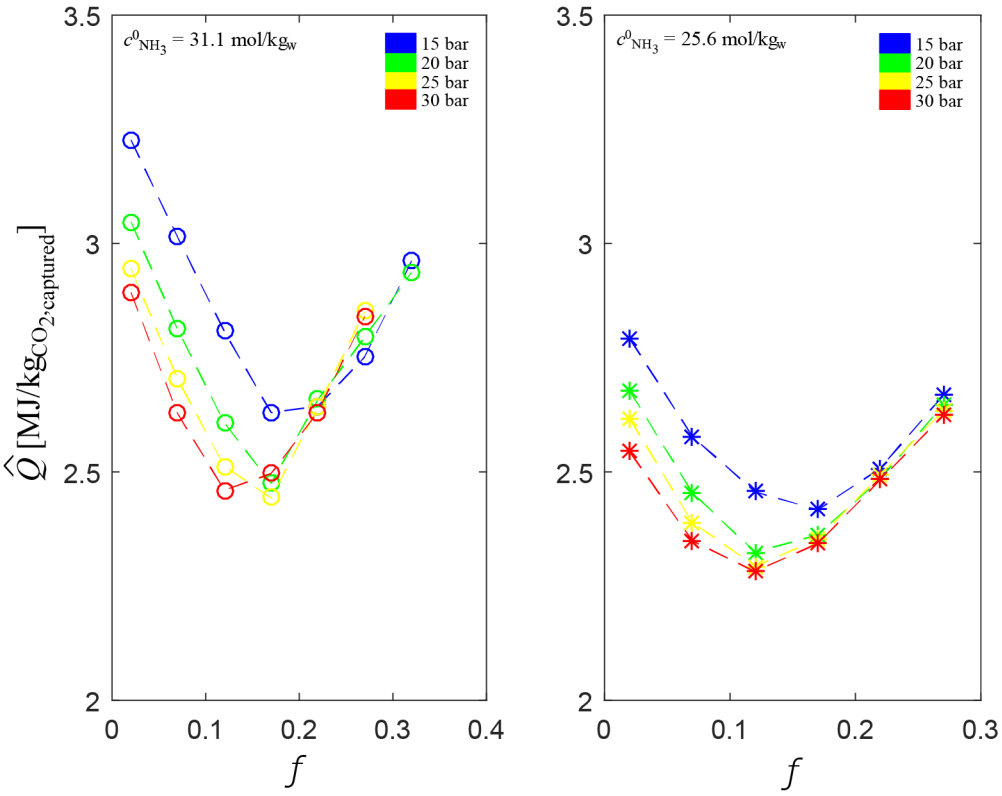

Figure 25: Results of the multi-variable sensitivity analysis. The plots show the specific reboiler as a function of the pressure P_{des} and the splitting factor f, when the pinch point is minimized, for two different ammonia composition of the absorptive solvent employed.

the pressure exploited in the regeneration section has been 10 bar. At this pressure, in this new CSF-CAP, the different compositions lead to different temperatures in the reboiler at the bottom of the desorber. In particular, much lower temperatures are obtained operating at 10 bar. For this reason, higher pressures have been explored. Nevertheless, the temperature at the bottom should not exceed 150 °C due to severe corrosion conditions. The second reason linked to the chose of operating at higher pressure is the ammonia partial pressure,

which decreases at higher pressures. So, a higher CO_2 purity in the vapor stream leaving the desorber is reached.

The multi-variable sensitivity analysis has led to draw several conclusions:

- The trends of the specific reboiler duty show that there is a minimum corresponding to a specific f, for each pressure and ammonia concentration. Therefore, an optimal f there exists.

- The difference in concentration of ammonia shows that the absolute value of the specific reboiler duty changes. In particular, at constant pressure and for a given f, a lower specific reboiler duty is obtained when lower ammonia concentrations are exploited.

- The required specific reboiler duty, at constant conditions, decreases with the pressure. However, the values of specific reboiler duty found at 30 bar are very close to the ones at 25 bar.

- The splitting factor f at which the minimum specific reboiler duty is found, for a given pressure, is very similar between the two cases at different ammonia concentration of the solvent.

In conclusion, values for f, ΔT and P_{des} have been chosen, which are reported in Table 6.

Table 6: Operating conditions chosen for the regeneration section

	Value chosen
P_{des}	25 bar
f	0.1
ΔT	3 °C

The results collected will be kept constant throughout the optimization of the plant. This allows to reduce the number of operating variables in the optimization process, so decrease the computational power required, still maintaining the robustness of the algorithm.

The Matlab code for the multi-variable sensitivity analysis is provided in Appendix A. The code launches simulations in Aspen Plus and clean results if any error, solid formation out of the crystallization section or formation of solids different from ammonium carbonate monohydrate occur.

5.2.2 Optimization

As explained before, the optimization is based on the minimization of the energy consumption within the plant:

$$\min(\hat{Q}_{\text{reboiler}} + \hat{Q}_{\text{chilling}}) \tag{41}$$

where the objective function is defined as the sum of $\hat{Q}_{\text{reboiler}}$ and $\hat{Q}_{\text{chilling}}$, which are the specific reboiler duty and the specific chilling duty within the plant, respectively.

The new optimization algorithm is based on a GPS-type optimization.This optimization starts from a set of operating conditions which lead to convergence, considered as base case, and from that it finds a sequence of points within a specified range, that approach the optimal set of operating conditions that minimizes the objective function. The objective function used in this optimization is the sum of the specific energy required as reboiler duty in the regeneration section and the specific chilling duty required from the plant. Six variables have been considered for the optimization, so the operating space is in 6 dimensions. In Figure 26 the algorithm is schematically explained for the case of 2 variables. After running the initial point simulation, the algorithm calculates the value of the objective function in the neighborhood of the initial point. The set of operating variables, referring to the point for which the smallest objective function value has been found, is taken as new starting point and the procedure is repeated. The GPS algorithm is a smart tool, which decides the right pathway to follow by "learning" from the results obtained, as well as from not converged simulations. This approach requires less computational power and less time to perform the calculations compared with a multi-variable sensitivity analysis.

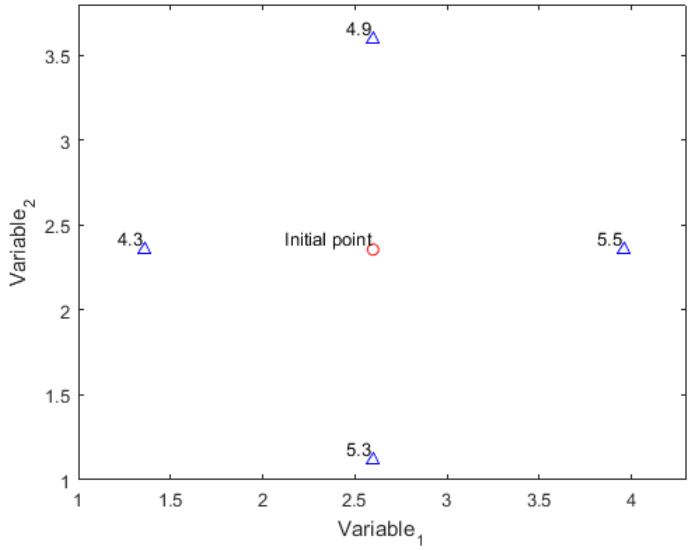

Figure 26: Scheme of the GPS-type optimization with 2 operating variables

The operating variables used in the optimization are the same used in the analysis of the absorption section, listed in Section 5.1.1. In addition, for convergence reasons, a sensitivity on the reboiler duty of the desorber is run for each set of operating conditions. The sensitivity goes from higher to lower value of reboiler duties specified, until the minimum is found. The minimum reboiler duty refers to the point where the CO_2 make-up of the plant is zero. The reason is linked to the fact that, when the set of operating conditions is changed, convergence in Aspen Plus is reached easier using higher reboiler duties.

The Matlab code for the optimization is provided in Appendix A. The same checks described in the code for the multi-variable sensitivity analysis (Section 5.2.1) have been done. Furthermore, the code returns results only if the CO_2 capture rate ψ_{CO_2} is higher than 85% and the ammonia slip is lower than 45000 ppm_v. The constrain on the ammonia slip has been chosen for two reasons:

- The preliminary analysis described in Section 5.1.1 has shown that values of ammonia slip above 45000 ppm_v lead to uncontrollable absorber operation.
- The energy duty in the flue-gas water wash section strongly depends on the ammonia slip. The higher the ammonia slip, the higher the energy required to operate the section. Although the energy duty of the flue-gas water wash section should not impact a lot the overall energy required in the plant, very high ammonia slip values could lead to excessive energy consumption.

In Table 7 the initial values and the ranges for the operating conditions provided to the optimizer are shown. The initial values come from Case 1. The ranges have been chosen among feasible values, coming from the feedback obtained in the previous analyses.

Table 7: Initial value and ranges for the operating conditions provided to the optimization code

	Initial value	Lower bound	Upper bound
$c^0_{NH_3}$ [mol/kg_{H_2O}]	25.73	15	30
$l_{CO_2\text{-lean}}$ [mol_{CO_2}/kg_{NH_3}]	0.34	0.3	0.35
L/G	3.23	2.00	4.00
T_{cry} [°C]	8	7	18
$T_{CO_2\text{-lean}}$ [°C]	21.2	18.0	21.2
α_l	0.18	0.1	0.25

Figure 27 shows the trend of the different variables conditions chosen for the optimization. Red points indicates the simulations performed. Red points circled in blue are the simulations converged. At the beginning, the optimizer screens the whole region for the different operating conditions. Then, when it is close to the optimum, it continuously narrows the region in that neighborhood, until the optimum is found. The last 600 simulations seems to have the same inputs, because the optimizer is moving very close to the optimum.

Figure 28 shows the optimization results. The overall specific chilling duty of the plant is shown as a function of the specific reboiler duty required from the desorber. As it can be noticed, the initial blue points are dispersed in the graph, while the yellow ones are more ordered. Although the optimization is not aimed to find a Pareto set of points, it seems that a Pareto has been found, shown with the red dotted line in Figure 28.

As expected, although the almost constant values for the reboiler duty, very different values for the chilling duty have been found. As it has been presented in the analysis on

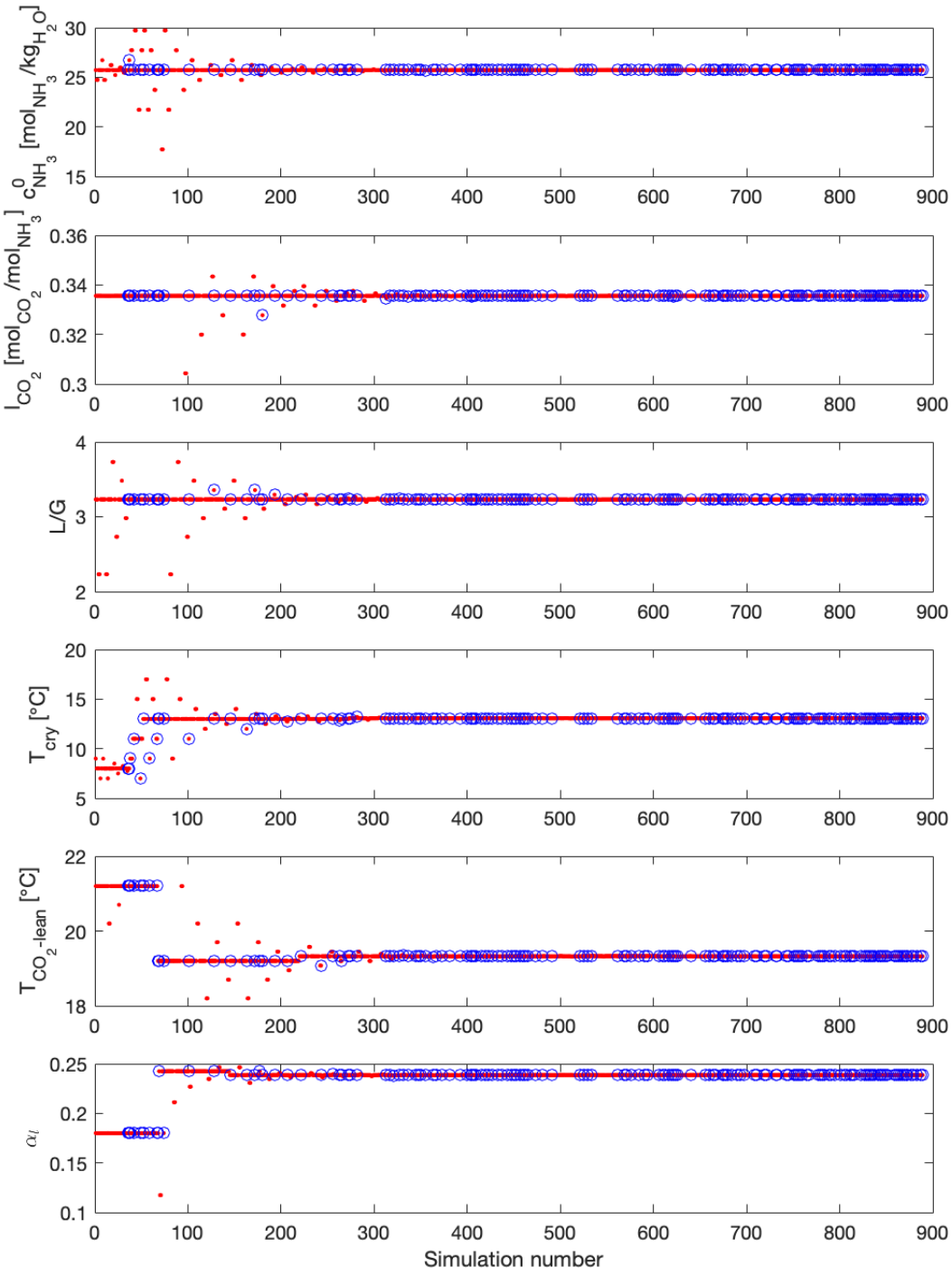

Figure 27: Trend of the different operating variables varied during the optimization with *patternsearch*

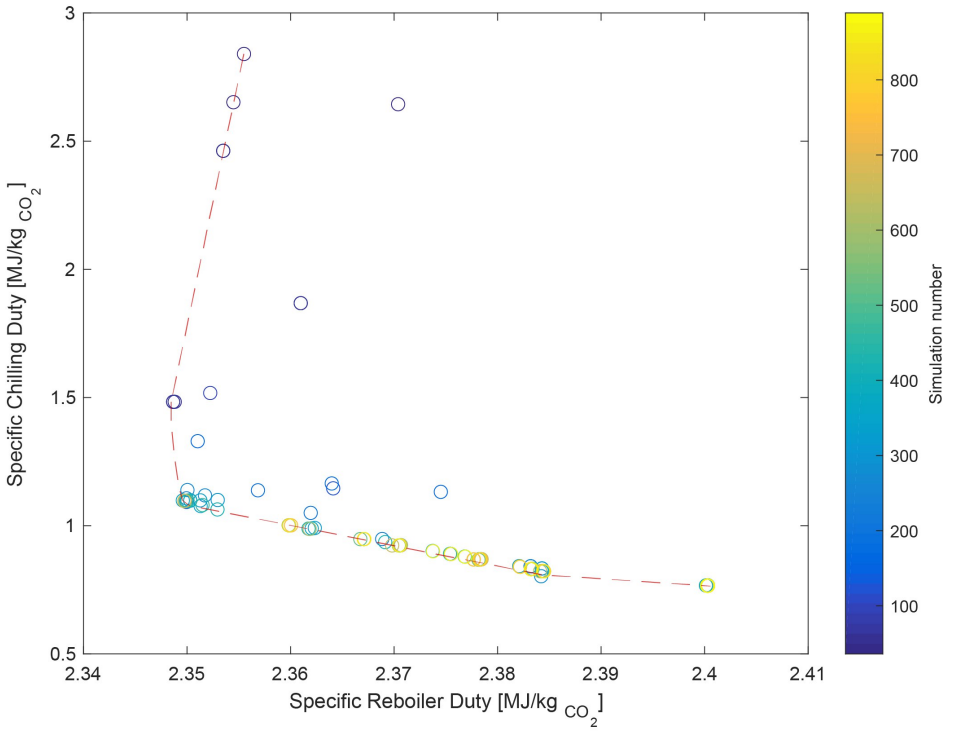

Figure 28: Results of the optimization with *patternsearch*, showing the specific chilling duty as a function of the specific reboiler duty. The color bar refers to the evolution of the simulations.

the regeneration section, shown in Figure 25, the reboiler duty of the desorber is almost constant, unless very different concentrations are exploited. Therefore, the optimizer has privileged the operating conditions which affects the chilling duty (*i.e.* T_{cry} and α_{l}), rather than the ones affecting the reboiler duty (*i.e.* $c^{0}_{\text{NH}_3}$ and $l_{\text{CO}_2\text{-lean}}$).

The reason for the low chilling duty is mainly linked with the exploitation of higher crystallization temperatures. In particular, as explained in Section 4, in comparison with the ammonium bicarbonate-crystallizing CSF-CAP, greater or equal solid yield can always be obtained with the ammonium carbonate monohydrate even with a lower temperature difference exploited in the crystallization section. Figure 29 shows the same results as Figure 28, but the colorbar refers to the crystallization temperature used. As shown, data referring to the lower chilling duty are linked to a higher crystallization temperature. Therefore, the theoretical potential of ammonium carbonate monohydrate presented in Section 4 resulted in a strong decrease of the chilling duty required in the plant.

Table 8 resumes the optimum process variables found, as well as the specific duties found with the optimization.

The flowscheme of the plant used in this optimization is reported in Appendix C. The Matlab code for the optimization is provided in Appendix B.

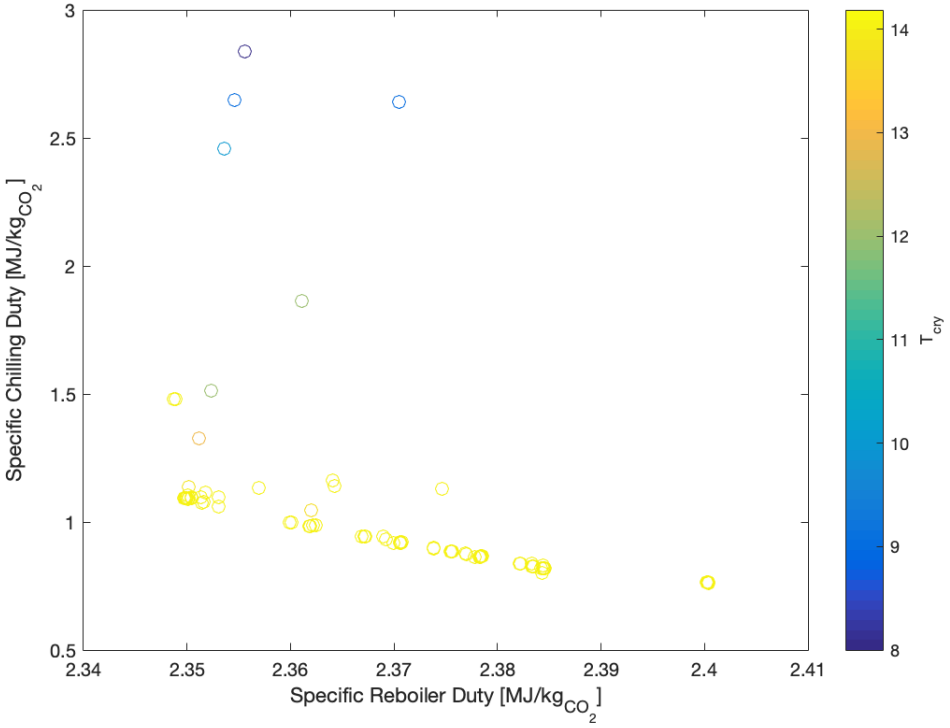

Figure 29: Results of the optimization with *patternsearch*, showing the specific chilling duty as a function of the specific reboiler duty. The color bar refers to the crystallization temperature exploited.

Table 8: Optimal operating conditions and duties for the CB-CSF-CAP

Optimal operating conditions	
$c^0_{NH_3}$ [mol/kg$_{H_2O}$]	25.73
$l_{CO_2\,-lean}$ [mol$_{CO_2}$ /kg$_{NH_3}$]	0.33
L/G	3.23
T_{cry} [°C]	14.06
$T_{CO_2\text{-lean}}$ [°C]	19.33
α_l	0.24
Optimal duties	
Specific reboiler duty [MJ$_{th}$/kg$_{CO_2\,,captured}$]	2.35
Specific chilling duty [MJ$_{th}$/kg$_{CO_2\,,captured}$]	1.09
Electric duty for auxiliaries [MJ$_{el}$/kg$_{CO_2\,,captured}$]	0.06

5.3 Optimization of the flue-gas water wash section

A detailed flowscheme of the flue-gas water wash section is show in Figure 30. The optimization has been done directly in Aspen Plus, by means of the optimization tool. The process is an absorption-desorption very similar to the CO_2 -capture section, but the easier computation allows the direct optimization in Aspen Plus.

Operating conditions and assumptions for the simualtions of the flue gas water wash sections are resumed in Table 9.

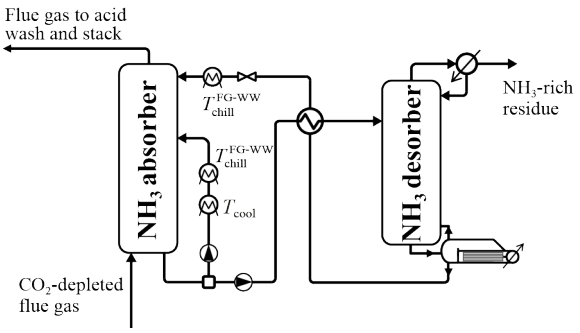

Figure 30: Flowscheme of the flue-gas water wash section

Table 9: Operating conditions and assumptions for the FG water wash section

Flue gas water wash section	
Temperature of chilled pumparound/NH_3 -lean ($T_{chill,FG-WW}$) [°C]	15/10
Temperature of condenser NH_3 desorber [°C]	68
Pressure of regeneration section [bar]	1.013
Purity lean solution (x_{H_2O})[molar fraction]	0.999
NH_3 removal efficiency [% mol.]	> 97.5
$\eta_M^{CO_2}$ absorber	0.015

The optimizer has been set to vary three operating variables, to reach the conditions imposed by the two given constraints. The varied operating variables are:

- The reboiler duty of the reboiler at the bottom of the NH_3 desorber:

$$\dot{Q}_{\text{reb,FG-WW}} \tag{42}$$

- The splitting factor of the liquid NH_3 -rich stream leaving the bottom of the absorber, defined as the mass flow rate of the NH_3 -rich stream recirculated to the absorber, divided by the total one:

$$f_{\text{FG-WW}} = \frac{\dot{m}_{\text{NH}_3\text{ -rich recycle}}}{\dot{m}_{\text{NH}_3\text{ -rich}}} \tag{43}$$

- The liquid-to-gas flow ratio of the absorber, defined as the ratio between the mass flow rate of solvent and the mass flow rate of CO_2 -depleted flue gas:

$$(L/G)_{\text{FG-WW}} = \frac{\dot{m}_{\text{solvent}}}{\dot{m}_{\text{CO}_2\text{ -depleted flue gas}}} \tag{44}$$

The constraints imposed are:

- Purity of the solvent leaving the bottom of the desorber in molar fraction of water:

$$x_{\text{H}_2\text{O}} > 0.999 \tag{45}$$

- Ammonia concentration in the flue gas exiting the absorber and sent to the acidic wash:

$$c_{NH_3}^{\text{FG to acidic wash}} < 200 \text{ ppm}_v \tag{46}$$

For the simulation for which the minimum of the objective function has been obtained in Section 5.2.2, the information on the CO_2 -depleted flue gas leaving the CO_2 -capture section has been used for the computation of the energy consumption in the flue gas water wash section.

The operating conditions and the results are reported in Table 10. A specific reboiler duty of 0.8 has been obtained for the NH_3 -stripper, while the chilling duty is almost negligible.

Table 10: Specifications and outputs for the flue gas water wash optimization

Exhaust flue gas specifications	
Mass flow rate [kg/ sec]	58.5
Temperature [°C]	14.06
Water mole fraction	0.013
Ammonia mole fraction	0.029
Carbon dioxide mole fraction	0.029
Air mole fraction	0.929
Optimal duties	
Specific reboiler duty [$MJ_{th}/kg_{CO_2,captured}$]	0.80
Specific chilling duty [$MJ_{th}/kg_{CO_2,captured}$]	0.09

The acidic wash is not simulated for the aim of this work, because the thermodynamic model does not account for acidic solutions. However, the acidic wash section has a negligible energy consumption with compared to the other sections of the plant. Therefore, this has been neglected in the energy duty evaluation.

The flowscheme used in this optimization is reported in Appendix D.

5.4 CO_2 compression duty evaluation

Similarly to Section 5.3, the information on the CO_2 gas stream leaving the CO_2 -wash section have been exploited for the calculation of the energy duty in the CO_2 -compression section.

General operating conditions and assumptions for the simulations of the CO_2 compression section are resumed in Table 11.

Table 11: Operating conditions and assumptions for the CO_2 compression section

CO_2 compression section	
Number of inter-cooled compression stages	6
Pressure at compressor outlet [bar]	80
Pressure at pump outlet [bar]	110

The compression duty is expected to be lower than the ammonium bicarbonate-crystallizing CSF-CAP, because a higher pressure has been used in the regeneration section.

CO_2 has to be compressed to be stored. This is achieved by means of a multi-stage compression with inter-cooler, up to around 80 bar, which leads to liquefaction of the CO_2 . A dehydration section is also provided to remove eventual water residues. Then, the liquid CO_2 is further compressed up to 110 bar by means of a pump. Further details about the assumptions made are reported in Table 12.

Table 12: Assumptions for the compressors in the CO_2 -compression section

CO_2 -compression section assumptions	
Isoentropic efficiency η_c	0.85
Mechanical efficiency η_m	0.95
Intercooler temperature $T_{\text{intercool}}$ [°C]	25

The electric energy consumption for compression is calculated. The compression duty has been evaluated only considering one of the CO_2 stream obtained from the previous simulations. The reason is that very similar capture rates have been obtained among the simulations, which means that the flow rate of the purified CO_2 stream is constant. Furthermore, a very high CO_2 purity (>99%) has also been obtained and the effect of the other components on the energy consumption can be neglected.

Table 13 shows the electric duty required for the compression of the purified CO_2 in the optimal case.

Table 13: Compression duty calculated for the optimized CB-CSF-CAP

Compression duty optimized case	
Compression duty [$MJ_{el}/kg_{CO_2\text{ ,captured}}$]	0.07

The flowscheme of the plant used in this optimization is reported in Appendix E.

6 Integration and performance evaluation

6.1 Integration

The energy consumption obtained as results from block 2, 3, and 4 of the optimization algorithm are shown in Table 14, have been integrated.

Table 14: Energy duties obtained from block 2, 3, and 4 of the optimization algorithm

Block 2: FG cooling section, CO_2 capture section, CO_2 wash section	
Specific reboiler duty [$MJ_{th}/kg_{CO_2,captured}$]	2.35
Specific chilling duty [$MJ_{th}/kg_{CO_2,captured}$]	1.08
Specific auxiliaries duty [$MJ_{el}/kg_{CO_2,captured}$]	0.06
Block 3: FG water wash section	
Specific reboiler duty [$MJ_{th}/kg_{CO_2,captured}$]	0.8
Specific chilling duty [$MJ_{th}/kg_{CO_2,captured}$]	0.09
Block 4: CO_2 compression section	
Specific electric duty [$MJ_{el}/kg_{CO_2,captured}$]	0.07

The CSF-CAP is characterised among others by desorption columns, pumps, and chillers. These kinds of units do not use the same type of energy. In particular, three different energy duties are required in the plant:

- thermal energy provided as reboiler duty;
- chilling duty;
- electric duty for compression and auxiliaries.

The overall energy duty for each energy category has been calculated and it is reported in Table 15.

Table 15: Overall energy consumption for each type of energy required

Overall energy consumption for the three type of energy required	
Specific reboiler duty [$MJ_{th}/kg_{CO_2,captured}$]	3.15
Specific chilling duty [$MJ_{th}/kg_{CO_2,captured}$]	1.18
Specific auxiliaries duty [$MJ_{el}/kg_{CO_2,captured}$]	0.07

6.2 Conversion and overall duty evaluation

The total energy cosumption of the plant cannot be assessed by directly summing the different energy demand. Consequently, it is not possible to directly compare the different energy requirement for different CAP plant, but they have to be transformed into comparable energy type. In particular, the electrical work has been chosen as the energy type for the

comparison. Therefore, the equivalent electrical work has been calculated for the thermal energy provided as reboiler duty and the chilling duty.

The general assumptions made for the calculations are resumed in Table 16.

Table 16: General assumptions made for the energy integration of the CB-CSF-CAP

Utilities and environment	
Cooling water temperature [°C]	15
Minimum ΔT for heat exchange	
Liquid/liquid [°C]	3
Evaporator of chilling utility [°C]	5
Condenser of chilling utility [°C]	10
η_{is} for COP calculation	0.6
η_{th} for equivalent electrical reboiler work	0.9
T_{sink} for equivalent electrical reboiler work [°C]	50

The equivalent electrical work of the thermal energy provided as reboiler duty has been calculated as follow:

$$\hat{W}_{\text{reboilers}} = \sum_i \hat{Q}_{reb,i} \eta_{\text{th}} (1 - \frac{T_{\text{amb}}}{T_{\text{reb,i}} + \Delta T_{\text{min}}}) \tag{47}$$

where $\hat{Q}_{\text{reb,i}}$ is the thermal energy demand for the reboiler *i* [$\text{MJ}_{\text{thermic}}$], η_{th} is the efficiency during energy transformation, T_{amb} is the ambient temperature [°C], $T_{\text{reb,i}}$ is the reboiler temperature for the reboiler *i* [°C], and ΔT_{min} is the minimum temperature difference between the reboiler and the steam used as thermal vector [°C]. Chilling duty can be transformed into electrical work as follow:

$$\hat{W}_{\text{chilling}} = \sum_j \frac{\hat{Q}_{\text{chill,j}}}{COP_{\text{j}}} \tag{48}$$

where $\hat{Q}_{\text{chill,j}}$ is the chilling demand for the chiller *j* [$\text{MJ}_{\text{thermic}}$], and COP_{j} is the coefficient of performance for the chiller *j*, which is calculated as follow:

$$COP = \frac{T_{\text{evap}}}{T_{\text{cond}} - T_{\text{evap}}} \times \eta_{\text{is}} \tag{49}$$

where T_{evap} is the evaporation temperature, defined as the crystallization temperature, minus 5 °C, T_{cond} is the condensation temperature, defined as the ambient temperature, plus 10 °C, and η_{is} is the efficiency used in COP calculation. The work required for auxiliaries and compression is already available as electric work from Aspen Plus, which also takes into account the all the efficiencies.

Each of the electrical work calculated is a specific value, weighted on the mass in kg of CO_2 captured.

Table 17 resumes the equivalent electrical work calculated from each type of energy required within the plant.

Table 17: Equivalent electrical work for each type of energy duty in the whole plant

Equivalent electrical work in MJ/kg_{CO_2}	
Reboiler CO_2 capture section	0.52
Reboiler FG-WW	0.11
Chillers	0.07
Auxiliaries	0.07
CO_2 compression	0.07

6.3 Comparison and conclusions

Figure 31 shows the specific equivalent electrical work for the different contributions to the overall energy consumption. L-CAP and BC-CSF-CAP values also refers to an optimized plant [1].

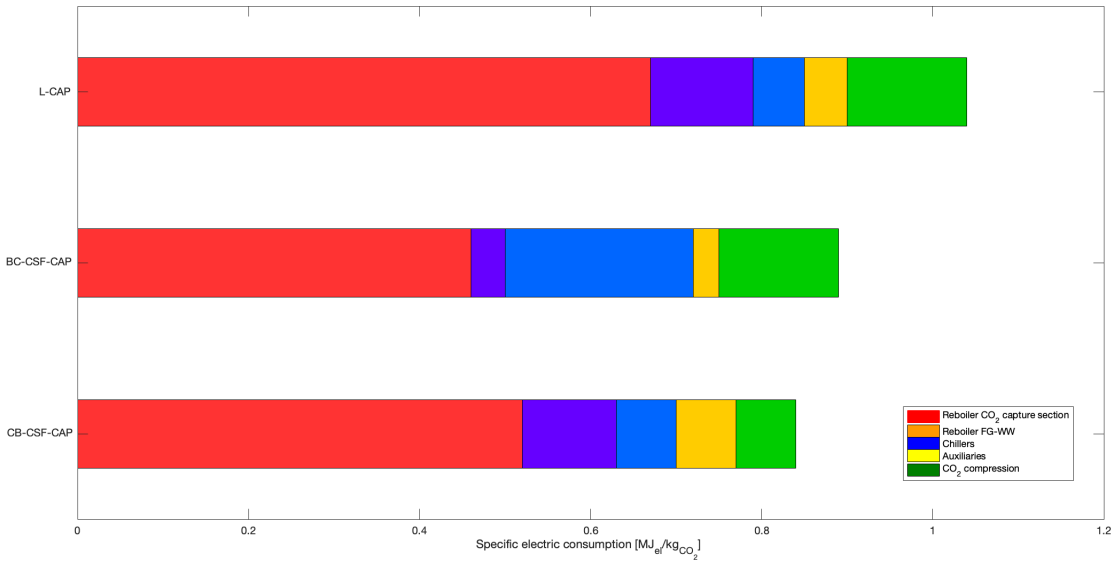

Figure 31: Specific equivalent electrical work for the different contributions to the overall energy consumption, for the L-CAP, BC-CSF-CAP, and CB-CSF-CAP

As shown, the ammonium carbonate monohydrate-crystallizing CSF-CAP has achieved an equivalent electrical penalty of $0.84\,MJ/kg_{CO_2}$, corresponding to a reduction of 5% compared to the ammonium bicarbonate-crystallizing CSF-CAP, which has an overall electrical penalty of $0.89\,MJ/kg_{CO_2}$. Compared to the L-CAP, which has achieved an overall equivalent electrical duty of $1.04\,MJ/kg_{CO_2}$, the reduction reaches 21%. Furthermore, in this work a heat integration has not been considered, whereas in the optimization of the BC-CSF-CAP, a heat integration for chilling duty within the crystallization section has been fixed to 48%

[1]. Therefore, the overall electrical energy penalty for the CB-CSF-CAP should be even lower if heat integration is considered.

Each type of energy duty obtained in the CB-CSF-CAP has a different value compared to the other CAPs. In particular:

- the value of the equivalent electrical work, relative to the reboiler duty of the CO_2 -capture section, is between the other two. This value strongly depends on the composition and the flow rate of the stream sent to regeneration, as well as other operating conditions chosen for that section. The L-CAP has a very high value compared with the other two cases, because the CO_2 concentration in the stream sent to regeneration is unchanged with respect to the CAP that exploits solid-formation.

- as expected, the equivalent electrical work, relative to the reboiler duty of the flue gas water wash section, is higher than the other CAPs. The higher energy duty is due to the higher ammonia content in the exhausted flue gas.

- the reduction of the overall equivalent energy penalty due to chilling is the strength of this process. Compared to the BC-CSF-CAP, the energy penalty is strongly reduced, due to higher temperatures have been exploited in the crystallization section. The L-CAP achieved a very low chilling duty, since the crystallization section, which is the major consumer of chilling duty, is not present.

- The auxiliaries of the CB-CSF-CAP requires more energy than the other CAPs, due to a higher pressure has to be reached in the regeneration section.

- Since higher pressure is exploited in the regeneration section compared to the other CAPs, the compression duty in the CB-CSF-CAP is highly reduced. In fact, the pressure change in the regeneration section is obtained by means of pumps, because a liquid phase has to be pressurized. Therefore, although higher energy is required for the auxiliaries, an overall reduction of compression energy is achieved.

In addition, a qualitative comparison can be done between the CB-CSF-CAP and the BC-CSF-CAP, concerning the unit operations. In particular:

- a smaller CO_2 -absorber can be used in the CB-CSF-CAP, due to higher absorption rates are achieved.

- the column of the CO_2 water wash section is bigger in the CB-CSF-CAP, because a higher capture of ammonia residues is required.

- the desorber has to be designed for higher pressure.

Thus, there are advantages and disadvantages in the CB-CSF-CAP compared with the BC-CSF-CAP, but the two processes can be qualitatively considered similar under the capital cost point of view.

Appendices

A Matlab code for the multi-variable sensitivity analysis on the regeneration section

```
%--------------------------------------------------------------------------%
% Davide Bernardo Preso
% ETH Zurich – Alma Mater Studiorum Universita' di Bologna
% Master Thesis
%--------------------------------------------------------------------------%


clc;
clear all;
close all;
% Connect to Aspen, define Aspen as a COM server object
Asp                     = actxserver('Apwn.Document');
CO2absorber_file        = strcat(pwd,'/','heat_work_p35.apw');

% Molar mass of compounds
MMCO2 = 44.0096; % gCO2/molCO2
MMNH3 = 17.0306; % gNH3/molNH3
MMH2O = 18.0385; % gH2O/molH2O

fgflow = 83.53846;

f          = 0.02:0.05:0.32;
deltaT     = 3:2:40;
reb1       = [8:-0.2:7.2]*1e4;
reb2       = [7:-0.1:4]*1e4;
rebduty    = [reb1, reb2];
SimName    = ['ABS_sensitivity' '_' num2str(length(f)) num2str(length(
    deltaT)) num2str(length(rebduty))];

% Compute the matrix of all cases [Nsim X 5]
SimulationsNumber=0;
AllCases        = zeros(length(f)*length(deltaT)*length(rebduty),3);

for j=1:length(f)
    for n=1:length(deltaT)
        for m=1:length(rebduty)
            SimulationsNumber=SimulationsNumber+1
            AllCases(SimulationsNumber,1)=f(j);
            AllCases(SimulationsNumber,2)=deltaT(n);
            AllCases(SimulationsNumber,3)=rebduty(m);
        end
    end
end
SensitivityNumber = SimulationsNumber/length(rebduty)

% Sensitivity analysis

Asp.InitFromFile2(CO2absorber_file); % activate aspen file for
    sensitivity
```

```
47
48 % Check sensitivity points and ASSIGN size to result matrix and fortran
       calculator text
49 n_sim               = 0;
50 Aspen_notentered    = 0;
51 AspenKilledFlag     = false;
52
53 % Define output variables
54 ResMatCAP_CO2mkup    = zeros(length(f),length(deltaT));
55 ResMatCAP_minpinch   = zeros(length(f),length(deltaT));
56 ResMatCAP_dT         = zeros(length(f),length(deltaT));
57 ResMatCAP_pressure   = zeros(length(f),length(deltaT));
58 ResMatCAP_rebduty    = zeros(length(f),length(deltaT));
59 ResMatCAP_split      = zeros(length(f),length(deltaT));
60 ResMatCAP_co2stora   = zeros(length(f),length(deltaT));
61 sens_rebdut          = zeros(1,24);
62
63 h=waitbar(0,'Calculating ABSORBER. Progress: ');
64 for j=1:length(f)
65     split  = f(j);
66     for n=1:length(deltaT)
67         dT = deltaT(n);
68         clear sens_rebdut
69         row_flag=1;
70         sens_rebdut = zeros(1,24);
71         for m=1:length(rebduty)
72             QN = rebduty(m);
73
74             desout2=50+dT;
75
76             tic;
77             tstart=tic;
78             waitbar(n_sim/(length(f)*length(deltaT)*length(rebduty)));
79             n_sim = n_sim+1
80
81             Asp.Tree.FindNode('\Data\Blocks\DESO\Input\QN').value = QN;
82             Asp.Tree.FindNode('\Data\Blocks\SPLITDES\Input\FRAC\TODES6')
                   .Value = split;
83             Asp.Tree.FindNode('\Data\Blocks\HECO\Input\VALUE\DESOUT2').
                   Value = desout2;
84
85             leanh2o_in = Asp.Tree.FindNode('\Data\Streams\LEANIN\Output\
                   STRM_UPP\WXAPP\MIXED\TOTAL\H2O').Value;
86             leannh3_in = Asp.Tree.FindNode('\Data\Streams\LEANIN\Output\
                   STRM_UPP\WXAPP\MIXED\TOTAL\NH3').Value;
87             leanco2_in = Asp.Tree.FindNode('\Data\Streams\LEANIN\Output\
                   STRM_UPP\WXAPP\MIXED\TOTAL\CO2').Value;
88
89             %initialization
90             n_start        = 0;
91             current_time   = 0;
92             Asp_didntwork  = 0;
93             SimStatus      = false;
94             MaxTime        = 30; % Time for a simulation to be stopped
95             MaxTimeReached= false;
96
97             % Run the simulation asynchronously (Run2(true)) assigning a
                   maximum
```

```
98          % time for convergence MaxTimes
99          tic
100         while current_time <= MaxTime
101             if n_start == 0 && Asp.Engine.Ready
102                 Asp.Engine.Run2(true);  % Runs the Aspen simulation
103                 n_start=1;
104             end
105             if Asp.Engine.IsRunning == 0
106                 break
107             end
108             current_time=toc;
109         end
110         if current_time >= MaxTime
111              MaxTimeReached = true;
112         end
113
114         % Check Results status and if possible acquire the results
115
116         Block_list=['ABSO';'DESO';'HCYC';'HECO'];
117
118         Block_list_str=cellstr(Block_list);
119
120         Block_status = true;
121
122         for p=1:length(Block_list_str)
123         valueStat=Asp.Tree.FindNode(strcat('\Data\Blocks\',char(
                Block_list_str(p)))).AttributeValue(12);
124             if valueStat == 8322
125                 Block_status = false;
126                 break
127             elseif valueStat == 9376
128                 Block_status = false;
129             end
130         end
131
132         % Accounts for solid formation within the absorber
133         SolidFormation = false;
134         valueSolids = Asp.Tree.FindNode('\Data\Blocks\ABSO').
                AttributeValue(12);
135         if valueSolids == 8324
136             SolidFormation = true;
137         elseif valueSolids == 9348
138             SolidFormation = true;
139         end
140
141         leanh2o_out = Asp.Tree.FindNode('\Data\Streams\LEANIN\Output
                \STRM_UPP\WXAPP\MIXED\TOTAL\H2O').Value;
142         leannh3_out = Asp.Tree.FindNode('\Data\Streams\LEANIN\Output
                \STRM_UPP\WXAPP\MIXED\TOTAL\NH3').Value;
143         leanco2_out = Asp.Tree.FindNode('\Data\Streams\LEANIN\Output
                \STRM_UPP\WXAPP\MIXED\TOTAL\CO2').Value;
144         lean_BC = Asp.Tree.FindNode('\Data\Streams\LEANIN\Output\
                STR_MAIN\MOLEFLOW\MIXED\NH4HCO3').Value;
145         lean_CB = Asp.Tree.FindNode('\Data\Streams\LEANIN\Output\
                STR_MAIN\MOLEFLOW\MIXED\CARBO').Value;
146         lean_SC = Asp.Tree.FindNode('\Data\Streams\LEANIN\Output\
                STR_MAIN\MOLEFLOW\MIXED\SESQUI').Value;
147         lean_CM = Asp.Tree.FindNode('\Data\Streams\LEANIN\Output\
```

```
    STR_MAIN\MOLEFLOW\MIXED\CARBAM').Value;
lean_IC = Asp.Tree.FindNode('\Data\Streams\LEANIN\Output\
    STR_MAIN\MOLEFLOW\MIXED\ICE').Value;
diffh2o = abs(leanh2o_in - leanh2o_out);
diffnh3 = abs(leannh3_in - leannh3_out);
diffco2 = abs(leanco2_in - leanco2_out);

if diffh2o>0.01 || diffnh3>0.01 || diffco2>0.01
    SolidFormation = true;
    disp('LEAN CHANGED');
end

if lean_BC>0 || lean_CB>0 || lean_SC>0 || lean_CM>0 ||
    lean_IC>0
    SolidFormation = true;
    disp('SOLIDS IN LEAN');
end

% Control on CO2 make-up
mkp= Asp.Tree.FindNode('\Data\Streams\CO2MKUP\Output\
    STR_MAIN\MASSFLOW\MIXED\CO2').Value;
error = abs(mkp-5.08);
if error<0.001
    SolidFormation = true;
    disp('ASPEN CRASHED');
end


telapsed=toc(tstart);
if MaxTimeReached || ~Block_status || SolidFormation
    Asp_didntwork = Asp_didntwork + 1;
else
    SimStatus = true;
    sens_rebdut(row_flag,1) = QN;
    sens_rebdut(row_flag,2) = Asp.Tree.FindNode('\Data\
        Streams\CO2MKUP\Output\STR_MAIN\MASSFLOW\MIXED\CO2').
        Value;
    for pin=3:23
        sens_rebdut(row_flag,pin) = Asp.Tree.FindNode(strcat
            ('\Data\Flowsheeting Options\Calculator\PINCH\
            Output\READ_VAL\',num2str(pin-2))).Value;
    end
    sens_rebdut(row_flag,24) = Asp.Tree.FindNode('\Data\
        Streams\CO2STORA\Output\STR_MAIN\MASSFLOW\MIXED\CO2')
        .Value;
    row_flag=row_flag+1;
    Aspen_notentered          = Aspen_notentered +
        Asp_didntwork;
end

Flagrunning=Asp.Engine.IsRunning;
if current_time > MaxTime && Flagrunning
    Aspen1_exe = 'apmain.exe';
    Aspen2_exe = 'AspenPlus.exe';
    taskkill = sprintf('taskkill /F /IM %s',Aspen1_exe);
    system(taskkill);
    taskkill = sprintf('taskkill /F /IM %s',Aspen2_exe);
    system(taskkill);
```

```
                AspenKilledFlag = true;
            else
                AspenKilledFlag = false;
            end
            if (~AspenKilledFlag)
                Asp.CloseDocument(false);
            end
            pause(3)
            if AspenKilledFlag
                Asp = actxserver('Apwn.Document');      % Connect to
                    Aspen, define Aspen as a COM server object
            end
            Asp.InitFromFile2(CO2absorber_file); % activate aspen file
                for sensitivity
            pause(1)
            system('Close_Notepad.bat');
        end

        % Find min. rebduty at min. co2 make-up, take minimum pinch
        [min_co2mkp,I] = min(sens_rebdut(:,2));
        min_pinch = min(sens_rebdut(I,[3 4 5 6 7 8 9 10 11 12 13 14 15
            16 17 18 19 20 21 22 23]));
        min_Q = sens_rebdut(I,1);
        min_co2 = sens_rebdut(I,24);

        ResMatCAP_pressure(j,n) = Asp.Tree.FindNode('\Data\Blocks\PUMP1\
            Input\PRES').Value;
        ResMatCAP_rebduty(j,n)  = min_Q;
        ResMatCAP_CO2mkup(j,n)  = min_co2mkp;
        ResMatCAP_minpinch(j,n) = min_pinch;
        ResMatCAP_dT(j,n)       = dT;
        ResMatCAP_split(j,n)    = split;
        ResMatCAP_co2stora(j,n) = min_co2;

        if min_pinch<4.9 && min_pinch>2.9
            break
        end

    end
end

waitbar(n_sim/n_sim);

indx=0;
for j=1:length(f)
    for n=1:length(deltaT)
            indx=indx+1;
            Final(indx,1)=ResMatCAP_pressure(j,n);
            Final(indx,2)=ResMatCAP_rebduty(j,n);
            Final(indx,3)=ResMatCAP_CO2mkup(j,n);
            Final(indx,4)=ResMatCAP_minpinch(j,n);
            Final(indx,5)=ResMatCAP_dT(j,n);
            Final(indx,6)=ResMatCAP_split(j,n);
            Final(indx,7)=ResMatCAP_co2stora(j,n);
    end
end

save pinch_study_p35.mat Final
```

B Matlab code for the main optimization

```
%
    ------------------------------------------------------------------------%
% Davide Bernardo Preso
% ETH Zurich – Alma Mater Studiorum Universita' di Bologna
% Master Thesis
%
    ------------------------------------------------------------------------%


function x = Optimization
clear all
close all
clc

%% Call of the optimizer
%Bounds
x0
    =[16.9687500000000,0.315673828125000,4,8,19.0031250000000,0.198071289062500];

lb = [15,  0.30, 2, 8, 18, 0.1];
ub = [30,  0.35, 4, 19, 21.2, 0.25];
nvars = size(x0,2);

options = optimoptions('patternsearch','PlotFcn','psplotparetof','
    InitialPoints',x0);

%Optimizer
[x] = patternsearch(@(y) AspenCall(y),x0,[],[],[],[],lb,ub,[],options)

end

%% Objective function call
function Obj = AspenCall(x)
%% Aspen COMtechnology port
% Connect to Aspen, define Aspen as a COM server object
Asp                     = actxserver('Apwn.Document');
CO2absorber_file        = strcat(pwd,'/','heat_work_finalv.apw');
%% Inputs for the Aspen simulation
% Molar mass of compounds
MMCO2 = 44.0096; % gCO2/molCO2
MMNH3 = 17.0306; % gNH3/molNH3
MMH2O = 18.0385; % gH2O/molH2O
%Flue-gas flow-rate in kg/s
fgflow = 83.53846;
%Inputs patternsearch
mNH3          = x(1);
LEANCO2       = x(2);
KLG           = x(3);
T_PumpAround  = x(4);
T_lean        = x(5);
SFRAC         = x(6);
reb11         = [9.0  8.0]*1e4;
reb12         = [8.0  7.0]*1e4;
reb2          = [7:-0.1:5]*1e4;
rebduty1      = [reb11, reb2];
```

```
rebduty2      = [reb12, reb2];
% Flags
n_sens              = 0;
Aspen_notentered    = 0;
Solid_cases         = 0;
sensanlength        = length(rebduty1);
n_stages            = 17;
sens_rebdut         = zeros(1,90);
Absorber_Flag       = 0;
%% Call Aspen
AspenKilledFlag=true; % fake flag to start the simulation
if AspenKilledFlag==true
    Asp.InitFromFile2(CO2absorber_file);
end
sens_rebdut = zeros(1,90);
Asp_didntwork = 0; % flag on the number of simulations not converged
%% Enter the reboiler sensitivity
% Loop for the reboiler duties
for z=1:length(rebduty1)
    if z==1 || z==2
        if mNH3<17
            QN = rebduty2(z);
            Asp.Tree.FindNode('\Data\Blocks\SPLITDES\Input\FRAC\TODES6')
                .Value=0.03;
        elseif mNH3>=17
            QN = rebduty1(z);
            Asp.Tree.FindNode('\Data\Blocks\SPLITDES\Input\FRAC\TODES6')
                .Value=0.1;
        end
    else
        QN = new_rebduty; % Assigned at a later stage based on the Q-
            iterations slope
    end
    % Internal variables calculation
    leanflow = KLG*fgflow;
    ammoflow = (leanflow*(mNH3 *17.0306/1000)/(1+(mNH3 /1000)
        *(17.0306+44.0096*LEANCO2 ))) ./ leanflow;
    cdioxflow = LEANCO2 *(44.0096/17.0306)*(ammoflow*leanflow)./leanflow
        ;
    waterflow = (leanflow-(ammoflow*leanflow)-(cdioxflow*leanflow))./
        leanflow;
    Tcry = T_PumpAround-1;
    %% Inputs of the Aspen simulation
    Asp.Tree.FindNode('\Data\Blocks\DESO\Input\QN').value = QN;
    Asp.Tree.FindNode('\Data\Streams\FAKELEAN\Input\TOTFLOW\MIXED').
        Value = leanflow;
    Asp.Tree.FindNode('\Data\Streams\FAKELEAN\Input\FLOW\MIXED\CO2').
        Value = cdioxflow;
    Asp.Tree.FindNode('\Data\Streams\FAKELEAN\Input\FLOW\MIXED\NH3').
        Value  = ammoflow;
    Asp.Tree.FindNode('\Data\Streams\FAKELEAN\Input\FLOW\MIXED\H2O').
        Value  = waterflow;
    Asp.Tree.FindNode('\Data\Blocks\HCYC\Input\FRACS\TODES1\MIXED\H2O').
        Value = SFRAC;
    Asp.Tree.FindNode('\Data\Blocks\HCYC\Input\FRACS\TODES1\MIXED\NH3').
        Value = SFRAC;
    Asp.Tree.FindNode('\Data\Blocks\HCYC\Input\FRACS\TODES1\MIXED\CO2').
        Value = SFRAC;
```

```
95      Asp.Tree.FindNode('\Data\Blocks\HCYC\Input\FRACS\TODES1\MIXED\NH4+')
            .Value = SFRAC;
96      Asp.Tree.FindNode('\Data\Blocks\HCYC\Input\FRACS\TODES1\MIXED\H+').
            Value = SFRAC;
97      Asp.Tree.FindNode('\Data\Blocks\HCYC\Input\FRACS\TODES1\MIXED\OH-').
            Value = SFRAC;
98      Asp.Tree.FindNode('\Data\Blocks\HCYC\Input\FRACS\TODES1\MIXED\CO3--'
            ).Value = SFRAC;
99      Asp.Tree.FindNode('\Data\Blocks\HCYC\Input\FRACS\TODES1\MIXED\HCO3-'
            ).Value = SFRAC;
100     Asp.Tree.FindNode('\Data\Blocks\HCYC\Input\FRACS\TODES1\MIXED\NH2COO
            -').Value = SFRAC;
101     Asp.Tree.FindNode('\Data\Blocks\HCYC\Input\FRACS\TODES1\MIXED\AIR').
            Value = SFRAC;
102     Asp.Tree.FindNode('\Data\Blocks\HCYC\Input\FRACS\TODES1\MIXED\
            NH4HCO3').Value = 1;
103     Asp.Tree.FindNode('\Data\Blocks\HCYC\Input\FRACS\TODES1\MIXED\ICE').
            Value = 1;
104     Asp.Tree.FindNode('\Data\Blocks\HCYC\Input\FRACS\TODES1\MIXED\CARBAM
            ').Value = 1;
105     Asp.Tree.FindNode('\Data\Blocks\HCYC\Input\FRACS\TODES1\MIXED\SESQUI
            ').Value = 1;
106     Asp.Tree.FindNode('\Data\Blocks\HCYC\Input\FRACS\TODES1\MIXED\CARBO'
            ).Value = 1;
107     Asp.Tree.FindNode('\Data\Blocks\HEX8\Input\TEMP').Value =
            T_PumpAround;
108     Asp.Tree.FindNode('\Data\Blocks\CRYS\Input\TEMP').Value = Tcry;
109     Asp.Tree.FindNode('\Data\Blocks\CHILLEAN\Input\TEMP').Value = T_lean
            ;
110     co2mkp_init = Asp.Tree.FindNode('\Data\Streams\CO2MKUP\Output\
            STR_MAIN\MASSFLOW\MIXED\CO2').Value;
111     % Initialized simulation parameters for convergence
112     n_start        = 0;
113     current_time   = 0;
114     SimStatus      = false;
115     MaxTime = 130; %s
116     MaxTimeReached= false;
117     ResTemp = zeros(length(sensanlength),8); % Defines the matrix for
            the temperature profile along the absorber at the stages
            selected in the sensitivity analysis, for each reboiler duty
            value
118
119     % Run the simulation asynchronously (Run2(true)) assigning a maximum
120     % time allowed for simulation MaxTimes
121     tic
122     while current_time <= MaxTime
123         if n_start == 0 && Asp.Engine.Ready
124             Asp.Run2(true);  % Runs the Aspen simulation
125             n_start=1;
126         end
127         if Asp.Engine.IsRunning == 0
128             break
129         end
130         current_time=toc;
131     end
132     if current_time >= MaxTime
133         MaxTimeReached = true;
134     end
```

```
135     %% Check on the most relevant problems encountered during the
            simulations
136     Run_Status = Asp.Tree.FindNode('\Data\Results Summary\Run-Status\
            Output\UOSSTAT2').Value;
137     if Run_Status == 9
138         Block_status = false; % Data is not saved
139     else
140         % Definition of the main problems encountered during the
141         % simulations
142         Block_list=['ABSO';'DESO';'HCYC';'HECO'];
143         Block_list_str=cellstr(Block_list);
144         Block_status = true;
145         for p=1:length(Block_list_str)
146             valueStat=Asp.Tree.FindNode(strcat('\Data\Blocks\',char(
                    Block_list_str(p)))).AttributeValue(12);
147             if valueStat == 8322 %8324 for cation umbalanced
148                 Block_status = false;
149             elseif valueStat == 9376
150                 Block_status = false;
151             end
152         end
153         % Accounts for solid formation within the absorber
154         SolidFormation = false;
155         valueSolids = Asp.Tree.FindNode('\Data\Blocks\ABSO').
                AttributeValue(12);
156         if valueSolids == 8324
157             SolidFormation = true;
158         elseif valueSolids == 9348
159             SolidFormation = true;
160         end
161         % Loading of the data necessary to run the other checks
162         leanh2o_out = Asp.Tree.FindNode('\Data\Streams\LEANIN\Output\
                STRM_UPP\WXAPP\MIXED\TOTAL\H2O').Value;
163         leannh3_out = Asp.Tree.FindNode('\Data\Streams\LEANIN\Output\
                STRM_UPP\WXAPP\MIXED\TOTAL\NH3').Value;
164         leanco2_out = Asp.Tree.FindNode('\Data\Streams\LEANIN\Output\
                STRM_UPP\WXAPP\MIXED\TOTAL\CO2').Value;
165         lean_BC = Asp.Tree.FindNode('\Data\Streams\LEANIN\Output\
                STR_MAIN\MOLEFLOW\MIXED\NH4HCO3').Value;
166         lean_CB = Asp.Tree.FindNode('\Data\Streams\LEANIN\Output\
                STR_MAIN\MOLEFLOW\MIXED\CARBO').Value;
167         lean_SC = Asp.Tree.FindNode('\Data\Streams\LEANIN\Output\
                STR_MAIN\MOLEFLOW\MIXED\SESQUI').Value;
168         lean_CM = Asp.Tree.FindNode('\Data\Streams\LEANIN\Output\
                STR_MAIN\MOLEFLOW\MIXED\CARBAM').Value;
169         lean_IC = Asp.Tree.FindNode('\Data\Streams\LEANIN\Output\
                STR_MAIN\MOLEFLOW\MIXED\ICE').Value;
170         diffh2o = abs(waterflow - leanh2o_out);
171         diffnh3 = abs(ammoflow - leannh3_out);
172         diffco2 = abs(cdioxflow - leanco2_out);
173         if diffh2o>0.01 || diffnh3>0.01 || diffco2>0.01
174             SolidFormation = true;
175             disp('LEAN CHANGED');
176         end
177         if lean_BC>0 || lean_CB>0 || lean_SC>0 || lean_CM>0 || lean_IC>0
178             SolidFormation = true;
179             disp('SOLIDS IN LEAN');
180         end
```

```
181         mkp = Asp.Tree.FindNode('\Data\Streams\CO2MKUP\Output\STR_MAIN\
                MASSFLOW\MIXED\CO2').Value;
182         if mkp == co2mkp_init
183             SolidFormation = true;
184             disp('ASPEN CRASHED');
185         end
186         slurry_BC = Asp.Tree.FindNode('\Data\Streams\SLURRY\Output\
                STR_MAIN\MOLEFLOW\MIXED\NH4HCO3').Value;
187         slurry_CB = Asp.Tree.FindNode('\Data\Streams\SLURRY\Output\
                STR_MAIN\MOLEFLOW\MIXED\CARBO').Value;
188         slurry_SC = Asp.Tree.FindNode('\Data\Streams\SLURRY\Output\
                STR_MAIN\MOLEFLOW\MIXED\SESQUI').Value;
189         slurry_CM = Asp.Tree.FindNode('\Data\Streams\SLURRY\Output\
                STR_MAIN\MOLEFLOW\MIXED\CARBAM').Value;
190         slurry_IC = Asp.Tree.FindNode('\Data\Streams\SLURRY\Output\
                STR_MAIN\MOLEFLOW\MIXED\ICE').Value;
191         if slurry_BC>0 || slurry_SC>0 || slurry_CM>0 || slurry_IC>0 ||
                slurry_CB==0
192             SolidFormation = true;
193             disp('SOLIDS DIFFERENT IN SLURRY');
194         end
195     end
196     %% Actions to be taken after the check
197     AspenKilledFlag = false; % Aspen, at this point of the simulation is
            not closed
198     if MaxTimeReached || ~Block_status || SolidFormation
199         Aspen1_exe = 'apmain.exe';
200         Aspen2_exe = 'AspenPlus.exe';
201         % Kill Aspen
202         taskkill = sprintf('taskkill /F /IM %s',Aspen1_exe);
203         system(taskkill);
204         taskkill = sprintf('taskkill /F /IM %s',Aspen2_exe);
205         system(taskkill);
206         AspenKilledFlag = true; % Aspen has been closed
207         if AspenKilledFlag
208             Asp = actxserver('Apwn.Document');   % Connect to Aspen,
                    define Aspen as a COM server object
209             Asp.InitFromFile2(CO2absorber_file); % activate aspen file
                    for sensitivity
210             pause(1)
211             AspenKilledFlag = false;
212         end
213         Asp_didntwork = Asp_didntwork + 1; % Info on the fact than the
                simulation has been discharged
214         if Asp_didntwork == 2
215             sens_rebdut(z:sensanlength,1:90)=NaN;
216             system('Close_Notepad.bat');
217             Obj = [Inf, Inf];  % Inf values for the Objective functions
                    are given
218             load Results.mat results
219             results(length(results(:,1))+1,:)=[x(1) x(2) x(3) x(4) x(5)
                    x(6) nan nan nan nan nan nan nan nan nan nan...
220                 nan nan nan nan nan nan nan nan nan nan nan nan nan nan
                        nan nan nan nan nan nan nan nan nan nan nan nan
                        nan nan nan...
221                 nan nan nan nan nan nan nan nan nan nan nan nan nan
                        nan nan nan nan nan nan nan nan nan nan nan
                        nan nan nan...
```

```
222                 nan nan nan nan nan nan nan nan nan nan nan nan nan nan
                        nan nan nan nan nan nan nan nan nan nan nan nan nan
                        nan nan nan...
223                 nan nan nan nan nan nan nan nan nan nan nan nan nan nan
                        nan nan nan nan nan nan nan nan nan nan nan nan nan
                        nan nan nan...
224                 nan nan nan nan nan nan nan nan nan nan nan nan nan nan
                        nan nan nan nan nan nan nan nan nan nan nan nan nan
                        nan nan nan...
225                 nan nan nan nan nan nan nan nan nan nan nan nan nan nan
                        nan nan nan nan nan nan nan nan nan nan nan nan nan
                        nan nan nan];
226             save Results.mat results
227             break % it exists the sensitivity on the desorber duty
                    giving back a Inf objective function value
228         else
229             sens_rebdut(z,1)     = QN;
230             sens_rebdut(z,2:90) = NaN;
231         end
232     else
233     %% Save data
234         Asp_didntwork = 0;
235         sens_rebdut(z,1) = QN;
236         sens_rebdut(z,2) = Asp.Tree.FindNode('\Data\Streams\CO2MKUP\
                Output\STR_MAIN\MASSFLOW\MIXED\CO2').Value;
237         for pin=3:23
238             sens_rebdut(z,pin) = Asp.Tree.FindNode(strcat('\Data\
                    Flowsheeting Options\Calculator\PINCH\Output\READ_VAL\',
                    num2str(pin-2))).Value;
239         end
240         sens_rebdut(z,24) = Asp.Tree.FindNode('\Data\Streams\CO2STORA\
                Output\STR_MAIN\MASSFLOW\MIXED\CO2').Value;
241         sens_rebdut(z,25) = Asp.Tree.FindNode('\Data\Flowsheeting
                Options\Calculator\CO2CAP\Output\WRITE_VAL\5').Value;
242         sens_rebdut(z,26) = Asp.Tree.FindNode('\Data\Flowsheeting
                Options\Calculator\CO2CAP\Output\WRITE_VAL\12').Value;
243         sens_rebdut(z,27) = Asp.Tree.FindNode('\Data\Flowsheeting
                Options\Calculator\CO2CAP\Output\WRITE_VAL\9').Value;
244         sens_rebdut(z,28) = Asp.Tree.FindNode('\Data\Flowsheeting
                Options\Calculator\CO2CAP\Output\WRITE_VAL\6').Value;
245         sens_rebdut(z,29) = Asp.Tree.FindNode('\Data\Streams\FGOUT\
                Output\STR_MAIN\MOLEFRAC\MIXED\CO2').Value;
246         sens_rebdut(z,30) = Asp.Tree.FindNode('\Data\Streams\FGOUT\
                Output\STR_MAIN\MOLEFRAC\MIXED\NH3').Value;
247         sens_rebdut(z,31) = Asp.Tree.FindNode('\Data\Streams\FGOUT\
                Output\STR_MAIN\MOLEFRAC\MIXED\H2O').Value;
248         sens_rebdut(z,32) = Asp.Tree.FindNode('\Data\Streams\FGOUT\
                Output\STR_MAIN\MOLEFRAC\MIXED\AIR').Value;
249         sens_rebdut(z,33) = Asp.Tree.FindNode('\Data\Streams\FGOUT\
                Output\STR_MAIN\TEMP\MIXED').Value;
250         sens_rebdut(z,34) = Asp.Tree.FindNode('\Data\Streams\FGOUT\
                Output\STR_MAIN\MASSFLMX\MIXED').Value;
251         sens_rebdut(z,35) = Asp.Tree.FindNode('\Data\Streams\DESOUT2\
                Output\STR_MAIN\TEMP\MIXED').Value;
252         sens_rebdut(z,36) = Asp.Tree.FindNode('\Data\Flowsheeting
                Options\Calculator\CO2CAP\Output\READ_VAL\14').Value;
253         sens_rebdut(z,37) = Asp.Tree.FindNode('\Data\Flowsheeting
                Options\Calculator\LLOADABS\Output\WRITE_VAL\7').Value;
```

```
254         sens_rebdut(z,38) = Asp.Tree.FindNode('\Data\Streams\WELTOT\
                Output\POWER_OUT').Value;
255         sens_rebdut(z,39) = Asp.Tree.FindNode('\Data\Streams\TODES3\
                Output\STR_MAIN\VFRAC\MIXED').Value;
256         sens_rebdut(z,40) = Asp.Tree.FindNode('\Data\Blocks\ABSO\Output\
                B_TEMP\1').Value;
257         sens_rebdut(z,41) = Asp.Tree.FindNode('\Data\Blocks\ABSO\Output\
                B_TEMP\3').Value;
258         sens_rebdut(z,42) = Asp.Tree.FindNode('\Data\Blocks\ABSO\Output\
                B_TEMP\5').Value;
259         sens_rebdut(z,43) = Asp.Tree.FindNode('\Data\Blocks\ABSO\Output\
                B_TEMP\7').Value;
260         sens_rebdut(z,44) = Asp.Tree.FindNode('\Data\Blocks\ABSO\Output\
                B_TEMP\9').Value;
261         sens_rebdut(z,45) = Asp.Tree.FindNode('\Data\Blocks\ABSO\Output\
                B_TEMP\11').Value;
262         sens_rebdut(z,46) = Asp.Tree.FindNode('\Data\Blocks\ABSO\Output\
                B_TEMP\13').Value;
263         sens_rebdut(z,47) = Asp.Tree.FindNode('\Data\Blocks\ABSO\Output\
                B_TEMP\15').Value;
264         sens_rebdut(z,48) = Asp.Tree.FindNode('\Data\Blocks\ABSO\Output\
                B_TEMP\17').Value;
265         sens_rebdut(z,49) = Asp.Tree.FindNode('\Data\Streams\QCHILLEA\
                Output\QCALC').Value;
266         sens_rebdut(z,50) = Asp.Tree.FindNode('\Data\Blocks\CHILLEAN\
                Output\B_TEMP').Value;
267         sens_rebdut(z,51) = Asp.Tree.FindNode('\Data\Streams\QCHILDCC\
                Output\QCALC').Value;
268         sens_rebdut(z,52) = Asp.Tree.FindNode('\Data\Blocks\CHILLH2O\
                Output\B_TEMP').Value;
269         sens_rebdut(z,53) = Asp.Tree.FindNode('\Data\Streams\QCRYST\
                Output\QCALC').Value;
270         sens_rebdut(z,54) = Asp.Tree.FindNode('\Data\Blocks\CRYS\Output\
                B_TEMP').Value;
271         sens_rebdut(z,55) = Asp.Tree.FindNode('\Data\Streams\QCO2WSH\
                Output\QCALC').Value;
272         sens_rebdut(z,56) = Asp.Tree.FindNode('\Data\Blocks\CO2COOL\
                Output\B_TEMP').Value;
273         sens_rebdut(z,57) = Asp.Tree.FindNode('\Data\Streams\QCO2WASH\
                Output\QCALC').Value;
274         sens_rebdut(z,58) = Asp.Tree.FindNode('\Data\Blocks\WASHCLR\
                Output\B_TEMP').Value;
275         sens_rebdut(z,59) = Asp.Tree.FindNode('\Data\Streams\QDCC\Output
                \QCALC').Value;
276         sens_rebdut(z,60) = Asp.Tree.FindNode('\Data\Blocks\COOLH2O\
                Output\B_TEMP').Value;
277         sens_rebdut(z,61) = Asp.Tree.FindNode('\Data\Streams\QCOOLER\
                Output\QCALC').Value;
278         sens_rebdut(z,62) = Asp.Tree.FindNode('\Data\Blocks\COOLER\
                Output\B_TEMP').Value;
279         sens_rebdut(z,63) = Asp.Tree.FindNode('\Data\Streams\QCOOLER\
                Output\QCALC').Value;
280         sens_rebdut(z,64) = Asp.Tree.FindNode('\Data\Blocks\COOLLEAN\
                Output\B_TEMP').Value;
281         sens_rebdut(z,65) = Asp.Tree.FindNode('\Data\Streams\QCOOLCRY\
                Output\QCALC').Value;
282         sens_rebdut(z,66) = Asp.Tree.FindNode('\Data\Blocks\COOLCRYS\
                Output\B_TEMP').Value;
```

```
283         sens_rebdut(z,67) = Asp.Tree.FindNode('\Data\Streams\CO2PROD3\
                Output\STRM_UPP\SOLINDEX\MIXED\LIQUID\NH4HCO3').Value;
284         sens_rebdut(z,68) = Asp.Tree.FindNode('\Data\Streams\CO2PROD3\
                Output\STRM_UPP\SOLINDEX\MIXED\LIQUID\CARBO').Value;
285         sens_rebdut(z,69) = Asp.Tree.FindNode('\Data\Streams\CO2PROD3\
                Output\STRM_UPP\SOLINDEX\MIXED\LIQUID\SESQUI').Value;
286         sens_rebdut(z,70) = Asp.Tree.FindNode('\Data\Streams\CO2PROD3\
                Output\STRM_UPP\SOLINDEX\MIXED\LIQUID\CARBAM').Value;
287         sens_rebdut(z,71) = Asp.Tree.FindNode('\Data\Streams\CO2PROD3\
                Output\STRM_UPP\SOLINDEX\MIXED\LIQUID\ICE').Value;
288         sens_rebdut(z,72) = Asp.Tree.FindNode('\Data\Streams\CO2STORA\
                Output\STR_MAIN\MOLEFRAC\MIXED\NH3').Value;
289         sens_rebdut(z,73) = Asp.Tree.FindNode('\Data\Streams\HEATHX8\
                Output\QCALC').Value;
290         sens_rebdut(z,74) = Asp.Tree.FindNode('\Data\Blocks\HEX8\Output\
                B_TEMP').Value;
291         sens_rebdut(z,75) = Asp.Tree.FindNode('\Data\Streams\HEATDISS\
                Output\QCALC').Value;
292         sens_rebdut(z,76) = Asp.Tree.FindNode('\Data\Blocks\DISSOL\
                Output\B_TEMP').Value;
293         sens_rebdut(z,77) = Asp.Tree.FindNode('\Data\Streams\DESOUT5\
                Output\STR_MAIN\TEMP\MIXED').Value;
294         sens_rebdut(z,78) = Asp.Tree.FindNode('\Data\Streams\CO2STORA\
                Output\STR_MAIN\MASSFLMX\MIXED').Value;
295         sens_rebdut(z,79) = Asp.Tree.FindNode('\Data\Streams\CO2STORA\
                Output\STR_MAIN\MASSFRAC\MIXED\H2O').Value;
296         sens_rebdut(z,80) = Asp.Tree.FindNode('\Data\Streams\CO2STORA\
                Output\STR_MAIN\MASSFRAC\MIXED\CO2').Value;
297         sens_rebdut(z,81) = Asp.Tree.FindNode('\Data\Streams\CO2STORA\
                Output\STR_MAIN\MASSFRAC\MIXED\NH3').Value;
298         sens_rebdut(z,82) = Asp.Tree.FindNode('\Data\Streams\CO2STORA\
                Output\STR_MAIN\MASSFRAC\MIXED\AIR').Value;
299         sens_rebdut(z,83) = Asp.Tree.FindNode('\Data\Streams\CO2STORA\
                Output\STR_MAIN\TEMP\MIXED').Value;
300         sens_rebdut(z,84) = Asp.Tree.FindNode('\Data\Streams\CO2STORA\
                Output\STR_MAIN\PRES\MIXED').Value;
301         sens_rebdut(z,85) = mNH3;
302         sens_rebdut(z,86) = SFRAC;
303         sens_rebdut(z,87) = LEANCO2;
304         sens_rebdut(z,88) = KLG;
305         sens_rebdut(z,89) = T_PumpAround;
306         sens_rebdut(z,90) = T_lean;
307         if Absorber_Flag == 0
308             for n_stages=1:n_stages
309             abs_h2o(n_stages)     = Asp.Tree.FindNode(strcat('\Data\
                    Blocks\ABSO\Output\X\', num2str(n_stages),'\H2O')).Value;
310             abs_co3(n_stages)     = Asp.Tree.FindNode(strcat('\Data\
                    Blocks\ABSO\Output\X\', num2str(n_stages),'\CO3--')).
                    Value;
311             abs_hco3(n_stages)    = Asp.Tree.FindNode(strcat('\Data\
                    Blocks\ABSO\Output\X\', num2str(n_stages),'\HCO3-')).
                    Value;
312             abs_nh3(n_stages)     = Asp.Tree.FindNode(strcat('\Data\
                    Blocks\ABSO\Output\X\', num2str(n_stages),'\NH3')).Value;
313             abs_nh4(n_stages)     = Asp.Tree.FindNode(strcat('\Data\
                    Blocks\ABSO\Output\X\', num2str(n_stages),'\NH4+')).Value
                    ;
314             abs_nh2coo(n_stages) = Asp.Tree.FindNode(strcat('\Data\
```

```
                Blocks\ABSO\Output\X\', num2str(n_stages),'\NH2COO-')).
                Value;
315             abs_co2(n_stages)     = Asp.Tree.FindNode(strcat('\Data\
                Blocks\ABSO\Output\X\', num2str(n_stages),'\CO2')).Value;
316             end
317             Absorber_Flag = 1;
318         end
319         if sens_rebdut(z,2)<0.5 % Threshold on the CO2 make-up limit
320             sens_rebdut(z+1:sensanlength,1:90)=NaN;
321             Aspen1_exe = 'apmain.exe';
322             Aspen2_exe = 'AspenPlus.exe';
323             % Kill Aspen
324             taskkill = sprintf('taskkill /F /IM %s',Aspen1_exe);
325             system(taskkill);
326             taskkill = sprintf('taskkill /F /IM %s',Aspen2_exe);
327             system(taskkill);
328             AspenKilledFlag = true; % Aspen has been closed
329             if AspenKilledFlag
330                 Asp = actxserver('Apwn.Document');       % Connect to
                    Aspen, define Aspen as a COM server object
331                 Asp.InitFromFile2(CO2absorber_file); % activate aspen
                    file for sensitivity
332                 pause(1)
333                 AspenKilledFlag = false;
334             end
335             break
336         end
337     end
338     if z>1 % Compute Q-Iterations slope
339     slope=(sens_rebdut(z,2)-sens_rebdut(z-1,2))/(sens_rebdut(z,1)-
            sens_rebdut(z-1,1));
340     intercept=sens_rebdut(z,2)-slope*sens_rebdut(z,1);
341     rebdut_zero=-intercept/slope;
342         if sens_rebdut(z,1)-rebdut_zero>5000
343             new_rebduty=sens_rebdut(z,1)-5000;
344         else
345             new_rebduty=sens_rebdut(z,1)-1000;
346         end
347     end
348 end
349 Result_index = find(sens_rebdut(:,2) == min(sens_rebdut(:,2)));
350 Ammonia_slip = sens_rebdut(Result_index,30)*1000000;
351 if ~isempty(Result_index)
352     if sens_rebdut(Result_index,25) > 85 && Ammonia_slip < 45000 &&
            sens_rebdut(Result_index,2) < 0.5
353         ResCap_QN               = sens_rebdut(Result_index,1);
354         ResCap_CO2Mkp           = sens_rebdut(Result_index,2);
355         ResCap_CO2Stora         = sens_rebdut(Result_index,24);
356         ResCap_CO2Cap1          = sens_rebdut(Result_index,25);
357         ResCap_CO2Cap2          = sens_rebdut(Result_index,26);
358         ResCap_SpecRebDut       = sens_rebdut(Result_index,27);
359         ResCap_CO2Balance       = sens_rebdut(Result_index,28);
360         ResCap_FG_CO2           = sens_rebdut(Result_index,29);
361         ResCap_FG_NH3           = sens_rebdut(Result_index,30);
362         ResCap_FG_H2O           = sens_rebdut(Result_index,31);
363         ResCap_FG_Air           = sens_rebdut(Result_index,32);
364         ResCap_FG_T             = sens_rebdut(Result_index,33);
365         ResCap_FG_M             = sens_rebdut(Result_index,34);
```

```
366 ResCap_Treb              = sens_rebdut(Result_index,35);
367 ResCap_DThex             = sens_rebdut(Result_index,36);
368 ResCap_CO2leanload       = sens_rebdut(Result_index,37);
369 ResCap_ElDuty            = sens_rebdut(Result_index,38)/1000;
370 ResCap_VapFracDes        = sens_rebdut(Result_index,39);
371 ResCap_Abs1              = sens_rebdut(Result_index,40);
372 ResCap_Abs3              = sens_rebdut(Result_index,41);
373 ResCap_Abs5              = sens_rebdut(Result_index,42);
374 ResCap_Abs7              = sens_rebdut(Result_index,43);
375 ResCap_Abs9              = sens_rebdut(Result_index,44);
376 ResCap_Abs11             = sens_rebdut(Result_index,45);
377 ResCap_Abs13             = sens_rebdut(Result_index,46);
378 ResCap_Abs15             = sens_rebdut(Result_index,47);
379 ResCap_Abs17             = sens_rebdut(Result_index,48);
380 ResCap_QChillea          = sens_rebdut(Result_index,49)/1000;
381 ResCap_TChillea          = sens_rebdut(Result_index,50);
382 ResCap_QChilDCC          = sens_rebdut(Result_index,51)/1000;
383 ResCap_TChilDCC          = sens_rebdut(Result_index,52);
384 ResCap_QCryst            = sens_rebdut(Result_index,53)/1000;
385 ResCap_TCryst            = sens_rebdut(Result_index,54);
386 ResCap_QCO2wash          = sens_rebdut(Result_index,55)/1000;
387 ResCap_TCO2wash          = sens_rebdut(Result_index,56);
388 ResCap_QCO2wsh           = sens_rebdut(Result_index,57)/1000;
389 ResCap_TCO2wsh           = sens_rebdut(Result_index,58);
390 ResCap_QDCC              = sens_rebdut(Result_index,59)/1000;
391 ResCap_TDCC              = sens_rebdut(Result_index,60);
392 ResCap_QCooler           = sens_rebdut(Result_index,61)/1000;
393 ResCap_TCooler           = sens_rebdut(Result_index,62);
394 ResCap_QCoolLean         = sens_rebdut(Result_index,63)/1000;
395 ResCap_TCoolLean         = sens_rebdut(Result_index,64);
396 ResCap_QCoolCry          = sens_rebdut(Result_index,65)/1000;
397 ResCap_TCoolCry          = sens_rebdut(Result_index,66);
398 ResCap_SIBCCO2Stora      = sens_rebdut(Result_index,67);
399 ResCap_SICBCO2Stora      = sens_rebdut(Result_index,68);
400 ResCap_SISCCO2Stora      = sens_rebdut(Result_index,69);
401 ResCap_SICMCO2Stora      = sens_rebdut(Result_index,70);
402 ResCap_SIICCO2Stora      = sens_rebdut(Result_index,71);
403 ResCap_CO2Sto_NH3molfr   = sens_rebdut(Result_index,72);
404 ResCap_QHX8              = sens_rebdut(Result_index,73);
405 ResCap_THX8              = sens_rebdut(Result_index,74);
406 ResCap_QDiss             = sens_rebdut(Result_index,75);
407 ResCap_TDiss             = sens_rebdut(Result_index,76);
408 ResCap_TDesout5          = sens_rebdut(Result_index,77);
409 ResCap_CO2Stora_M        = sens_rebdut(Result_index,78);
410 ResCap_CO2Sto_H2Omasfr   = sens_rebdut(Result_index,79);
411 ResCap_CO2Sto_CO2masfr   = sens_rebdut(Result_index,80);
412 ResCap_CO2Sto_NH3masfr   = sens_rebdut(Result_index,81);
413 ResCap_CO2Sto_AIRmasfr   = sens_rebdut(Result_index,82);
414 ResCap_CO2Sto_Temp       = sens_rebdut(Result_index,83);
415 ResCap_CO2Sto_Pres       = sens_rebdut(Result_index,84);
416 ResCap_wnh3_in           = sens_rebdut(Result_index,85);
417 ResCap_spltfr_in         = sens_rebdut(Result_index,86);
418 ResCap_CO2wt_in          = sens_rebdut(Result_index,87);
419 ResCap_klg_in            = sens_rebdut(Result_index,88);
420 ResCap_TempPA_in         = sens_rebdut(Result_index,89);
421 ResCap_Tlean_in          = sens_rebdut(Result_index,90);
422 ResVecCap_H2O            = abs_h2o(1:n_stages);
423 ResVecCap_CO3            = abs_co3(1:n_stages);
```

```
424         ResVecCap_HCO3          = abs_hco3(1:n_stages);
425         ResVecCap_NH3           = abs_nh3(1:n_stages);
426         ResVecCap_NH4           = abs_nh4(1:n_stages);
427         ResVecCap_NH2COO        = abs_nh2coo(1:n_stages);
428         ResVecCap_CO2           = abs_co2(1:n_stages);
429         Obj_RebDut    = ResCap_SpecRebDut;
430         Obj_ChillDut = (ResCap_QChilDCC + ResCap_QCryst +
                ResCap_QCO2wash)/(sens_rebdut(Result_index,78)*sens_rebdut(
                Result_index,80))
431 %         Obj_Sum_Energies = Obj_RebDut + Obj_ChillDut;
432         Obj = [Obj_RebDut, Obj_ChillDut];
433         load Results.mat results
434         results(length(results(:,1))+1,:)=[x(1) x(2) x(3) x(4) x(5) x(6)
                ResCap_QN ResCap_CO2Mkp ResCap_CO2Stora ResCap_CO2Cap1
                ResCap_CO2Cap2 ResCap_SpecRebDut ResCap_CO2Balance
                ResCap_FG_CO2 ResCap_FG_NH3 ResCap_FG_H2O ResCap_FG_Air...
435             ResCap_FG_T ResCap_FG_M ResCap_Treb ResCap_DThex
                    ResCap_CO2leanload ResCap_ElDuty ResCap_VapFracDes
                    ResCap_Abs1...
436             ResCap_Abs3 ResCap_Abs5 ResCap_Abs7 ResCap_Abs9 ResCap_Abs11
                    ResCap_Abs13 ResCap_Abs15 ResCap_Abs17 ResCap_QChillea
                    ResCap_TChillea ResCap_QChilDCC...
437             ResCap_TChilDCC ResCap_QCryst ResCap_TCryst ResCap_QCO2wsh
                    ResCap_TCO2wsh ResCap_QCO2wash ResCap_TCO2wash
                    ResCap_QDCC...
438             ResCap_TDCC ResCap_QCooler ResCap_TCooler ResCap_QCoolLean
                    ResCap_TCoolLean ResCap_QCoolCry ResCap_TCoolCry
                    ResCap_SIBCCO2Stora...
439             ResCap_SICBCO2Stora ResCap_SISCCO2Stora ResCap_SICMCO2Stora
                    ResCap_SIICCO2Stora ResCap_CO2Sto_NH3molfr ResCap_QHX8
                    ResCap_THX8...
440             ResCap_QDiss ResCap_TDiss ResCap_TDesout5 ResCap_CO2Stora_M
                    ResCap_CO2Sto_H2Omasfr ResCap_CO2Sto_CO2masfr
                    ResCap_CO2Sto_NH3masfr...
441             ResCap_CO2Sto_AIRmasfr ResCap_CO2Sto_Temp ResCap_CO2Sto_Pres
                    ResCap_wnh3_in ResCap_spltfr_in ResCap_CO2wt_in
                    ResCap_klg_in ResCap_TempPA_in ResCap_Tlean_in...
442             ResVecCap_H2O ResVecCap_CO3 ResVecCap_HCO3 ResVecCap_NH3
                    ResVecCap_NH4 ResVecCap_NH2COO ResVecCap_CO2 Obj_RebDut
                    Obj_ChillDut];
443         save Results.mat results
444         system('Close_Notepad.bat');
445     else
446     Obj = [Inf, Inf];
447     load Results.mat results
448     results(length(results(:,1))+1,:)=[x(1) x(2) x(3) x(4) x(5) x(6) nan
            nan nan nan nan nan nan nan nan nan...
449         nan nan nan nan nan nan nan nan nan nan nan nan nan nan nan nan
                nan nan nan nan nan nan nan nan nan nan nan nan nan...
450         nan nan nan nan nan nan nan nan nan nan nan nan nan nan nan nan
                nan nan nan nan nan nan nan nan nan nan nan nan nan...
451         nan nan nan nan nan nan nan nan nan nan nan nan nan nan nan nan
                nan nan nan nan nan nan nan nan nan nan nan nan nan...
452         nan nan nan nan nan nan nan nan nan nan nan nan nan nan nan nan
                nan nan nan nan nan nan nan nan nan nan nan nan nan...
453         nan nan nan nan nan nan nan nan nan nan nan nan nan nan nan nan
                nan nan nan nan nan nan nan nan nan nan nan nan nan...
454         nan nan nan nan nan nan nan nan nan nan nan nan nan nan nan nan
```

```
                nan nan nan nan nan nan nan nan nan nan nan nan nan nan];
455         save Results.mat results
456         system('Close_Notepad.bat');
457         end
458     else
459         Obj = [Inf, Inf];
460         load Results.mat results
461         results(length(results(:,1))+1,:)=[x(1) x(2) x(3) x(4) x(5) x(6) nan
                nan nan nan nan nan nan nan nan nan...
462             nan nan nan nan nan nan nan nan nan nan nan nan nan nan nan nan
                    nan nan nan nan nan nan nan nan nan nan nan nan nan nan...
463             nan nan nan nan nan nan nan nan nan nan nan nan nan nan nan nan
                    nan nan nan nan nan nan nan nan nan nan nan nan nan nan...
464             nan nan nan nan nan nan nan nan nan nan nan nan nan nan nan nan
                    nan nan nan nan nan nan nan nan nan nan nan nan nan nan...
465             nan nan nan nan nan nan nan nan nan nan nan nan nan nan nan nan
                    nan nan nan nan nan nan nan nan nan nan nan nan nan nan...
466             nan nan nan nan nan nan nan nan nan nan nan nan nan nan nan nan
                    nan nan nan nan nan nan nan nan nan nan nan nan nan nan...
467             nan nan nan nan nan nan nan nan nan nan nan nan nan nan nan nan
                    nan nan nan nan nan nan nan nan nan nan nan nan nan nan];
468         save Results.mat results
469         system('Close_Notepad.bat');
470     end
471     end
```

C Flowsheet from Aspen Plus used in the main optimization

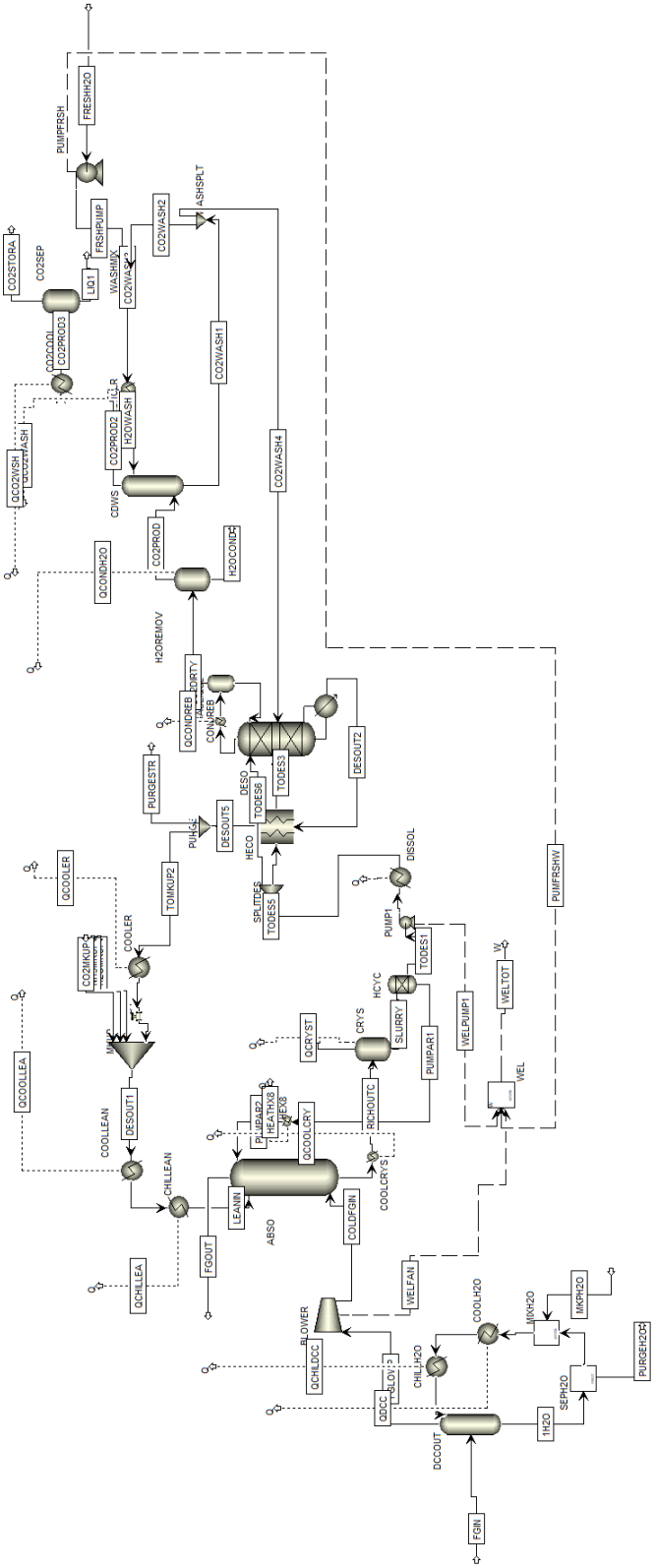

Figure 32: Flowsheet from Aspen Plus used in the main optimization

D Flowsheet from Aspen Plus used in the FG-WW section optimization

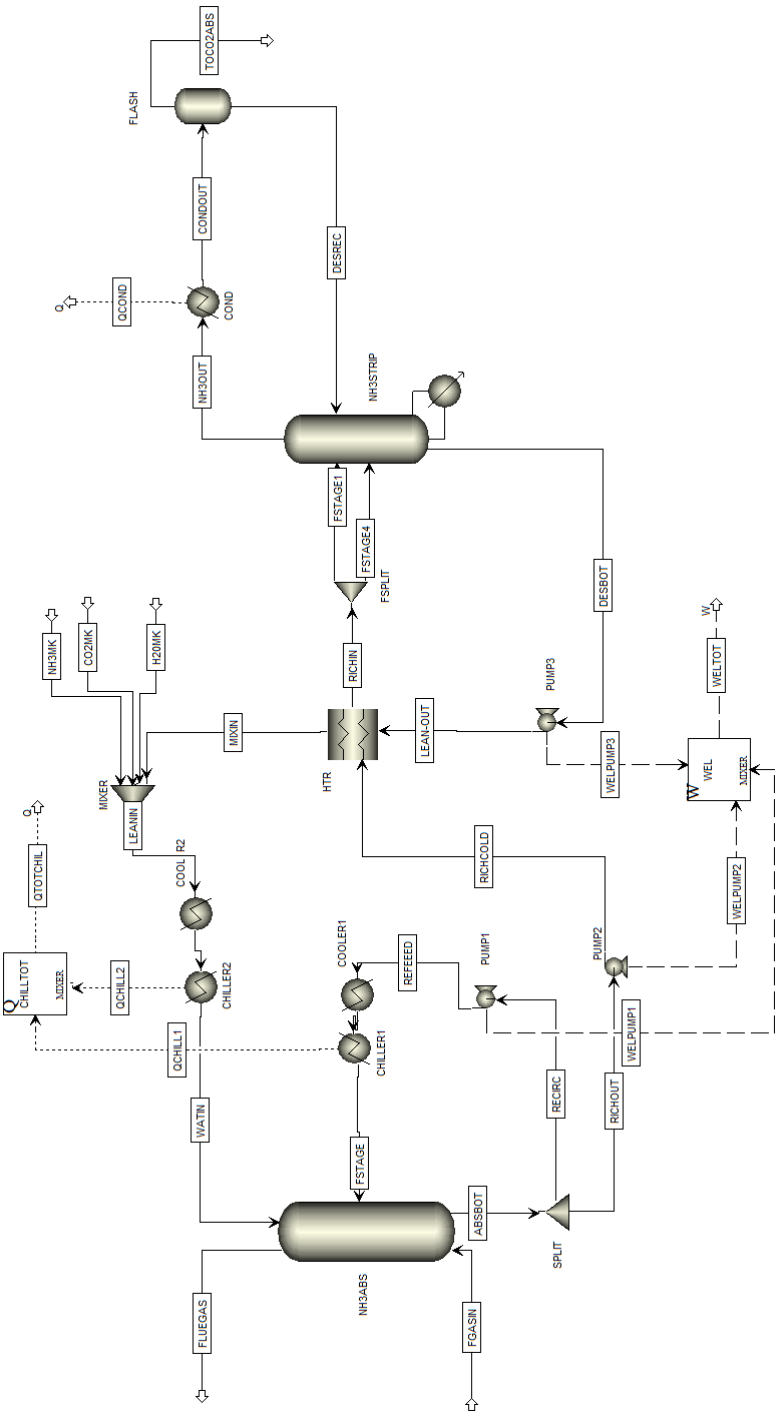

Figure 33: Flowsheet from Aspen Plus used in the flue gas water wash section optimization

E Flowsheet from Aspen Plus of the CO_2 compression section

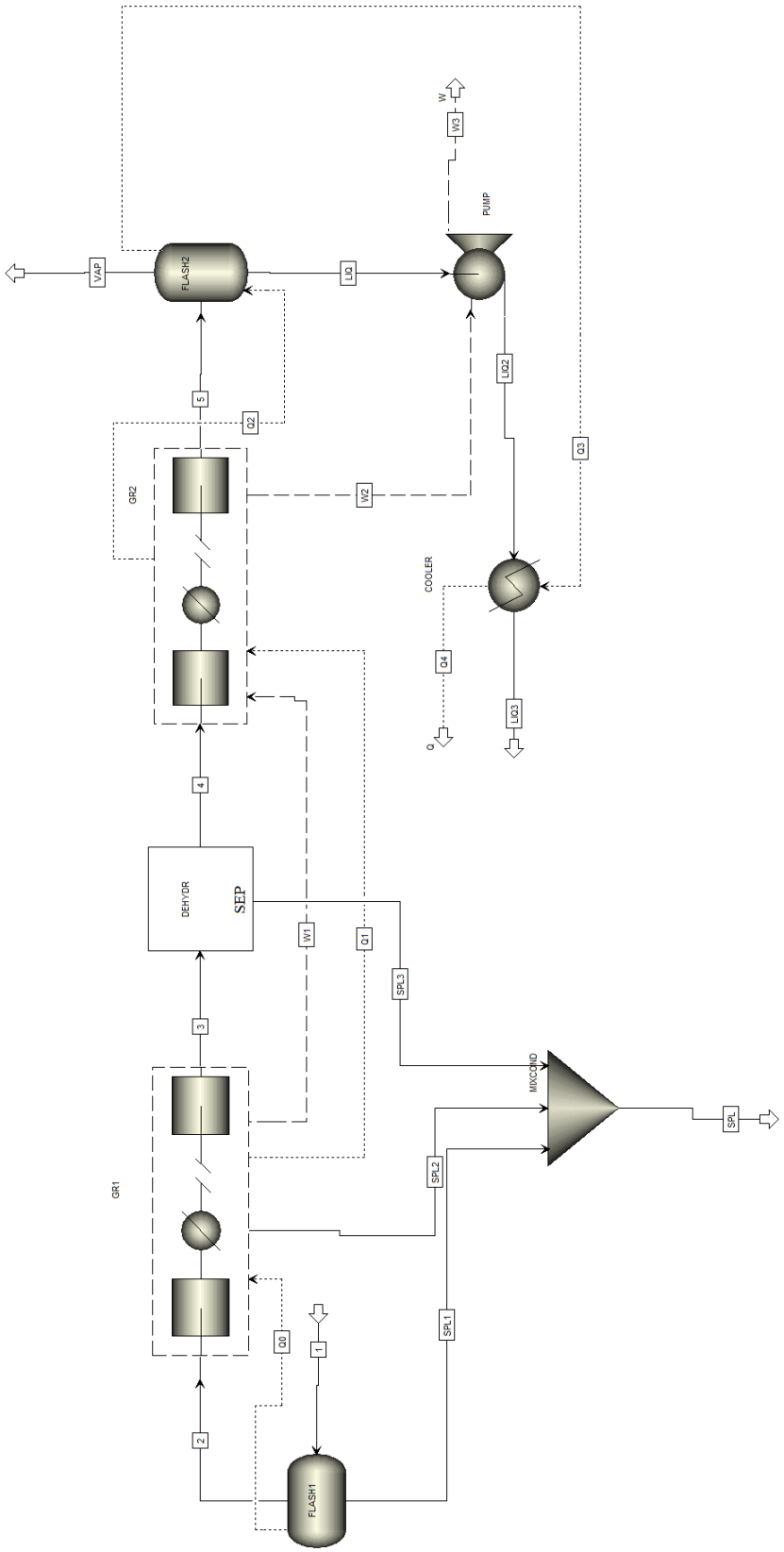

Figure 34: Flowsheet from Aspen Plus of the CO_2 compression section

References

[1] Daniel Sutter, Matteo Gazzani, and Marco Mazzotti. A low-energy chilled ammonia process exploiting controlled solid formation for post-combustion CO2 capture. *Faraday Discussions*, 192:59–83, 2016.

[2] Kaj Thomsen and Peter Rasmussen. Modeling of VLS equilibrium in gas-aqueous electrolyte systems. *Chemical Engineering Science*, 54:1787–1802, 1999.

[3] IPPC. Climate Change 2013: The Physical Science Basis. Working Group I Contribution to the Fifth Assessment Report of the Intergovernmental Panel on Climate Change, 2013.

[4] Amitava Bandyopadhyay. Amine versus ammonia absorption of CO2 as a measure of reducing ghg emission: a critical analysis. *Clean Techn. Environ. Policy*, 13:269–294, 2011.

[5] Brian R. Strazisar, Richard R. Anderson, and Curt M. White. Degradation pathways for monoethanolamine in a CO2 capture facility. *Energy and Fuels*, 17:1034–1039, 2003.

[6] United Nations Framework Convention on Climate Change (UNFCCC). Adoption of the Paris Agreement, 2015.

[7] International Energy Agency (IEA). Energy Technology Analysis: Prospects for CO2 Capture and Storage, 2012.

[8] S Fuss, W F Lamb, M. W. Callaghan, J Hilaire, Felix Creutzig, T Amann, T Beringer, W De Oliveira Garcia, J Hartmann, T Khanna, G Luderer, G F Nemet, J Rogelj, P Smith, J V Vicente, J Wilcox, M Del Mar Zamora Dominguez, and J C Minx. Negative emissions - Part 2: Costs, potentials and side effects. *Environmental Research Letters*, 13, 2018.

[9] Teeradet Supap, Raphael Idem, Paitoon Tontiwachwuthikul, and Chintana Saiwan. Kinetics of sulfur dioxide- and oxygen-induced degradation of aqueous monoethanolamine solution during CO2 absorption from power plant flue gas streams. *International Journal of Greenhouse Gas Control*, 3:133–142, 2009.

[10] Patricia Luis. Use of monoethanolamine (MEA) for CO2capture in a global scenario: Consequences and alternatives. *Desalination*, 380:93–99, 2016.

[11] Y. A. C. Jande, M. Asif, S. M. Shim, and W. S. Kim. Energy minimization in monoethanolamine-based CO2 capture using capacitive deionization. *International Journal of Energy Research*, 38:1531–1540, 2014.

[12] Alicia J. Reynolds, T. Vincent Verheyen, Samuel B. Adeloju, Erik Meuleman, and Paul Feron. Towards commercial scale postcombustion capture of CO2 with monoethanolamine solvent: Key considerations for solvent management and environmental impacts. *Environmental Science and Technology*, 46:3643–3654, 2012.

[13] Jason E. Bara. What chemicals will we need to capture CO2? *Greenhouse Gas Sci Technol.*, 2:162–171, 2012.

[14] Arthur L. Kohl and Richard Nielsen. *Gas Purification*. Gulf Professional Publishing, 5th editio edition, 1997.

[15] Daniel Sutter, Matteo Gazzani, and Marco Mazzotti. Formation of solids in ammonia-based CO2 capture processes — Identification of criticalities through thermodynamic analysis of the CO2–NH3–H2O system. *Chemical Engineering Science*, 133:170–180, 2015.

[16] Victor Darde, Kaj Thomsen, Willy J M van Well, and Erling H. Stenby. Chilled ammonia process for CO2 capture. *International Journal of Greenhouse Gas Control*, 4:131–136, 2010.

[17] R. Strube, G. Pellegrini, and G. Manfrida. The environmental impact of post-combustion CO2 capture with MEA, with aqueous ammonia, and with an aqueous ammonia-ethanol mixture for a coal-fired power plant. *Energy*, 36:3763–3770, 2011.

[18] International Energy Agency. Technology Roadmap - Low-Carbon Transition in the Cement Industry. Technical report, 2018.

[19] International Energy Agency (IEA). Cement Technology Roadmap 2009 - Carbon Emissions Reductions up to 2050. Technical report, 2009.

[20] Victor Darde, Willy J.M. Van Well, Erling H. Stenby, and Kaj Thomsen. Modeling of carbon dioxide absorption by aqueous ammonia solutions using the extended UNIQUAC model. *Industrial and Engineering Chemistry Research*, 49:12663–12674, 2010.

[21] J.M. Prausnitz and Denis S. Abrams. Statistical thermodynamics of liquid mixtures : A new expression for the excess Gibbs energy of partly or completely miscible systems. *AIChE Journal*, 21:116–128, 1975.

[22] G. Maurer and J. M. Prausnitz. On the derivation and extension of the UNIQUAC equation. *Fluid Phase Equilibria*, 2:91–99, 1978.

[23] Kaj Thomsen, Peter Rasmussen, and Rafiqul Gani. Correlation and prediction of thermal properties and phase behaviour for a class of aqueous electrolyte systems. *Chemical Engineering Science*, 51:3675–3683, 1996.

[24] Victor Darde, Bjørn Maribo-Mogensen, Willy J.M. van Well, Erling H. Stenby, and Kaj Thomsen. Process simulation of CO2capture with aqueous ammonia using the Extended UNIQUAC model. *International Journal of Greenhouse Gas Control*, 10:74–87, 2012.

[25] Victor Darde. *CO2 capture using aqueous ammonia*. PhD thesis, DTU, 2011.

[26] Bernd Rumpf and Gerd Maurer. Solubility of ammonia in aqueous solutions of phosphoric acid: Model development and application. *Journal of Solution Chemistry*, 23:37–51, 1994.

[27] Kaj Thomsen. *Aqueous electrolytes : model parameters and process simulation*. PhD thesis, DTU, 1997.

[28] Sepideh Ziaii, Gary T. Rochelle, and Thomas F. Edgar. Dynamic modeling to minimize energy use for CO 2 capture in power plants by aqueous monoethanolamine. *Industrial and Engineering Chemistry Research*, 48:6105–6111, 2009.

[29] Eli Gal. Ultra cleaning of combustion gas including the removal of CO2, 2008.

[30] Victor Darde, Kaj Thomsen, Willy J M van Well, and Erling H. Stenby. Chilled ammonia process for CO2 capture. *Energy Procedia*, 1:1035–1042, 2009.

[31] Guojie Qi, Shujuan Wang, Hai Yu, Paul Feron, and Changhe Chen. Rate-based modeling of CO2 absorption in aqueous NH3 in a packed column. *Energy Procedia*, 37:1968–1976, 2013.

[32] Peter Versteeg and Edward S. Rubin. A technical and economic assessment of ammonia-based post-combustion CO2 capture at coal-fired power plants. *International Journal of Greenhouse Gas Control*, 5:1596–1605, 2011.

[33] Matlab optimization toolbox, R2016a.

[34] Kangkang Li, Hai Yu, Paul Feron, and Moses Tade. Modelling and experimental study of SO2 removal and NH3 recycling in an ammonia based CO2 capture process. *Energy Procedia*, 63:1162–1170, 2014.

List of Figures

List of Tables